Curved Pi-Conjugation, Aromaticity, and the Related Chemistry of Small Fullerenes (<C_{60}) and Single-Walled Carbon Nanotubes

Xin Lu*,† and Zhongfang Chen*,‡

State Key Laboratory of Physical Chemistry of Solid Surfaces & Center for Theoretical Chemistry, Department of Chemistry, Xiamen University, Xiamen 361005, China, and Department of Chemistry, University of Georgia, Athens, Georgia 30602-2525

Received March 17, 2005

Contents

1. Introduction 3644
2. Curved π-Conjugation within Small Fullerenes and the Related Chemistry 3644
   2.1 Curved π-Conjugation and Aromaticity within Small Fullerenes 3644
   2.2 The Smallest Fullerene C_{20} and Its Molecular and Solid Derivatives 3646
      2.2.1 Geometric and Electronic Structures of Fullerene C_{20} 3646
      2.2.2 Synthesis and Characterization of Fullerene C_{20} 3647
      2.2.3 Dimer, Oligomer, and Polymeric Solid of Fullerene C_{20} 3647
      2.2.4 Perhydrogenated Derivative of Fullerene C_{20}: Dodecahedrane $C_{20}H_{20}$ 3649
      2.2.5 Other Exohedral Derivatives of Fullerene C_{20} 3650
      2.2.6 Dodecahedral Heterofullerenes 3651
      2.2.7 Endohedral Derivatives of $C_{20}H_{20}$ and C_{20} 3652
   2.3 C_{28} Fullerene and Its Molecular and Solid Derivatives 3652
      2.3.1 Geometric and Electronic Structures of Fullerene C_{28} 3652
      2.3.2 Endohedral Fullerenes of C_{28} 3653
      2.3.3 Exohedral Fullerenes of C_{28} 3653
      2.3.4 Heterofullerenes of C_{28} 3653
      2.3.5 Solid of C_{28}: Hyperdiamond 3654
   2.4 C_{36} and Its Molecular and Solid Derivatives 3654
      2.4.1 Synthesis of C_{36} and Its Derivatives 3654
      2.4.2 Geometric and Electronic Structures of C_{36} 3654
      2.4.3 Exohedral Derivatives of C_{36} 3655
      2.4.4 Endohedral Derivatives of C_{36} 3656
      2.4.5 Heterofullerene Analogues of C_{36} 3657
      2.4.6 Oligomers of C_{36} 3657
      2.4.7 Polymers and Solids of C_{36} 3658
   2.5 C_{50} and Its Molecular and Solid Derivatives 3661
      2.5.1 Geometric and Electronic Structures of C_{50} 3661
      2.5.2 Exohedral Derivatives of C_{50} 3662
      2.5.3 Endohedral Derivatives of C_{50} 3663
      2.5.4 Heterofullerenes of C_{50} 3663
      2.5.5 Oligomers of C_{50} 3663
   2.6 Other Small Fullerenes and Their Derivatives 3663
      2.6.1 C_{24} and Its Derivatives 3663
      2.6.2 C_{32} and Its Derivatives 3665
      2.6.3 C_{40} and Its Derivatives 3666
      2.6.4 C_{44} and Its Derivatives 3667
      2.6.5 C_{26}, C_{30}, C_{34}, C_{38}, C_{42}, C_{46}, C_{48}, C_{52}, C_{54}, C_{56}, C_{58}, and Their Derivatives 3668
   2.7 Small Metal-Substituted Metallofullerenes MC_n 3671
3. π-Conjugation in the Sidewalls of Single-Walled Carbon Nanotubes (SWCNTs) and the Related Sidewall Chemistry 3672
   3.1 Geometric and Electronic Structures of SWCNTs 3672
      3.1.1 Zone-Folding Approximation 3672
      3.1.2 Curvature Effects 3672
      3.1.3 Intertube Interactions in Nanotube Bundles 3673
   3.2 Aromaticity of SWCNTs 3673
      3.2.1 Clar Valence Bond (VB) Model Description 3673
      3.2.2 Aromaticity and Chemical Reactivity: A Chemist's View 3675
   3.3 Curvature-Induced Pyramidalization and Misalignment of π-Orbitals 3675
   3.4 Sidewall Chemistry of SWCNTs Related to the Curved π-Conjugation and Aromaticity 3676
      3.4.1 Fluorination 3676
      3.4.2 1,3-Dipolar Cycloadditions: A Facile Way to Sidewall Functionalization 3677
      3.4.3 Diels-Alder Cycloaddition 3680
      3.4.4 Sidewall Osmylation: Base-Catalyzed and Photo-Promoted Reactions 3681
      3.4.5 [2+1] Cycloadditions 3682
      3.4.6 [2+2] Cycloaddition of Singlet O_2 and Sidewall Oxidation 3684
      3.4.7 Sidewall Epoxidation or Sidewall Opening by Oxidation 3684
      3.4.8 Sidewall Hydrogenation 3684
      3.4.9 Addition of Radicals 3685
      3.4.10 Chemical Reactivity of Sidewall Defects 3685
   3.5 Hybrid Materials Consisting of Small Fullerenes and Single-Wall Carbon Nanotubes: Peapods 3687
4. Pros and Cons of Different Approaches in Computational Nanotube Chemistry 3688
5. Concluding Remarks 3689
6. Acknowledgment 3690
7. Notes Added in Proof 3690
8. References and Notes 3690

* To whom correspondence should be addressed. E-mail: xinlu@xmu.edu.cn; chen@chem.uga.edu.
† Xiamen University.
‡ University of Georgia.

10.1021/cr030093d CCC: $53.50
Published on Web 09/29/2005

Xin Lu was born in Changning, Hunan Province, China, in 1969. He received his chemistry education at Xiamen University. After his Ph.D. work with Profs. Qianer Zhang and Nanqin Wang, he joined the faculty at Xiamen University and the State Key Laboratory for Physical Chemistry of Solid Surfaces in 1996, where he is now Professor of Physical Chemistry. During the 1999–2000 academic year, he enjoyed a nine-month sabbatical visit at the Cherry L. Emerson Center for Scientific Computation, Emory University, hosted by Prof. M. C. Lin. He received the Young Chemist's Award of Chinese Chemical Society (2000), the Fok Ying-Tung Fund from the Fok Ying-Tung Education Foundation (2002), and the National Science Fund for Distinguished Young Scholars. He has published over 90 scientific papers in peer-reviewed journals, including three review articles. His research interests include theoretical simulations of chemical processes on solid surfaces and the chemistry of carbon nanotubes and fullerenes.

Zhongfang Chen was born in Liaoyang, P. R. China, in 1971. He earned his B.Sc. (organic chemistry, in 1994), M.Sc. (physical chemistry, with Xuezhuang Zhao, in 1997), and Ph.D. (physical chemistry, with Xuezhuang Zhao and Auchin Tang, in 2000) at Nankai University, Tianjin, P. R. China. In late 1999, he began to work in Germany with Andreas Hirsh (Universität Erlangen-Nürnberg) and Walter Thiel (Max-Planck-Institute für Kohlenforschung in Mülheim/Ruhr) as a postdoc, under the support of the Alexander von Humbolt Foundation and the Max-Planck Society. He joined Paul v. R. Schleyer's group in late 2002 but physically remained in Erlangen until his move to the University of Georgia (Athens, GA) in October 2003. His early research was on the synthesis of fullerenes and their derivatives. Tempted by the charm of modern computational chemistry, in 1997, he switched to apply these powerful tools to characterize the experimentally synthesized structures, to design new materials with novel chemical bonding and potential applications, and to investigate rules and trends in chemistry. His main research areas are fullerenes, nanotubes, aromaticity of spherical molecules and clusters, and molecules with novel chemical bonding. He enjoys his extensive collaborations with peer experimentalists and theoreticians. So far, he has given over 30 lectures and has about 70 publications.

1. Introduction

The successive discoveries of fullerenes[1] and carbon nanotubes[2] (CNTs) around 1990 triggered a hot wave of scientific research to explore the properties and applications of these new forms of carbonous materials over the past two decades. Figure 1 shows

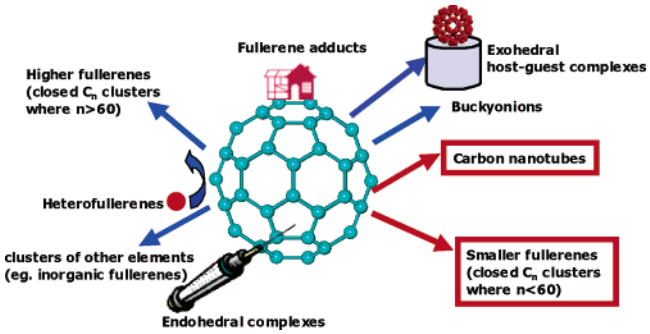

Figure 1. Research areas centered on fullerene C_{60}.

schematically the research area centered at fullerene C_{60}. Differing from the two long-known allotropes of carbon, i.e., diamond and graphite, fullerenes and carbon nanotubes have displayed brand-new, unique, and fascinating structural, electronic, electric, mechanic, and optical properties and should find their power in a wide variety of applications.[3,4] Some of their unique properties can be related to the curved π-conjugation within their curved hexagonal (for CNTs) or hybrid hexagon−pentagon (for fullerenes) carbon−carbon networks. The curved π-conjugation and aromaticity, as well as the related chemistry, of fullerene[60] and its larger homologues have been the subject of several review articles. Herein we review recent studies on the curved π-conjugation within small fullerenes ($<C_{60}$) and single-walled carbon nanotubes (SWCNTs) as well as their unusual chemical properties that are related to their curved π-conjugation and aromaticity.

2. Curved π-Conjugation within Small Fullerenes and the Related Chemistry

2.1 Curved π-Conjugation and Aromaticity within Small Fullerenes

Fullerenes are convex carbon cages comprising hexagons and exactly 12 pentagons. This building principle follows Euler's Theorem stating that exactly 12 pentagons must be accommodated to allow closure of a carbon network consisting of n hexagons. The geometry and stability of fullerenes are, in most cases, governed by the so-called isolated-pentagon rule (IPR),[5] i.e., the pentagons within the most stable fullerenes are surrounded by five hexagons and, hence, are isolated from each other. The smallest carbon cage that faithfully fulfills this rule is the icosahedral C_{60} (I_h).[6]

Only C_{60} and fullerenes not smaller than C_{70} can fulfill the IPR. Non-IPR fullerenes with adjacent pentagons are always unstable, due to enhanced steric strain (steric effect) and resonance destabilization pertaining to the pentalene-type 8π-electron system (electronic effect). For fullerenes that cannot follow the IPR rule, such as small fullerenes reviewed in this article (Table 1), the relative stability of the different isomers is directly related to the number of adjacent pentagons; the isomer with the least adja-

Table 1. Total Numbers (N_i) of Fullerenic Isomers for C_n (n = 2−58)[a]

C_n	N_i	C_n	N_i	C_n	N_i	C_n	N_i
C_{20}	1	C_{30}	3	C_{40}	40	C_{50}	271
C_{22}	0	C_{32}	6	C_{42}	45	C_{52}	437
C_{24}	1	C_{34}	6	C_{44}	89	C_{54}	580
C_{26}	1	C_{36}	15	C_{46}	116	C_{56}	924
C_{28}	2	C_{38}	17	C_{48}	199	C_{58}	1205

[a]Data extracted from ref 6.

cent pentagons is most favorable energetically.[7] This is known as the pentagon adjacency penalty rule (PAPR).[8] Nevertheless, stabilization of non-IPR fullerenes larger than C_{60} can be attainable by charging or encapsulating electron-donating metal atoms and clusters.[9] Stable derivatives of non-IPR large fullerenes are exemplified by $Sc_2@C_{66}$,[10] $Sc_3N@C_{68}$,[11] and $La_2@C_{72}$,[12] whose carbon cages have two or three fused pentagons.

Fullerenes smaller than C_{60} unavoidably possess adjacent pentagons and, meanwhile, a much higher pentagon-to-hexagon ratio. Consequently, the curvature of the carbon surface of small fullerenes is much higher than that of their large homologues, which results in a much severer steric strain on the small fullerene carbon surface.[5,6] Even worse, the π-conjugation within small fullerenes is more severely curved and weakened, especially at those pentagon−pentagon (PP) fusion sites. Accordingly, small fullerenes have been predicted to have narrow HOMO−LUMO gaps and high reactivity, e.g., subject to coalescence. Because of their high lability, thus far they can only be observed and experimented upon in the gas phase,[13] whereas the efforts made for bulk synthesis of them have proven to be mostly fruitless.[14] As such, most of our knowledge regarding small fullerenes comes from gas-phase experiments and theoretical investigations. Yet, it has been shown that for carbon clusters C_n generated in the gas phase the most stable structures are probably fullerenes with $n \geq 30$, whereas small carbon clusters prefer chain or ring structures.[15]

Much encouraging is the recently reported synthesis of dodecachlorofullerene[50] ($C_{50}Cl_{10}$),[16] which unambiguously provides evidence that small fullerenes can definitely be stabilized and thus synthetically approachable by functionalizing their active pentagon abutments.[17,18] Other recent exciting progresses in small fullerenes include the synthesis of covalently bonded assembly of C_{36} and its derivatives ($C_{36}H_4$, $C_{36}H_4O$, and $C_{36}H_6$),[14] the gas-phase production of endohedral metallofullerenes $M@C_{28}$ (M = U, Zr, Hf, and Ti),[19] and the gas-phase production and characterization of the smallest fullerene C_{20}[20] from its long-known derivatives ($C_{20}H_{20}$)[21] followed by bromination.

Because of their spherical shapes, fullerenes suffer large strain energy introduced by the deviation from planarity. The curvature-induced pyramidalization of the carbon atoms weakens the π-conjugation and in the meantime demands rehybridization of the atomic π-orbitals with incorporation of fractional s-character, resulting in the atomic π-orbitals of s^mp-character ($m \ll 1$).[22] The curved-π conjugations within the unsaturated carbon networks of fullerenes thus have not only π-character but also substantial s-character, remarkably different from the planar π-conjugations within graphite and planar polycyclic aromatic hydrocarbons that are solely of p_π-character. The chemical reactivity of conventional fullerenes is primarily driven by such type of curved π-conjugation.

The curved π-conjugation within the carbon surfaces of fullerenes and SWCNTs can be easily analyzed using the π-orbital axis vector (POAV) method proposed by Haddon.[22] In general, an sp^2-hybridized carbon atom prefers to form planar σ-framework with its neighbors, leaving its p_π-orbital perpendicular to the σ-bonds. In fullerenes, the sp^2-hybrized carbon atom is pyramidalized; the angle between its p_π-orbital and the σ-bonds is larger than 90°. The pyramidalization angle (θ_p) for such a nonplanar sp^2-hybrized carbon atom can be defined as the angle between its π-orbital and the σ-bonds minus 90° (Figure 2).[22] Thus an sp^3-hybridized carbon atom

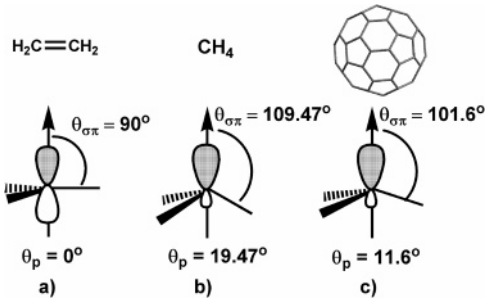

Figure 2. Pyramidalization angle ($\theta_p = (\theta_{\sigma\pi} - 90)°$) for (a) an ideally planar sp^2-hybridized carbon atom (e.g., in C_2H_4), (b) an ideally tetrahedral sp^3-hybridized carbon atom, and (c) for a nonplanar sp^2-hybridized carbon atom in C_{60}.

(ideally tetrahedral) has a 19.5° pyramidalization angle, θ_p, while a regular sp^2 carbon (as in a planar benzene) has a θ_p of 0°. All carbon atoms in the icosahedral C_{60} have the same θ_p of ~11.6°. The pyramidalization angle θ_p of a carbon atom in the curved carbon surface is a good measure of the curvature-induced local weakening of π-conjugation, which in turn results in the chemical reactivity of fullerenes. The larger pyramidalization angle is of an unsaturated carbon atom in a fullerene, the higher reactivity it is toward addition reactions.[22] For small fullerenes, their PP fusion apices always have the largest pyramidalization angles, thus are the most active sites subject to addition reactions.

While the pyramidalization angle can be used to assess the local reactivity of carbon atoms in a fullerene and to advocate the importance of steric strain effect, the global aromaticity of such spherical molecules (electronic effect) is another factor to determine their global stability. However, it is worth noting that aromaticity is only one factor to determine the overall stability of a molecule and can only be decisive when other factors are similar or unimportant; the most stable isomers do not necessarily have the largest aromaticities and vice versa.

Hirsch et al.[23] proposed the spherical aromaticity rule, i.e., $2(N+1)^2$ electron-counting rule, to explain the aromaticity of I_h symmetrical fullerenes. Follow-

ing this rule, the icosahedral C_{60} and C_{20} are neither of maximum aromaticity, whereas their charged forms, C_{60}^{10+} and C_{20}^{2+}, have much more enhanced spherical aromaticity. Such a rule can also be extended to assess the aromaticity of fullerenes with lower symmetries[24] as well as to deduce the stability of heterofullerenes and endohedral metallofullerenes, such as $C_{48}N_{12}$[25] and $Sc_2@C_{66}$.[10] As summarized below, this rule is also very useful in explaining the distinguished kinetic stability of some magic-number small fullerenes (e.g., C_{32} and C_{50})[1,5] and derivatives (e.g., $M@C_{28}$ (M = Ti, Zr, U))[19] observed in the gas-phase experiments. For an up-to-date review on the concept and applications of spherical aromaticity, please refer to the "Spherical Aromaticity" paper by Chen and King[26] in this thematic issue. However, it was argued that the $2(N+1)^2$ electron-counting rule based on the scalar surface harmonic theory is sometimes too simple to account for the unusual stability of those fullerenes (e.g., C_{60} and C_{70}) in which the spherical harmonic count breaks down around the HOMO−LUMO gap.[27] Nevertheless, the effects of local and global electron delocalization for the curved π-conjugation within a fullerenic molecule may be further characterized with the use of nucleus-independent chemical shifts (NICS)[28] at the ring and cage centers that can be readily computed with state-of-the-art quantum chemical methods. For an up-to-date review on the definition and applications of NICS, please refer to the paper by Chen et al. in this thematic issue.[29]

2.2 The Smallest Fullerene C_{20} and Its Molecular and Solid Derivatives

2.2.1 Geometric and Electronic Structures of Fullerene C_{20}

The dodecahedral fullerene C_{20} is the smallest possible fullerene consisting solely of 12 pentagons with extreme curvature. Owing to its fascinating structure, this elusive molecule has been the subject of many theoretical investigations.[30,31] However, the fullerenic cage structure of C_{20} has been computed to be less stable than the ring- and bowl-shaped structures, although the relative energies between these three types of isomers depend on the sophistication of the theoretical methods employed.[30] Some investigations even favored bicyclic rings[32] and linear chains.[33] Nevertheless, it has been shown theoretically that the dodecahedral fullerene C_{20} is of the lowest energy among all the mathematically possible 20-vertex polyhedral cages.[34]

It is also interesting to note that dodecahedral fullerene C_{20} does not adopt the perfect I_h symmetry due to Jahn−Teller distortion,[23] whereas its lowest energy form is still in dispute.[31,35] In total five possible dodecahedral structures (with C_2, C_{2h}, C_i, D_{3d} and D_{2h} symmetries, respectively) have been computed to be its lowest-energy candidates, but their relative stability depends on the theoretical methods used. Nevertheless, the recent work by Chen et al.[31] demonstrates that all these five isomers are isoenergetic (within 0.2 kcal/mol^{-1} at B3LYP/6-31G*, and within 0.5 kcal/mol^{-1} at MP2/6-31G*) and have essentially the same structural parameters at both

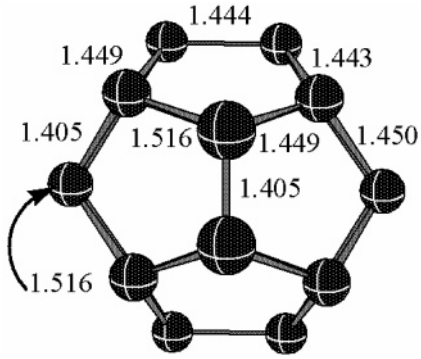

Figure 3. The B3LYP/6-31G* optimized structure of C_{20} (C_2). The arrow points to the invisible C−C bond (Reprinted with permission from ref 31. Copyright 2004, VCH).

B3LYP and MP2 levels. The B3LYP/6-31G* optimized C_2 structure is shown in Figure 3.

Hence, it is inferable that the dodecahedral C_{20} cage is highly fluxional and can readily convert from one structure to another with negligible barriers. In addition, all these structures have narrow HOMO−LUMO gaps, e.g., 1.95 eV for the C_2 isomer predicted at the B3LYP/6-31G* level.

The extreme curvature of the dodecahedral fullerene C_{20} is evidenced by the rather large pyramidalization angles ranging from 19.1 to 22.0° (calculated using the B3LYP/6-31G* optimized geometry of C_2 symmetry) at its carbon atoms, which are very close to the θ_p value of a regular sp^3-hybridized carbon (19.5°). Thus each carbon atom of the fullerene C_{20} is nearly sp^3-hybridized with one dangling bond unsaturated. Accordingly, the unsaturated C_{20} cage is highly labile and is subject to isomerization,[20] oligomerization,[36,37] or polymerization to form fullerite solid.[31,38−40] The high lability of C_{20} fullerene can be demonstrated by the high exothermicities of its hydrogenation reactions (eqs 1−3).[31] Hence, production of C_{20} fullerene in its molecular form seems to be an impossible mission.

$$C_{20} + 4\ H_2 = C_{20}H_8\ (T_h) \qquad \Delta H\ (\text{per } H_2) = -67.0\ \text{kcal/mol} \quad (1)$$

$$C_{20} + 6\ H_2 = C_{20}H_{12}\ (T_h) \qquad \Delta H\ (\text{per } H_2) = -36.5\ \text{kcal/mol} \quad (2)$$

$$C_{20} + 10\ H_2 = C_{20}H_{20}\ (I_h) \qquad \Delta H\ (\text{per } H_2) = -61.9\ \text{kcal/mol} \quad (3)$$

Although neutral C_{20} fullerene has a symmetry lower than the perfect I_h, its dication, C_{20}^{2+}, does have an I_h symmetry.[41] Density functional theory (DFT) calculations at the B3LYP/6-31G* level of theory predicted that the C−C bond lengths in C_{20}^{2+} are identical at 1.448 Å but vary from 1.405 to 1.517 Å in the neutral C_{20} (C_2 isomer), suggesting a much more pronounced degree of electron delocalization in the dication. This was confirmed by GIAO−SCF calculations.[23,24,42] The NICS values (GIAO−B3LYP/6-31G* prediction) at individual ring centers of neutral C_{20} range from 6.3 to −9.2 ppm, whereas the NICS value at each pentagon center of dication is −23.7 ppm (Figure 4). Meanwhile, the NICS value

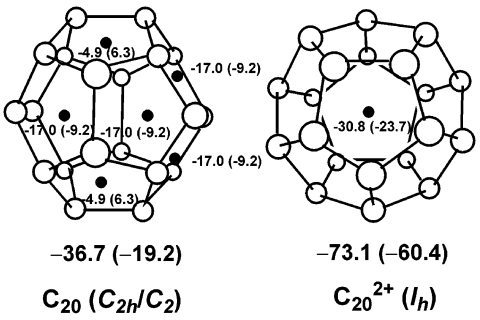

Figure 4. Nucleus-independent chemical shift (NICS) values (ppm) from GIAO-HF/6-31G* (B3LYP/6-31G* in parentheses). The NICS at the cage centers are given in bold below each structure, while those at individual ring centers are shown in the corresponding ring.

at the center of the dodecahedral cage is predicted to be −60.4 ppm for C_{20}^{2+} and −19.2 ppm for neutral C_{20} (C_2 symmetry). This indicates more uniform and higher diatroptic ring current effects in all the pentagons of the dication, which in turn results in much more diatropic shielding at the dication cage center.[24,42] This huge difference between C_{20} and C_{20}^{2+} was ascribed to the completely filled valence shell with $2(N+1)^2$ π-electrons ($N = 2$) and reflects the perfect spherical aromaticity in C_{20}^{2+}.[23,24] In accordance with the higher aromaticity of C_{20}^{2+}, its calculated ^{13}C chemical shift is uniformly 207.3 ppm, whereas the δ ^{13}C's are upfield (ranging from 165.1 to 191.8 ppm) for the neutral C_{20}.[42] Such a dicationic C_{20} cage might be synthetically approachable in ionic solid, with which the predicted δ ^{13}C's could be confirmed.

2.2.2 Synthesis and Characterization of Fullerene C_{20}

Despite its labile nature, C_{20} fullerene was successfully generated in the gas phase with a lifetime on the microsecond time scale by Prinzbach et al. in 2000.[20] The synthetic strategy employed is schematically depicted in Figure 5. The starting material is the dodecahedrane ($C_{20}H_{20}$) that can be synthesized through an optimized "isodrin-pagodane route".[21]

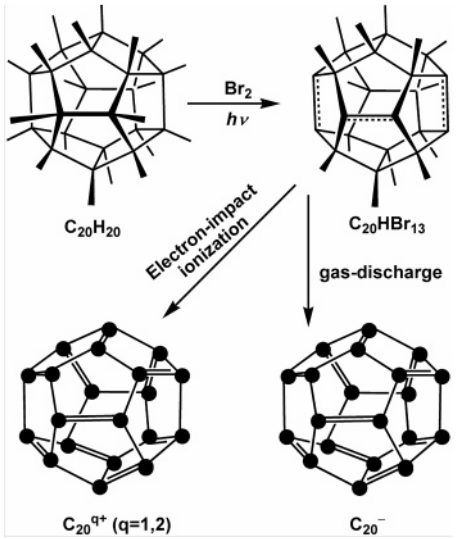

Figure 5. Strategy for the synthesis of dodecahedral C_{20} (ref 20).

Bromination of dodecahedrane was performed in solution with dry, deoxygenated bromine under visible light irradiation for 3 days. Isomeric $C_{20}H_mBr_{14-m}$ ($m = 0-3$) trienes were produced as primary products. Electron-impact mass spectroscopy of the $C_{20}H_mBr_{14-m}$ ($m = 0-3$) trienes using 70 eV electron energy for ionization gave a spectrum that unambiguously demonstrates the generation of C_{20}^+ and C_{20}^{2+} in the gas phase. The intensive C_{20}^{2+} signals observed in the mass spectrum imply its remarkable kinetic stability due to its unusually high spherical aromaticity.[24] On the other hand, upon gas discharge of the $C_{20}H_mBr_{14-m}$ ($m = 0-3$) trienes, $C_{20}Br_n^-$ ($n = 0-9$) anions were also observed in the mass spectrum, among which C_{20}^- had the largest abundance. The photoelectron spectrum of the as-generated C_{20}^- cluster revealed that neutral dodecahedral C_{20} fullerene has an electron affinity (EA) of 2.25 ± 0.03 eV and a vibrational progression of 730 ± 70 cm^{-1}, in sharp contrast to the corresponding data measured for its ring- and bowl-shaped isomers. Table 2 summarizes electron affinities and vibrational progressions of fullerene C_{20} and its ring- and bowl-shaped isomers detected by photoelectron spectroscopy (PES).[20] Density functional calculations at the BLYP/6-311G* level by Saito et al. faithfully reproduced the PES spectra of these C_{20} isomers and suggested that neutral C_{20} fullerene most probably adopts a symmetry of C_i or C_{2h}.[30p]

Table 2. Electron Affinities (EA) and Vibrational Progressions (VP) of C_{20} Isomers[a]

properties	cage	bowl	ring
EA (eV)	2.25 ± 0.03 (2.21)[b]	2.17 ± 0.03 (2.18)[b]	2.44 ± 0.03 (2.86)[b]
VP (cm^{-1})	730 ± 70	2060 ± 70	2260 ± 0.03

[a] Experimental data extracted from ref 20. [b] Data predicted at the BLYP/6-311G* level of theory are extracted from ref 30p.

2.2.3 Dimer, Oligomer, and Polymeric Solid of Fullerene C_{20}

As mentioned before, fullerene C_{20} is subject to coalescence. In their gas-phase production of fullerene C_{20}, Prinzbach et al. also found that a series of $(C_{20})_n^+$ ($n = 1-13$) oligomers were produced upon coalescence of the as-generated C_{20} fullerenes, among which C_{60}^+ shows the largest abundance.[36] Yet, it is not clear whether the thus-produced C_{60}^+ cluster adopts the well-known buckminsterfullerene structure[1] or other structures that are formed by simple additions of C_{20} cages.[31,37]

Recently, the crystallized solid of C_{20} fullerene was claimed to be prepared in the ultrahigh molecular weight polyethylene samples during Ar^+ ion beam irradiation; preliminary electron diffraction experiments suggested a hexagonal crystal structure for the as-prepared C_{20} solid.[38] More recently, Iqbal et al.[40a] reported the preparation of a C_{20}-based solid phase in thin diamond-like carbon films deposited by ultraviolet laser ablation from diamond onto nickel substrates at room temperature in the presence of 10^{-4} Torr of cyclohexane or benzene. Desorption of

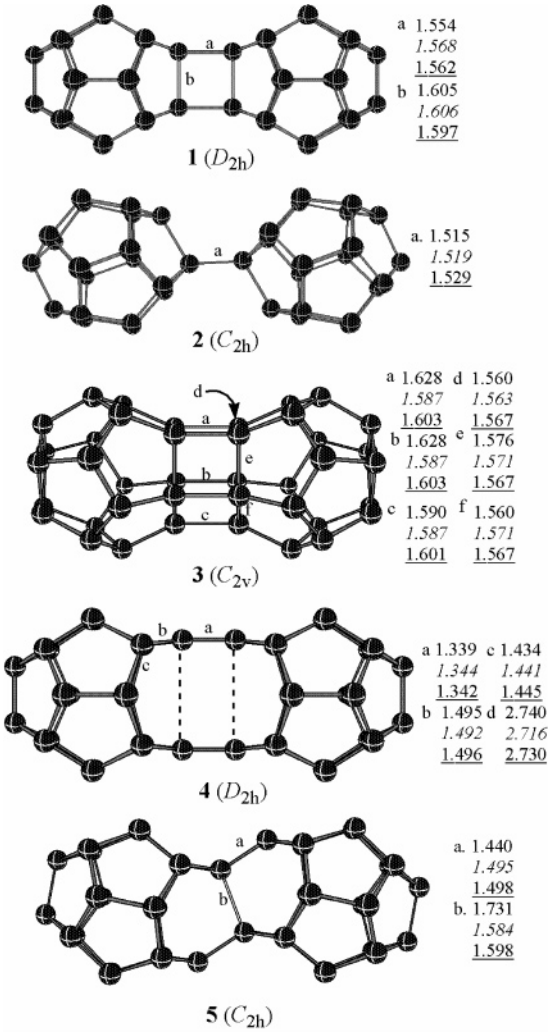

Figure 6. The B3LYP/6-31G* optimized structures of $(C_{20})_2$ and its dianion (normal for singlet, italic for triplet, underlined for dianion). Reprinted with permission from ref 31. Copyright 2004, VCH.

C_{20}, C_{21}, and C_{22} species from their C_{20}-based solid was detected by laser desorption mass spectrometry. Micro-Raman spectroscopy and electron diffraction from selected particles together with first principle density-functional calculations indicated a cubic solid with dodecahedral C_{20} cages as building blocks. However, in their proposed structure, the dodecahedral C_{20} cages were linked with bridging carbon atoms at interstitial tetrahedral sites to form a face-centered-cubic lattice with 22 carbon atoms per unit cell.[40a]

Several theoretical investigations have been reported on the geometric and electronic structures of oligomers, polymers, and solids formed from C_{20} cages.[31,37,39,40] Choi et al.[37] conducted a systematic theoretical investigation on the dimerization of fullerene C_{20}. Eight dimers, corresponding to the [2+2], open-[2+2], [1+1], [5+2], di-[5+5], tri-[5+5], tetra-[5+5], and tetra-[4+4] addition patterns, were studied in their HF/6-31G* and B3LYP/6-31G* calculations; all these dimerization patterns were predicted to be thermodynamically favorable with substantial exothermicity ranging from 24 kcal/mol (for the tetra-[4+4] addition) to 145 kcal/mol (for the open-[2+2] addition) at the B3LYP/6-31G* level of theory. A stepwise mechanism with no net activation barriers was elucidated for the formation of the most favorable open-[2+2] dimer from C_{20} cage monomers. The first step is the barrierless formation of the metastable [1+1] isomer, followed by the smooth formation of the [2+2]-cycloaddition product. Such facile [2+2] cycloaddition of fullerene C_{20} demonstrates its high reactivity. The [2+2] isomer can undergo further isomerization to form the energetically more favorable open-[2+2] isomer. Similar dimerization patterns have been found by Chen et al. in a subsequent theoretical study.[31] Figure 6 depicts five isomers of $(C_{20})_2$ predicted at the B3LYP/6-31G* level by Chen et al.,[31] among which the open-[2+2] isomer is the most favorable.

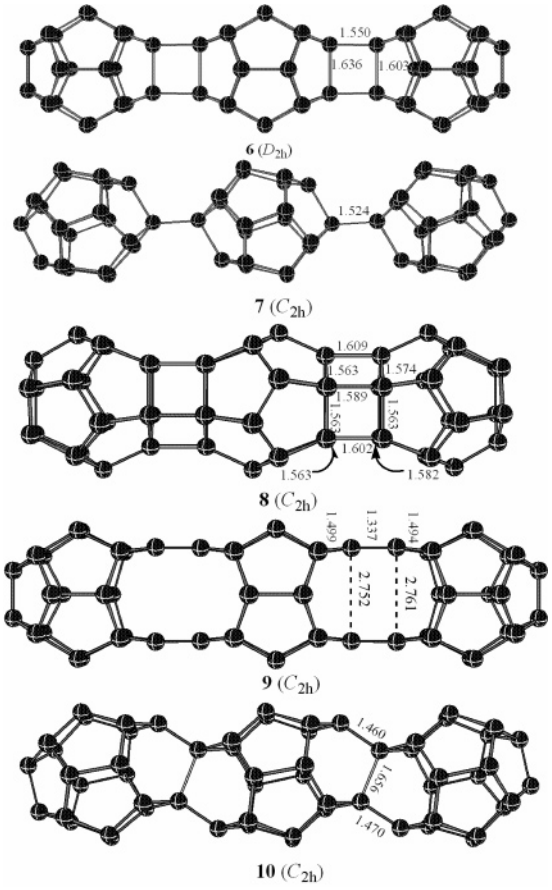

Figure 7. The B3LYP/6-31G* optimized structure of $(C_{20})_3$. Reprinted with permission from ref 31. Copyright 2004, VCH.

Besides dimers of C_{20} cage, the structures of trimers, tetramers, and one-dimensional infinite chains of C_{20} have been computed by Chen et al.[31] The optimized structures of these oligomers and infinite chains are depicted in Figures 7−9, respectively. The most stable forms of these oligomeric and 1-D polymeric structures are exclusively derived from open-[2+2] additions of C_{20} monomers. In light of these oligomeric and 1-D polymeric structures, six three-dimensional solid structures were designed and computed with the density functional tight-binding (DFTB) method. The content of tetracoordinated carbons in these *bcc*-structured solids derived from C_{20} cages ranges within 0−80%. The thermodynami-

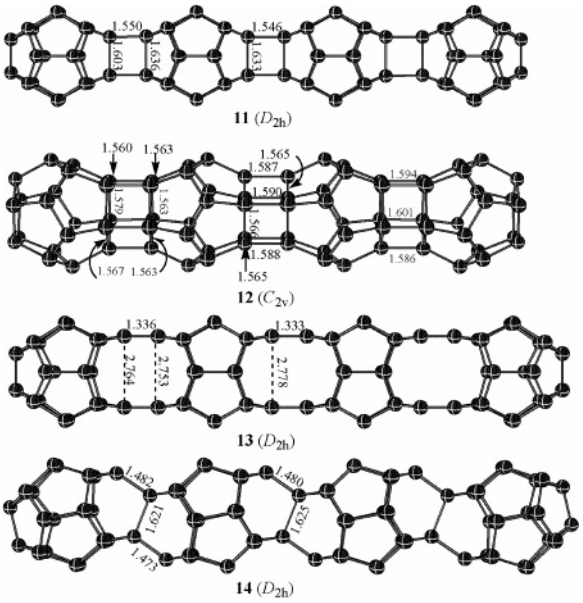

Figure 8. The B3LYP6-31G* optimized structure of $(C_{20})_4$. Reprinted with permission from ref 31. Copyright 2004, VCH.

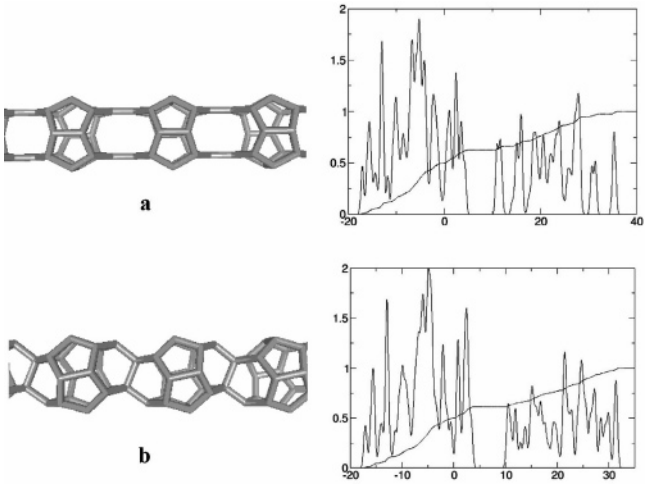

Figure 9. The DFTB-optimized structures and DOS of infinite chains of C_{20}: (a) an open [2+2] chain and (b) a twisted chain. Reprinted with permission from ref 31, Copyright 2004, VCH.

cally most favorable solid structure (Figure 10) was found to have moderate content (50%) of tetracoordinated carbons, i.e., 10 carbon atoms within a C_{20} monomer have been involved to form intercage C−C bonds in the according solid. Such a C_{20} solid was predicted to have a binding energy of 8.7 eV/atom and a band gap of ~2 eV, thus being a semiconductor. Earlier DFT calculations[39a] by Miyamoto and Saito found that a simple-cubic-like solid phase of C_{20} shows metallic properties, but it is much less stable than that proposed by Chen at al.[31] Another interesting finding by Miyamoto et al.[39a] is that a metastable 1-D chain phase could be a semiconductor with high density of states near the Fermi level, suggesting that the 1-D polymer of C_{20} could become a superconductor upon carrier doping.

Most recently, a new allotropic form of carbon $[C_{28}]_n$ based on fullerene C_{20} and cubic cluster C_8 was proposed. This hypothetic solid has a simple cubic

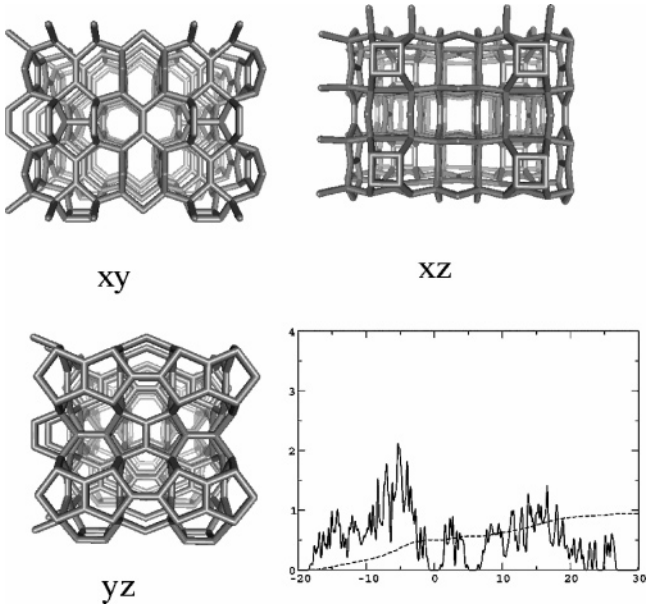

Figure 10. The DFTB optimized structure and DOS of the most stable three-dimensional C_{20} solid. Reprinted with permission from ref 31. Copyright 2004, VCH.

lattice, in which the C_{20} cages are located at the vertices of a cube, and was computed to be dielectric with an energy gap of 3.3 eV.[43]

2.2.4 Perhydrogenated Derivative of Fullerene C_{20}: Dodecahedrane $C_{20}H_{20}$

The dodecahedrane $C_{20}H_{20}$, the chemical transliteration of the platonic dodecahedron,[44] once had been widely and actively sought in organic synthesis.[45−47] The motivation was 2-fold, i.e., the aesthetic appeal to approach the translation of platonic dodecahedron into real molecules and the synthetic challenge that "requires the bonding together properly of twenty methine units".[45b] Early attempts to synthesize this molecule had been unsuccessful until 1982. The first successful synthesis of dodecahedrane was realized by Paquette et al. in 1982.[46a,b] In their industrious synthetic work, the authors eventually prepared anion dodecahedrane along with its monosubstituted derivative in 23 steps from cyclopentadienide. Subsequently, Prinzbach et al. developed an optimized "isodrin-pagodane-dodecahedrane" route,[21,47] with which the production of dodecahedrane became much more efficient. We do not discuss their synthetic strategies in detail here; for more information on this topic, please refer to refs 21 and 46.

The expected high symmetry of dodecahedrane was fully manifested by the measured infrared (IR), Raman, ^{1}H and ^{13}C NMR spectra.[46b] Only three IR-active frequencies appeared aptly at 2945, 1298, and 728 cm^{-1}, whereas eight Raman-active bands were observed at 2954, 2938, 1124, 1164, 1092, 840, 676, and 480 cm^{-1}. In its ^{1}H and ^{13}C NMR spectra measured in $CDCl_3$ solution, only singlets were observed at δ 3.38 (^{1}H) and δ 66.93 (^{13}C) ppm, respectively.

The estimated heat of formation from experiments is about 18.2 ± 1 kcal/mol for dodecahedrane.[48] Because of its high symmetry, all the CH bonds in dodecahedrane are eclipsed, giving rise to substantial

strain energy. Indeed, a strain energy of 61.4 ± 1 kcal/mol was estimated by Prinzbach et al.[48]

Except the tremendous efforts of the experimentalists to achieve the synthesis and to explore the properties of this fascinating molecule, dodecahedrane has been studied intensively at various theoretical levels with regard to the energy (e.g., heat of formation and strain energy),[49,50] vibrational frequencies,[51] NMR chemical shifts,[42] and coupling constants[50a] for ^{13}C and ^{1}H nuclei, inelastic neutron-scattering spectrum,[52] substituent effects,[21a] and charge density.[53] The GIAO-B3LYP/6-31G* calculations[42] gave a fairly good prediction with regard to the ^{1}H and ^{13}C NMR chemical shifts [δ 3.4 (^{1}H) and δ 73.1 (^{13}C) ppm] of dodecahedrane. The RMP2/6-31G* calculations[50f] reproduced the experimental enthalpy of formation (17.4−18.9 kcal/mol by theory vs 18.2 kcal/mol by experiment), whereas the MM2 method did quite well with the strain energy (65.4 kcal/mol by MM2 vs 61.4 by experiment).[49c]

Note that the synthesis of dodecahedranes was achieved three years before finding the first fullerene, the buckminsterfullerene C_{60}.[1] Unfortunately, despite its close relation to the smallest fullerene C_{20}, dodecahedrane has long been neglected as, frankly speaking, the first fullerene derivative made by mankind. More significantly, this compound is also the first fullerene derivative that can be prepared by means of rational organic chemistry. Note that except for dodecahedrane, only the rational chemical synthesis of the buckminsterfullerene C_{60} has been reported.[54]

2.2.5 Other Exohedral Derivatives of Fullerene C_{20}

Following the successful synthesis of dodecahedrane $C_{20}H_{20}$, a large number of exohedral derivatives of fullerene C_{20} have been synthesized with dodecahedrane as starting point. For example, under "brutal" conditions all of the hydrogen atoms in dodecahedrane could be replaced, giving rise to perhalogenated derivatives of C_{20}, e.g., $C_{20}Br_{20}$, and polyhalogenated dodecahedrenes, e.g., $C_{20}Cl_{16}$ and $C_{20}H_{0-3}Br_{14-11}$.[21] As mentioned previously, these halogenated derivatives of C_{20} could work as precursors for the gas-phase generation of fullerene C_{20}.[20] Ever since its creation, rich chemistry centering at dodecahedrane has been disclosed and was recently reviewed by Parquette[46d] and Prinzbach et al.[21b,47a−c] In this subsection, we summarize only the chemistry of polyunsaturated dodecahedranes that is closely related to the theme of the current review.

Among various exohedral derivatives of C_{20}, of particular interest are the polyunsaturated dodecahedranes $C_{20}R_n$ (n = 18, 16, 14, 12, 10; R = H or other substituents) that have one to five highly bent unsaturated C=C bonds (Chart 1).[21b] Note that pyramidalization of an unsaturated C=C bond reduces remarkably its energy gap between the π (bonding) and π^* (antibonding) molecular orbitals, leading to "diradical" character and, of course, much higher reactivity.[55] Hence, due to the presence of highly pyramidalized C=C bonds, polyunsaturated dodecahedranes can undergo thermally activated [$\pi_2 + \pi_2$] cycloadditions,[21b] which are generally symmetry-forbidden for simple alkenes with a planar C=C bond.[56] Selective [2+2] dimerization or even trimerization of polyunsaturated dodecahedranes (Chart 2) were found experimentally upon heating,

Chart 1

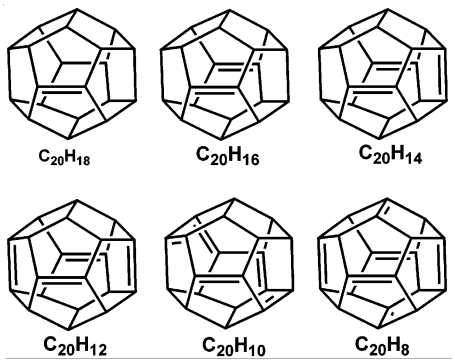

Chart 2

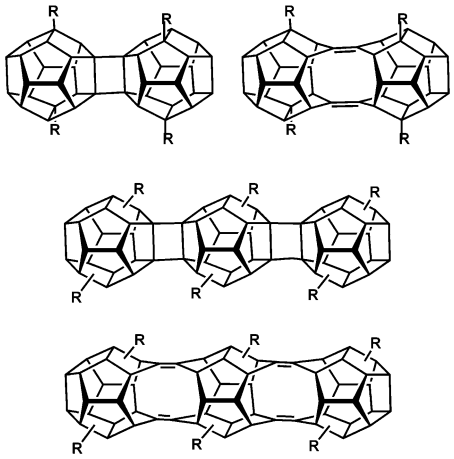

for example, dodecahedrene diester (exclusion of O_2) to about 300 °C.[21b] Indirect evidence for the formation of higher oligomers from polyunsaturated dodecahedranes is also available.[57] A laser desorption time-of-flight mass spectroscopic study disclosed that C_{40} "dimers" to C_{100} "pentamers" were formed from the 1,6-dibromododecahedrane after desorption with a 248-nm excimer laser. Dodecahedrenes and dodecahedradienes were suspected to be key intermediates in the formation of these oligomers. Upon release of all hydrogen atoms at higher ion velocities, these oligomers could even rearrange to pure fullerenes, preferably C_{60}.

In addition to the unexpected [2+2] cycloadditions, unsaturated dodecahedranes, as a dienophile, readily undergo normal [4+2] cycloadditions (Diels−Alder reaction), for example, with 1,3-butadiene and furan even at room temperature (Chart 3).[58]

Chart 3

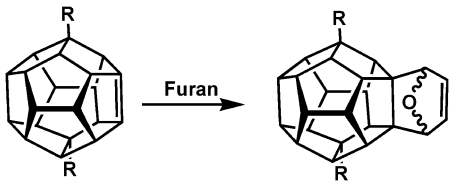

Polyunsaturated dodecahedranes have much shorter inner-shell diameters than the fully saturated one. For instance, the shortest transannular $\pi-\pi$ distance in the 1,16-dodecahedrodiene is about ~3.5 Å,[59] by 1.0 Å shorter than that of dodecahedrane. It is thus possible for polyunsaturated dodecahedranes to have through-space homoconjugation.[60] However, ab initio calculations (HF/3-21G)[59b] predicted insignificant transannular $\pi-\pi$ interaction either in the 1,16-dodecahedradiene or in its cations (Chart 4). The

Chart 4

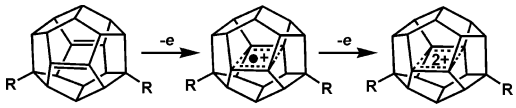

transannular $\pi-\pi$ distance in this cage-shaped diene decreases with increasing its oxidation number but is longer than 3.2 Å even in the dication. The dication, although having two π-electrons and fulfilling the Hückel ($4n + 2$) rule of aromaticity, is more like a bis(radical cation). Obviously, its high structural rigidity hinders the through-space homoconjugation.[59] The theoretical prediction was confirmed experimentally by subsequent ESR, PE, and CV studies.[61]

In contrast to the insignificant through-space π-electron delocalization in 1,16-dodecahedradiene and its cations, remarkable in-plane cyclic π-electron delocalization was found in the [10]trannulene subunit of dodecahedrapentaene $C_{20}H_{10}$ (Chart 5) by means

Chart 5

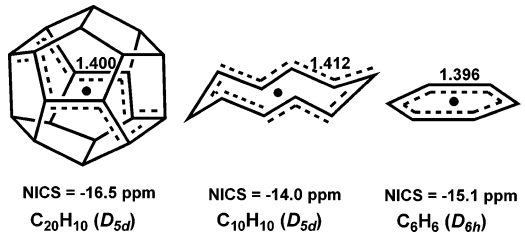

of MNDO-CI calculations.[62a] Such a "in-plane" delocalization due to the overlap of adjacent p_π-orbitals results in unusual "in-plane aromaticity" when fulfilling the Hückel ($4n+2$) rule of aromaticity.[63] The in-plane aromaticity in dodecahedrapentaene was further confirmed by CSGT-B3LYP/6-31G* calculations.[62b] The molecule was predicted to be in D_{5d} symmetry with all the central C−C bonds in the same length of 1.400 Å; the NICS value of −16.5 ppm at the cage center is comparable with NICS −15.2 ppm for benzene and NICS −14.0 ppm for the parent [10]-trannulene $C_{10}H_{10}$ calculated at the same theoretical level. Evidently, the in-plane delocalization gives rise to a pronounced degree of diatropic ring current effect within the [10]trannulene subunit of dodecahedrapentaene.[62]

2.2.6 Dodecahedral Heterofullerenes

While the highly strained fullerene C_{20} was manifested to be unstable with a microsecond-scale lifetime observed in the gas phase,[20] the search for its stable analogues, namely, heterofullerene[20], becomes appealing. In 1992, Castleman et al. discovered the first metallocarbohedrene (Met-Car) Ti_8C_{12}.[64] Subsequently, a series of Met-Cars have been also discovered with the stoichiometry M_8C_{12} (M = V, Zr, Hf, Cr, Nb, Fe, Mo) or Ti8-xM$_x$C$_{12}$ (M = Zr, Hf, Y, W, Nb, Mo, and Si),[65] forming an important new class of molecular clusters. Being one of the highlights in nanoscience, Met-Cars have attracted much attention from both experimentalists and theoreticians to explore their properties.[66] Interestingly, the Ti_8C_{12} cluster was originally proposed to have a T_h symmetry dodecahedron structure, in which each face of a Ti_8 cube was capped by a C=C group (Chart 6).[64]

Chart 6

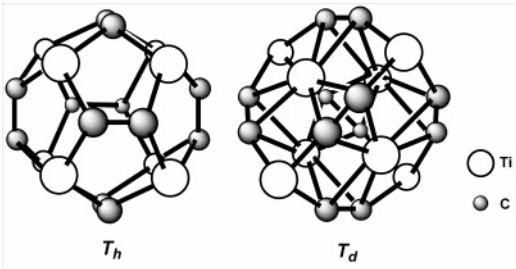

However, first-principle calculations overthrew such a heterofullerene model and revealed that it can be readily transformed into a much more stable structure with a T_d symmetry (Chart 6).[67] The latter was confirmed to be more realistic by a critical comparison of the measured ionization potentials[68] and vibrational frequencies[69] for Ti_8C_{12} with the theoretical predictions. In the T_d symmetry structure of M_8C_{12}, an inner $(Ti^i)_4$ tetrahedron was capped by an outer $(Ti^o)_4$ tetrahedron, with the six C=C groups aligned along the Ti^o-Ti^o edges of the outer $(Ti^o)_4$ tetrahedron. So the M_8C_{12} Met-Cars could not be a heterofullerene analogue of dodecahedral C_{20} at all.

While the M_8C_{12} Met-Cars cannot be regarded as heterofullerenes, the T_h symmetry P_8C_{12} [more exactly $P_8(C{=}C)_6$] cluster was recently predicted to be a stable, dodecahedral heterofullerene (Figure 11).[70]

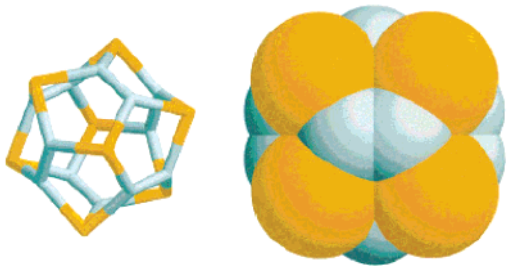

Figure 11. Skeletal and space filling models of P_8C_{12} (the latter is oriented perpendicular to one cubic face) (extracted from ref 70).

In their density functional study using the B3LYP/6-311G* method, Alder et al.[70] investigated the relative strain energies for a series of T_h symmetry X_8C_{12} (X = P, N, CH) molecules by computing the energy of isodesmic reaction, $X_8C_{12}H_{12} + C_{20}H_{12} \rightarrow X_8C_{12} + C_{20}H_{20}$. The reaction was predicted to be highly exothermic (by 86.7 kcal/mol) for X = P but highly endothermic (by 148.1 kcal/mol) for X = N. Thus, the strain energy of the P_8C_{12} heterofullerene

is far smaller than that of the T_h symmetry dodecahedratetraene. In accordance with its reduced strain energy, the optimized geometry of the T_h-P_8C_{12} appears to be nearly cubic with its alkenic >C=C< groups being less pyramidal than those in C_{60}. The alkene pyramidalization angle, φ,[55,71] was calculated to be 30.0° for T_h-P_8C_{12}, 31.7° for C_{60}, much smaller than that in the known dodecahedrene (43.7°).[47e] In addition, T_h-P_8C_{12} has 28 π-electrons distributed spherically and was predicted to be mildly aromatic with an NICS value of −15 ppm at its cage center. On the contrary, the isoelectronic (valence shell only) T_h-N_8C_{12}[72] was found to be nonaromatic due to the lack of effective vinylic delocalization between the nitrogen lone pair and the adjacent double bonds. Containing uniformly distributed P atoms, this minimally strained heterofullerene[20] was envisioned to be an interesting ligand for metals in the synthesis of novel inorganic−organic hybrid materials.

Similar to T_h-P_8C_{12}, heterofullerene $C_{12}Si_8$ was also calculated to adopt a T_h-dodecahedral structure, whereas $C_{12}Ge_8$ and $C_{12}Sn_8$ prefer quite different D_{2h} and D_2 structures, respectively.[73] But the kinetic stability of T_h-$C_{12}Si_8$ should be much lower than that of T_h-P_8C_{12} because of the following two factors: (i) T_h-P_8C_{12} is aromatic, but T_h-$C_{12}Si_8$ is not; (ii) the Si atoms in T_h-$C_{12}Si_8$ do not provide the same strain relief as the P atoms in T_h-P_8C_{12}.[70]

Very recently, the substitution patterns of mono-BN-substituted fullerene[20] were[74] explored by means of semiempirical MNDO and DFT computations. The structures with adjacent B and N atoms were preferred. BN-substituted heterofullerenes were predicted to have larger HOMO−LUMO gap, higher IP and EA values than the pristine dodecahedral C_{20}, implying enhanced kinetic stability upon BN-substitution.

2.2.7 Endohedral Derivatives of $C_{20}H_{20}$ and C_{20}

Dodecahedrane $C_{20}H_{20}$ has an inner void of ~ 4.5 Å in diameter, thus capable of encapsulating various guest atoms and ions. Indeed, the "inside chemistry" of $C_{20}H_{20}$ was already a popular area of research[50a,b,75] far prior to the emergence of the endohedral chemistry of fullerenes.[76] For example, early quantum chemical calculations[50a,b,75] using various semiempirical methods and ab initio HF/STO-3G methods showed that the inclusion of small ions (H^+, Li^+, Be^{2+}, Mg^{2+}) is favorable with no energy cost, whereas the accommodation of an electron or atoms such as He and Li is energy-costing. Using an ab initio MP2(FC)/6-311G** method, the binding energies and equilibration constants for the formation of He- and Ne-encapsulated $C_{20}H_{20}$ were computed by Jiménez-Vázquez et al.[77] The predicted inclusion energies are 33.8 kcal/mol for He and 98.3 kcal/mol for Ne. The equilibrium constant for He@ $C_{20}H_{20}$ was calculated, and the pressure corresponding to the experimentally synthesized compound is 4×10^{26} atm.[77] Thereafter, more systematic and sophisticated theoretical studies have been done by Schleyer and co-workers[78] with regard to the structures and stabilities of a number of endohedral dodecahedrane complexes X@$C_{20}H_{20}$ (X = $H^{0/+}$, He, Ne, Ar, $Li^{0/+}$, $Be^{0/+/2+}$, $Na^{0/+}$, $Mg^{0/+/2+}$, N, P, C^-, Si^-, O^+, S^+). Interestingly, they found that H^+ does not bind endohedrally but escapes from the cavity to bridge a C−C bond exohedrally.[78b] Among these endohedral minifullerenes, of particular interest is the H@$C_{20}D_{20}$ that has been proposed for use as single quantum bits (qubits) in solid-state quantum computers.[79] Similar use has been proposed of large endohedral fullerenes whose dopants atoms retain their isolated atomic states.[80]

Despite the intensive efforts made by theoreticians, experimental investigation on the endohedral dodecahedrane complexes is scarce. So far only He@$C_{20}H_{20}$ has been successfully obtained with a low yield (~0.01%)[81] by using an experimental procedure developed for large fullerenes.[82]

2.3 C_{28} Fullerene and Its Molecular and Solid Derivatives

2.3.1 Geometric and Electronic Structures of Fullerene C_{28}

Thanks to the amazing finding of endofullereneic M@C_{28}^+ (M = U, Hf, Zr) clusters by Guo et al. in 1992,[19] C_{28} fullerene has been one of the most intensively investigated small fullerenes.[19,42,83,74] This carbon cluster, together with its two smaller neighbors C_n (n = 24 and 26), is located at the crossover from ring- or bowl-shaped carbon clusters (C_{10}−C_{20}) to fullerenic ones (C_n, $n \geq 30$).[12,84] Under suitable conditions, its cationic species, C_{28}^+, can be produced even with an abundance nearly as great as that of C_{60} in the laser vaporization of graphite.[19]

As disclosed by spin-polarized HF and DFT calculations,[19,83] C_{28} has a ground-state fullerenic structure of T_d symmetry (Figure 12a). This small fullerene

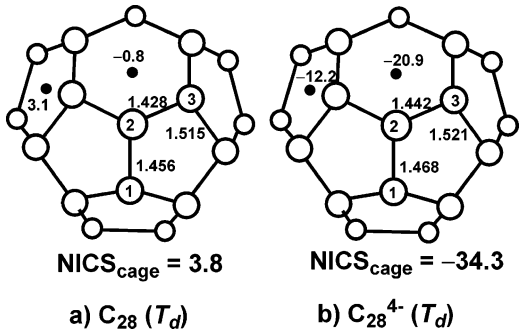

Figure 12. Structures of (a) neutral and (b) tetraanion of C_{28} (T_d) fullerene. B3LYP/6-31G* bond lengths (Å) and NICS values (ppm) from GIAO−B3LYP/6-31G* are also given. Reprinted with permission from ref 42. Copyright 2001, Springer.

contains four separated six-membered rings connected by four carbon atoms at each vertex of a tetrahedron. In its open-shell $^5A_2$ ground state, there are four singly occupied frontier orbitals, i.e., the $14t_2$ and $8a_1$ orbitals. Hence, fullerene C_{28} is highly reactive, with four dangling bonds localized on the triplet-pentagon-fusion apecies (i.e., the C1 atoms in Figure 12a), and works as a "superatom" of tetrahedral valence subject to formation of molecular derivatives, e.g., endohedral[19,83b,85] and exohedral derivatives,[19,83b,85a,c,86] and solid assembly.[87] However, Paulus[30x] found that the $^3T_1$ state is 0.11 eV lower in energy than the quintet $^5A_2$ state when electron

correlation is included in the coupled cluster level, which shows the great influence of correlations especially for open shell systems.

C_{28} fullerene has in total 28 π-electrons delocalized around its carbon surface; its curved π-conjugation does not obey the spherical aromaticity rule at all.[23,24] The most stable electronic configuration is an open-shell quintet with T_d symmetry and is nonaromatic either globally or locally. This nonaromatic character was confirmed by recent GIAO-B3LYP/6-31G* calculations; the computed NICS values at the cage center and each individual ring centers (cf. Figure 12a) are so small (3.8 ppm at the cage center, 3.1 ppm at the pentagon center and −0.8 ppm at the hexagon center) which reflects the very weak ring current effects.[42] Once its valence shell is completely filled upon reduction, the resulting C_{28}^{4-} anion (Figure 12b) is highly aromatic both globally and locally because its curved 32-electron π-conjugation follows the $2(N+1)^2$ rule for spherical aromaticity.[23,24] The highly negative NICS values at the cage center and ring centers (ranging from −12.2 at pentagon center to −30.3 ppm for the cage center) computed by Chen et al. clearly indicated the very strong diatropic ring current effects around each individual rings and the whole carbon surface in the C_{28}^{4-} anion (Figure 12b).[42] Accompanying the reduction-enhanced aromaticity of the C_{28}^{4-} anion might be a drastic increase in its kinetic stability. That is why C_{28} is preferentially tetravalent and prefers to encapsulate a Group-IV metal atom (e.g., Zr and Hf) inside to form endohedral metallofullerenes M@C_{28}.[19]

2.3.2 Endohedral Fullerenes of C_{28}

The first endohedral metallofullerene of C_{28}, U@C_{28}, was produced in the cationic form by laser vaporization of a mixture of UO_2/graphite in a cluster FT-ICR apparatus.[19] Further experiments on other MO_2/graphite composites (M = Zr, Hf, and Ti) led to the finding of the corresponding endohedral metallofullerenes M@C_{28}^+.[19] XPS spectroscopic investigation on the as-prepared U@C_{28}-containing thin solid film indicates a formal 4+ valence state for the encapsulated uranium atom as well as substantial covalent bonding between the encapsulated metal atom and the C_{28} cage. Hence, these metallofullerenes can be better described as M^{4+}@C_{28}^{4-}.[19] Following this experimental study, Guo et al. performed a systematic theoretical investigation on the electronic structures of a series of endohedral fullerenes M@C_{28} (M = Mg, Al, Si, S, Ca, Sc, Ti, Ge, Zr, and Sn).[83b] Their SCF−HF calculations showed that only two endohedral compounds, Zr@C_{28} and Sc@C_{28}, have a large binding energy (2.8 and 1.5 eV, respectively), whereas formation of the rest of the compounds is thermodynamically unfavorable. In accordance with such a theoretical prediction, La@C_{28}, which is valence isoelectronic with the Sc@C_{28}, was observable in the laser vaporization experiments.[88]

A series of endohedral compounds that encapsulate tetravalent atoms such as Zr, Ti, C, Si, Ge, and Sn[85a,b] were explored by means of density functional calculations, which predict that the inclusion of Zr, Ti, Si, or Ge in the C_{28} cage is thermodynamically favorable. Other endohedral fullerenes containing a nonmetal atom such as B@C_{28}, N@C_{28}, and O@C_{28} has been considered theoretically, but the possibility of forming these compounds could be very low.[85c,d]

In addition to the aforementioned endohedral fullerenes, the possibility of simultaneous bonding from the inside and outside of the C_{28} cage, as in a hybrid compound Ti@$C_{28}H_4$, has also been considered theoretically by Dunlap et al.[85e] and Guo et al.[83b] In Ti@$C_{28}H_4$, the encapsulated Ti remains in its neutral atomic state, differing significantly from that of Ti@C_{28}.

2.3.3 Exohedral Fullerenes of C_{28}

Because of the four dangling bonds at the tetrahedron apices, T_d C_{28}'s exohedral compounds, $C_{28}X_4$ (X = H, F, Cl, Br, I), have been sought theoretically.[83b,85a,c,86] The attachment of four monovalent atoms to the active C1 sites of the C_{28} cage (see Figure 12a for definition) greatly enhances its kinetic stability due to saturation of the dangling bonds. For example, a moderate HOMO−LUMO gap (~2.5 eV) of $C_{28}H_4$ (T_d) was predicted by LDA calculations.[85a] In these exohedral derivatives ($C_{28}X_4$), the four separated benzene-like rings are aromatic.[42] Exohedral adduct of C_{28} (T_d) was predicted to the best isomer of $C_{28}Si$, in which the Si is attached to the pentagon junctions (atom type 3, see Figure 12).[89]

2.3.4 Heterofullerenes of C_{28}

Besides endohedral encapsulation and exohedral functionalization, another way to stabilize the highly reactive C_{28} cage is to substitute some of the cage carbon atoms by heteroatoms.[42,90] Indeed, the T_d symmetrical heterofullerene $C_{24}N_4$ (Figure 13a), which

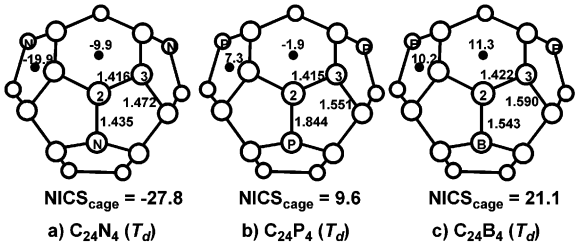

Figure 13. Structures of heterofullerenes: (a) $C_{24}N_4$, (b) $C_{24}P_4$, and (c) $C_{24}B_4$. B3LYP/6-31G* bond lengths (Å) and NICS values (ppm) from GIAO-B3LYP/6-31G* are also given. Reprinted with permission from ref 42. Copyright 2001, Springer.

is isoelectronic with the highly aromatic C_{28}^{4-} anion, was proven to have rather high local and global aromaticity.[42] A highly negative NICS value (−27.8 ppm) at the cage center of $C_{24}N_4$ was predicted by GIAO-B3LYP/6-31G* calculations,[42] indicating the overall spherical aromaticity of this heterofullerene and, meanwhile, suggesting a high delocalization of the electrons rather than isolated electron lone pairs at the nitrogen atoms. On the contrary, the valence isoelectronic $C_{24}P_4$ (Figure 13b) was found to be nonaromatic with a positive NICS value (9.6 ppm) at the cage center because of localization of the phosphorus lone pairs. For the boron-substituted heterofullerene, $C_{24}B_4$ (Figure 13c), which has a total

of 24 π-electrons, spherical antiaromaticity was expected on account of the incomplete filling of the valence orbitals in T_d symmetry. Indeed, the highly positive NICS value (21.1 ppm) at its cage center computed by GIAO-B3LYP/6-31G* calculations implies remarkable paratropic ring current effects. Among the three heterofullerenes, the N-substituted one, $C_{24}N_4$, might be synthetically viable owing to its high aromaticity.

2.3.5 Solid of C_{28}: Hyperdiamond

Because of the presence of four dangling bonds located at its tetrahedron apices, the tetravalent T_d symmetrical C_{28} fullerene is undoubtedly isolobal with an sp^3-hybridized carbon atom. Therefore, an arrangement of the superatomic C_{28} unit in a diamond lattice should give rise to a new crystalline form of pure carbon (Figure 14), which was called

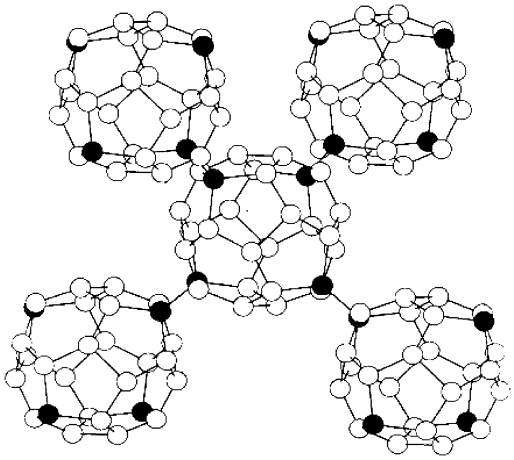

Figure 14. Structure of the hyperdiamond lattice. The C_{28} clusters are connected together at the black atoms. Reprinted with permission from ref 87b (http://link.aps.org/abstract/PRB/v49/p8446). Copyright 1994, APS.

"hyperdiamond." Properties of the hyperdiamond from first-principle density functional calculations[87] are summarized as follows:

(i) The hyperdiamond carbon is a high-energy material. Its cohesive energy was estimated to be 0.6772 eV/atom (or 5.43 kJ/g) lower than that of diamond.[87a] The energy release upon hyperdiamond-to-diamond conversion would be as much as that of trinitrotoluene (TNT).

(ii) The hyperdiamond carbon is a wide-gap semiconductor. Its band gap was predicted to be ~1.6 eV by LDA computations but was empirically scaled up to ~3.0 eV. [87b]

However, the presence of local defects in the hyperdiamond would be unavoidable since a perfect orientation of all C_{28} units in the solid would be hardly approached due to the size of the C_{28} unit.[87b] Accordingly, a C_{28} solid experimentally attainable would probably be amorphous and porous with a large pore size and may find its various applications such as gas-storage, support of catalysts, etc.

2.4 C_{36} and Its Molecular and Solid Derivatives

2.4.1 Synthesis of C_{36} and Its Derivatives

C_{36} was one of the magic-number small fullerenes detected by mass spectroscopy in the very early days of fullerene science.[5,91] After that, few experiments have been done on C_{36} exclusively in the gas phase[92] until 1998 when Zettl's group[14a] claimed the first preparation of C_{36} in the solid form by the arc-discharge method.[93] Together with C_{60} and C_{70}, C_{36} was found with a remarkable percentage in the soot that was produced by repeated arc-discharge runs in 400 Torr helium. The C_{36} solid was found to be soluble in pyridine and carbon disulfide (CS_2) under ultrasonic heating. ^{13}C NMR spectrum of the purified "C_{36} solid powder" showed two prominent peaks at 146.1 and 137.5 ppm. On the basis of this spectrum, the synthesized solid was assigned to be aggregation of molecular C_{36} fullerene in a D_{6h} symmetry, for which density functional calculations predicted a ^{13}C NMR spectrum with one peak at 135 ppm and two peaks around 158 ppm. However, the electron-diffraction pattern of their C_{36}-based solid suggested an intercage distance shorter than 1.7 Å, strongly implying the presence of covalent intercage bonding. Indeed, subsequent theoretical investigations revealed that molecular C_{36} should be unstable and prone to polymerize.[17,94] Further scanning tunneling spectroscopic study of the "C_{36} solid" indicated an 0.8 eV electronic gap, a phenomenon that was better reproduced by density functional calculations on the covalent dimeric and trimeric assemblies of C_{36}.[95] Hence, the nature of the "C_{36}-based solid" is in controversy, since sp^3 hybridized carbon signals were not found in the ^{13}C NMR spectrum.[14a] Moreover, various attempts to reproduce the production of C_{36} by arc-discharge failed.[14c] Stimulated by Zettl's work, Shinohara et al. prepared several derivatives of C_{36}, e.g., $C_{36}H_4$, $C_{36}H_4O$, and $C_{36}H_6$.[14c,d] Their structural characterization is unfortunately not available to date. Very recently, individual C_{36} fullerenes, in addition to C_{60} and C_{70}, were observed in flame-generated soots using high-resolution transmission electron microscopy.[96] Nevertheless, the limited and controversial experimental findings on the synthesis of C_{36} and its derivatives have invoked intensive theoretical investigations, the results of which will be summarized and compared with the limited available experimental information in the following subsections.

2.4.2 Geometric and Electronic Structures of C_{36}

C_{36} has 15 conventional fullerene isomers;[6] among them, the D_{6h} and D_{2d} isomers (Chart 7) have a minimal number of adjacent pentagons and, hence, are candidates for the most stable structure.[6] Intensive theoretical studies have been reported on the

Chart 7

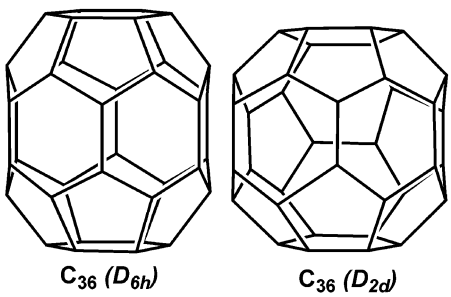

structure and bonding of C_{36}[30x,21y,42,94,97] and its charged species.[97i,98] The most systematic structural searching work was done separately by Slanina et al.[97a] and Fowler et al,[97b] using various semiempirical quantum chemical methods. Slanina et al. searched through 598 cage structures of C_{36} by the semiempirical method and predicted the D_{2d} isomer to be the lowest energy.[97a] Fowler et al. gave a similar prediction after optimizing in total 88 C_{36} fullerene structures with the DFTB, QCFF/PI, MNDO, AM1, and PM3 methods.[94a] Furthermore, their QCFF/PI calculations revealed that the D_{6h} isomer is highly diradicaloid in nature and should work as a hexavalent group in redox reactions.[94] On the other hand, various DFT calculations showed that the D_{2d} and D_{6h} singlet states and D_{6h} triplet state are quasi-isoenergetic, but their exact stability order depends on the type of functional used.[97b−i] More elaborate ab initio calculations at the CASSCF, MP2, and MRMP2 level of theory convincingly demonstrated that the D_{6h} singlet state is the lowest energy state with substantial diradical character, followed by the D_{6h} triplet, D_{2d} triplet, and D_{2d} singlet states.[97u] Because of its diradical character, it is extremely difficult to obtain the pure molecular form of C_{36} fullerene because it tends to form polymeric solid[14a] or react with other molecules/atoms/ions available in the synthetic process to form derivatives.[14b,c] Interestingly, the D_{6h} and D_{2d} isomers can transform via Stone-Wales (SW) transformation,[99] and a transformation barrier of ca. 6 eV was computed at DFT level.[100]

Few experimental data are available on the properties of C_{36} molecule. From the photoelectron spectrum of selected C_{36}^- anion generated in the gas phase, an electron affinity ~3.0 eV and a HOMO−LUMO gap of ~0.8 eV were estimated for neutral C_{36}.[92d] These properties have also been predicted by different theoretical means. Table 3 lists the EA's and IP's predicted for the D_{2d} and D_{6h} isomers of C_{36}. It appears that the theoretical calculations tend to underestimate the electron affinity of C_{36}, except LDA, which overestimated the electron affinity. Because of the inherent diradical nature of the D_{6h} C_{36} ground state,[97u] the inaccuracy of these predictions listed in Table 3 is not unexpected at all, because none of them could give a correct description with regard to the ground-state electronic structure of C_{36}. This is also the reason the HF/6-31G* prediction is the worst.

Table 3. Adiabatic Ionization Potentials (IP) and Electron Affinities (EA) of the D_{2d} and D_{6h} Isomers of C_{36} Predicted by Different Theoretical Means[a] (eV)

isomer	parameter	HF	LDA	GGA	B3LYP	B3PW91
D_{2d}	IP	5.15	7.19	6.58	6.41	6.58
	EA	1.68	3.01	2.43	2.31	2.50
D_{6h}	IP	7.16	7.50	6.91	6.70	6.89
	EA	0.28	3.25	2.66	2.50	2.67

[a] The standard split-valence basis set 6-31G* was employed in the computations. All the data listed are extracted from ref 97f.

The global and local aromaticities of the neutral and charged species of D_{6h} C_{36} were assessed by Chen et al.[97i] and Tanaka et al.[98] using an NICS probe. The NICS values at the center of the cages and the pentagons and hexagons of (Figure 12) D_{6h} C_{36}^q (q = 0, +2, −2) were computed using the GIAO-SCF/6-31G* method and are schematically shown in Figure 15. For the neutral species, its singlet state is more aromatic (either locally or globally) than the triplet state; the hexagons are locally more aromatic than the pentagons. Interestingly, a decrease of aromaticity is insignificant upon oxidation to the dication but very remarkable upon reduction to the dianion.

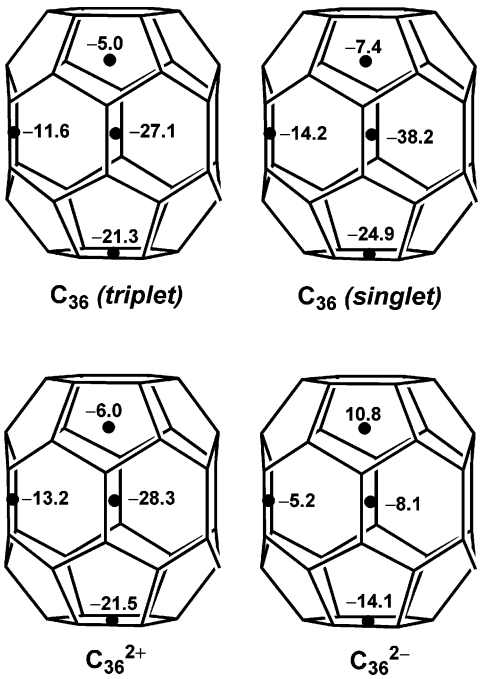

Figure 15. NICS values (ppm) calculated by the GIAO-SCF/6-31G* method for D_{6h} C_{36}^q (q = 0, +2, −2) (ref 97i).

In contrast to the very high global aromaticity of the D_{6h} C_{36} (singlet state), the global aromaticity of the singlet-state D_{2d} C_{36} isomer was found to be much lower with an NICS value of −15.4 ppm at the cage center.[42] In addition, the local aromaticities of pentagons and hexagons in the singlet-state D_{2d} C_{36} isomer (NICS values ranging from 11.2 to −14.2 ppm) are mostly lower than those of the D_{6h} C_{36} isomer.

2.4.3 Exohedral Derivatives of C_{36}

Few exohedral derivatives of C_{36} have been disclosed experimentally. Shinohara et al. reported the production and characterization of several C_{36}-related materials, including $C_{36}H_4$, $C_{36}H_4O$, $C_{36}H_6$, and $C_{36}H_6O$, by a high-temperature laser vaporization (laser-furnace) method and the conventional DC arc-discharge method.[14c,d] Upon laser-vaporization of a Ni/Co-doped graphite rod, an enhanced production of $C_{36}H_4$ together with $C_{36}H_4O$ was obtained. However, transformation from the as-prepared $C_{36}H_4$ and $C_{36}H_4O$ to $C_{36}H_6$ and $C_{36}H_6O$ was observed during the extraction process using CS_2 as solvent. Such a transformation suggests $C_{36}H_4$ and $C_{36}H_4O$ are reactive with two free valences available for further chemical transformation. A MALDI mass analysis on a dried $C_{36}H_6$ solid prepared by evaporating a purified CS_2 extract revealed that upon desorption/

ionization, fragmentation of $C_{36}H_6$ occurs, preferentially giving the magic fragment $C_{18}H_3$.[14d] Unfortunately, no further experimental information is available about the structural characterization of these C_{36} derivatives.

The lack of experimental information on the structures of hydrides and hydroxides of C_{36} has motivated a number of theoretical investigations.[17,97g,i,m,n,r,t,] A lot of exohedral derivatives have been investigated theoretically, including $C_{36}H_{2n}$ (n = 1, 2, 3, 6),[17,97,101] $C_{36}F_2$,[102] $C_{36}O$,[103] and $C_{36}OH^+$.[104]

Fowler et al.[17,94a] have conducted a rather systematic search for the lowest energy isomers of $C_{36}H_{2n}$ (n = 1, 2, 3) derived from the D_{6h} and D_{2d} C_{36} cages by means of DFTB optimizations. It was concluded that (i) hydrogen atoms are preferentially added to the pentagon fusions of the carbon cages; (ii) the lowest-energy isomers for $C_{36}H_6$ and $C_{36}H_4$, adopt the D_{6h} C_{36} cage with a 1,4-addition pattern of hydrogen distribution (Figure 16); (iii) the lowest-energy isomer

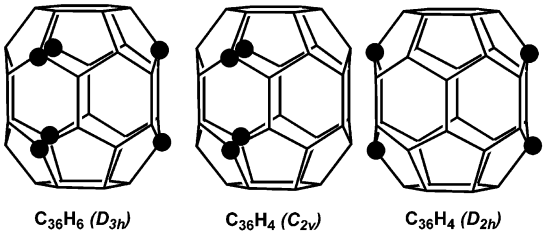

Figure 16. Structures of the most stable $C_{36}H_6$ and $C_{36}H_4$ isomers. The black dot denotes the carbon atom on which H atom is attached (from ref 17).

for $C_{36}H_2$ adopts the D_{2d} C_{36} cage with a 1,4-addition pattern of hydrogen distribution (Figure 17a), followed by several quasi-isoenergetic isomers derived from the D_{6h} C_{36} cage (Figure 17b−d). The ^{13}C NMR spectra for various low-energy isomers of $C_{36}H_{2n}$ (n = 2, 3) have also been computed by Heine et al. using the density-functional PBE method.[101d]

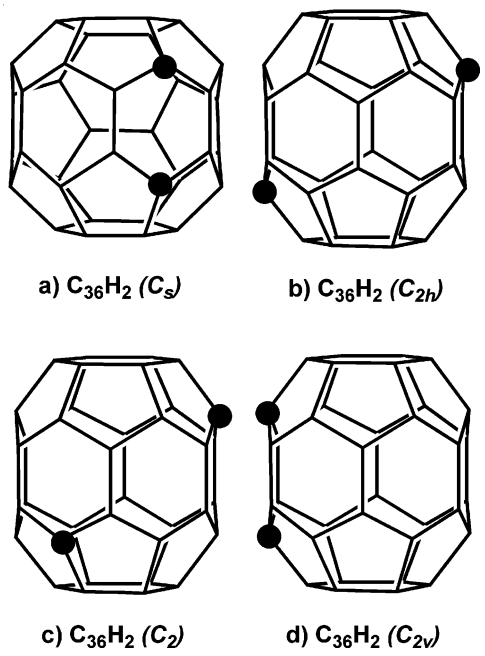

Figure 17. Structures of the most stable $C_{36}H_2$ isomers. The black dot denotes the carbon atom on which H atom is attached (from ref 17).

The local and global aromaticity of $C_{36}H_6$, $C_{36}H_{12}$, and $C_{36}H_{36}$ was studied by Chen et al.[97i] The D_{3h} isomer of $C_{36}H_6$ (Figure 18a) was found to be globally

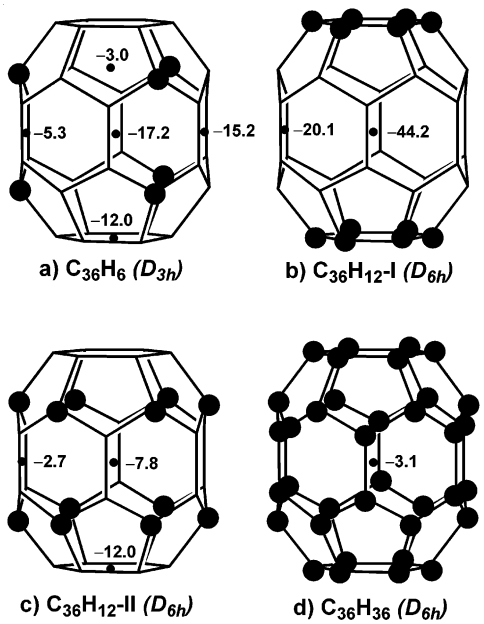

Figure 18. NICS values (ppm) calculated by the GIAO-SCF/6-31G* method for $C_{36}H_6$, $C_{36}H_{12}$, and $C_{36}H_{36}$. The black dot denotes the carbon atom on which H atom is attached (ref 97i).

aromatic; the intact hexagons are aromatic, whereas the hexagons with 1,4-addition of hydrogens are nonaromatic. Two isoenergetic isomers have been found for $C_{36}H_{12}$; the isomer I (Figure 18b) has a [6]-cyclacene belt, thus having higher aromaticity than isomer II (Figure 18c). The perhydrogenated C_{36}, $C_{36}H_{36}$ (Figure 18d), is nonaromatic and should behave as a normal saturated hydrocarbon.

Hundreds of $C_{36}F_2$ isomers derived from C_{36} carbon cages were optimized by Zhao et al.[102] using the semiempirical AM1 and PM3 methods. The lowest-energy isomer of $C_{36}F_2$ was found to have a structure identical to that of $C_{36}H_2$.[17] It was concluded that the addition pattern of H or F atoms for the formation of $C_{36}X_2$ (X = F, H) is predominantly determined by the conjugation effect, rather than by relaxation of strain.[17,101c,102]

Zhao et al. have also performed HF/STO-3G calculations to search for the low-energy isomers of $C_{36}O$.[103] Four lowest-energy isomers derived from the D_{6h} and D_{2d} cages of C_{36} proposed by them are depicted Figure 19. It appears that they all have an epoxy-like local structure. Among them, the isomer-I (Figure 19a) derived from the D_{2d} C_{36} cage was predicted to be the most stable at the HF/6-31G//HF/STO-3G level of theory.

2.4.4 Endohedral Derivatives of C_{36}

To the best of our knowledge, the only endohedral metallofullerene of C_{36} so far produced in experiments was U@C_{36} by Guo et al.[19] However, no further information is available on its structure characterization.

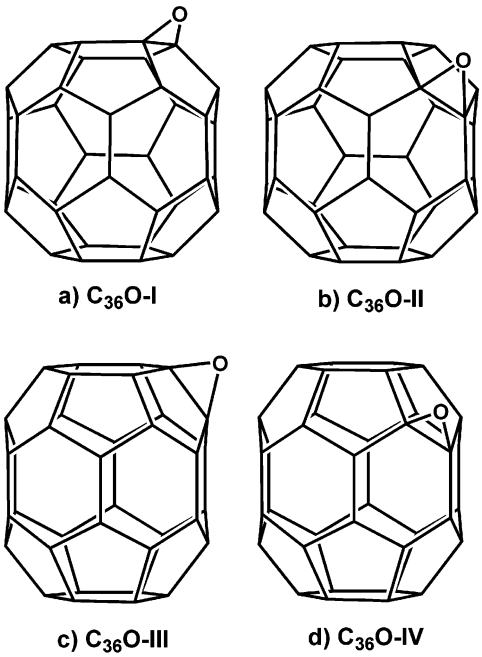

Figure 19. Four lowest-energy isomers of $C_{36}O$ (ref 103).

Except U@C_{36}, several endohedral complexes of C_{36}, X@C_{36} (X = N, He,[105] H, Li, Na, K[97g]), have been investigated theoretically. It has been shown that in N@C_{36}, the N atom is located at the center of the D_{6h} cage with no explicit covalent bond but prefers to covalently bond to a C−C bond of the D_{2d} cage.[105] In He@C_{36}, He atom is located exclusively at the cage center for both the D_{6h} and D_{2d} cages. For the hypothetic endohedral complexes X@C_{36} (X = H, Li, Na, K),[97g] the encapsulated monovalent atoms were found to locate at the center of the D_{6h} carbon cage with charge transfer from the trapped atom to the carbon cage. The inclusion energy predicted at the B3LYP/6-311+G* level of theory was −41.6, −24.0, 8.4, and 15.3 kcal/mol for Li, Na, H, and K, respectively. Hence, the inclusion is thermodynamically favorable for Li and Na, whereas the encapsulation of H or K is unfavorable.

2.4.5 Heterofullerene Analogues of C_{36}

The geometries and electronic structures of the monosubstituted [36]fullerenes $C_{35}X$ (X = B, N, Si),[106] the mono-BN-substituted [36]fullerene $C_{34}BN$,[74,97v] and the multisubstituted heterofullerenes $C_{30}X_6$ and $C_{24}X_{12}$ (X = B, N)[97i] were investigated by means of density functional calculations. Ding et al.[106] studied the monosubstitution fullerenes $C_{35}X$ (X = B, N, Si) using LDA and GGA methods and found that the dopant atom prefers to occupy the site where the replaced carbon atom has significant contribution to the frontier orbitals of C_{36} (Chart 8). The computed IP, EA, and chemical hardness of these monosubstituted heterofullerenes suggested that the chemical stability of the monosubstituted heterofullerenes should be slightly lower than that of the pristine C_{36}.

In the mono-BN-substituted heterofullerene $C_{34}BN$, the B and N dopants prefer to pair up and to occupy a hexagon−pentagon fusion rather than a PP fusion (Chart 8).[74] Mono-BN substitution of C_{36} (D_{6h}) raises the IP and EA simultaneously, along with a small increase of the HOMO−LUMO gap. This suggests an enhanced chemical stability due to mono-BN substitution.

Chart 8

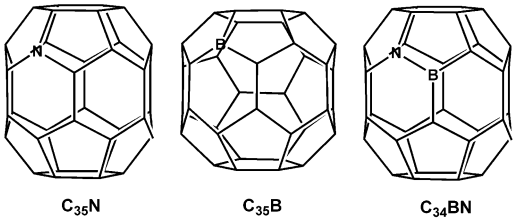

The geometries and electronic properties of various isomers of disubstituted heterofullerene $C_{34}X_2$ (X = B, N) have been computed using the B3LYP and TDB3LYP methods by Li et al very recently.[97v] The calculations suggest that the disubstituted heterofullerenes could perform better in the two-photon excitation process than does the pristine C_{36}.

Several multisubstituted heterofullerene[36]s, $C_{30}X_6$ and $C_{24}X_{12}$ (X = B, N), were proposed by Chen et al.[97i] The NICS values at the center of the cages and the pentagons and hexagons (Figure 20) were computed (using the GIAO−SCF/6-31G* method) to assess the global and local aromaticity of these heterofullerenes. The computed NICS values indicate that the $C_{30}X_6$ (X = B,N) and $C_{24}N_{12}$ heterofullerenes are less aromatic than the pristine D_{6h} C_{36} (cf. Figure 15), whereas the $C_{24}B_{12}$ species has a highly delocalized structure and is more aromatic than the pristine D_{6h} C_{36}.

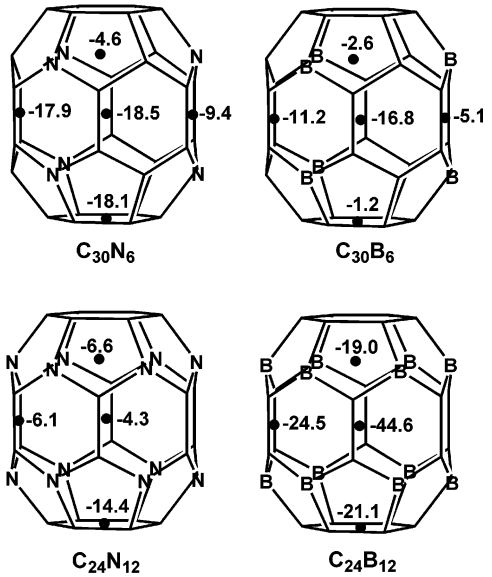

Figure 20. Structures of several hypothetical multisubstituted heterofullerene[36]s and NICS values (ppm) calculated by GIAO-SCF/6-31G* calculations. (Reprinted with permission from ref 97i. Copyright 2000, Elsevier.

2.4.6 Oligomers of C_{36}

Dimers. The preliminary density functional calculations[95,97b,g] demonstrated that dimerization of the diradicaloid D_{6h} C_{36} fullerene is highly favorable with a face-to-face 1,4-connection of two hexagons, forming a dimer structure in D_{2h} symmetry (Figure 21a). The

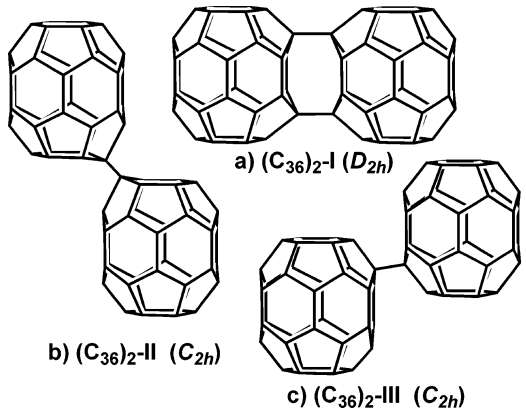

Figure 21. Structures of $(C_{36})_2$ derived from D_{6h} C_{36} cage.

inter-cage bond length is about 1.60 Å, slightly longer than normal C−C bond (~1.55 Å) in simple alkanes. The exothermicity for the dimerization was predicted to be 73 kcal/mol at the DFTB level,[94a] about 10 times higher than that of $(C_{60})_2$.[107] In addition to this di-σ-bonded dimer, mono-σ-bonded dimers in C_{2h} symmetry (Figure 21b,c) were also found to be energetically favorable but less stable than the di-σ-bonded one.[95] A more systematic theoretical work to search the dimeric structures derived from D_{6h} C_{36} was reported by Huang et al.[108] A total of 16 dimeric structures were considered in their B3LYP/3-21G calculations, among which the D_{2h} structure shown in Figure 21a was confirmed to be the most stable. Furthermore, their recent DFT-B3LYP/6-31G* calculations[109] revealed that a C_{2v} dimeric structure (Figure 22) can be formed by [2+2] addition of two D_{2d} C_{36} cages; such a [2+2] dimerization is exothermic with an estimated dimerization energy of 29.7 kcal/mol, far lower than that of the D_{2h} dimer of D_{6h} C_{36}.

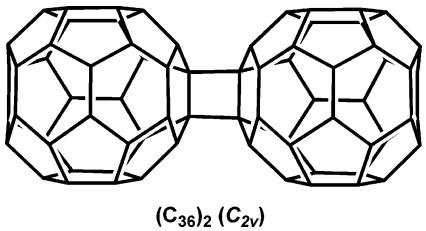

Figure 22. $(C_{36})_2$ derived from D_{2d} C_{36} cage.

Trimers, Tetramers, and Hexameric "Superbenzene". The diradicaloid nature of the D_{6h} C_{36} cage as well as its inherent hexavalence[94] also facilitates the formation of highly symmetric trimer and tetramer with the face-to-face 1,4-connection mode as proposed by Fowler et al.[79b,110] The exothermicities for the formation of the D_{3h} trimer (Figure 23a) and the D_{2h} tetramer (Figure 23b) from free D_{6h} C_{36} cages were predicted to be 137.8 and 259.3 kcal/mol, respectively, at the DFTB theoretical level. Note that free valences are available within the hexavalent D_{6h} C_{36} cages involved in the formation of these oligomers, e.g., each C_{36} cage in the trimer has two free valences. Attachment of more C_{36} cages at the edge of these oligomers should be highly plausible. Hence, the oligomers shown in Figure 23 could be precursors leading to higher oligomers and polymers.

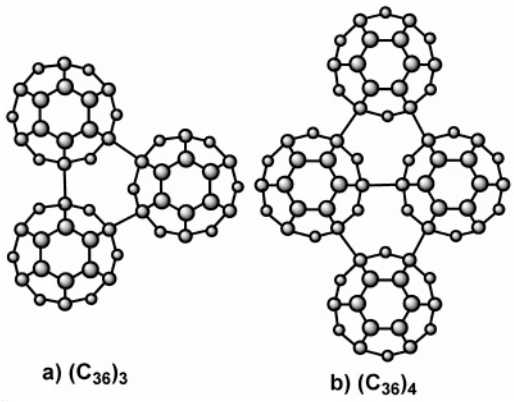

Figure 23. Trimer (a) and tetramer (b) formed by the D_{6h} C_{36} carbon cage.

In the presence of hydrogen, the free valences at the edge of C_{36}-based oligomer can be saturated. Indeed, Fowler et al.[94a] proposed a hexamer of C_{36} whose free valences are saturated by hydrogens. The structure of such a hexameric "superbenzene" is depicted in Figure 24. With no free valence at any monomer, this "superbenzene" is quite stable with a large HOMO−LUMO gap. This implies that a stable 2D polymer of C_{36}, namely, "supergraphite",[94a] can be obtained with the hexagonal hexamer as building blocks.

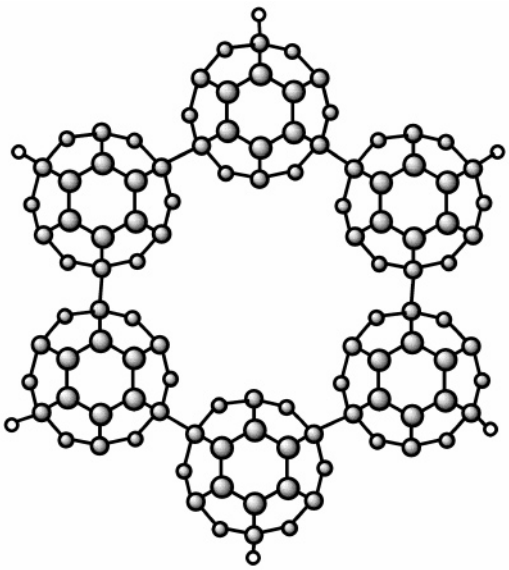

Figure 24. Hexameric "superbenzene" $(C_{36}H_2)_6$ in D_{6h} symmetry.

2.4.7 Polymers and Solids of C_{36}.

In light of the oligomeric structures, various C_{36}-based one-dimensional (1D)[94a,111] and 2D polymers, and 3D-polymeric solids[94a,97c,110,112,113] have been proposed and investigated by means of quantum chemical methods.

1D Polymer. An infinite linear chain of D_{6h} C_{36} cages (Figure 25a) was designed by Fowler et al.[94a] Their DFTB calculation revealed that this 1D-polymer, with a D_{2h} symmetry and an optimal inter-cage bond length of 1.61 Å, has a band gap of 1.28 eV (semiconductive!) and a binding energy of 66.3

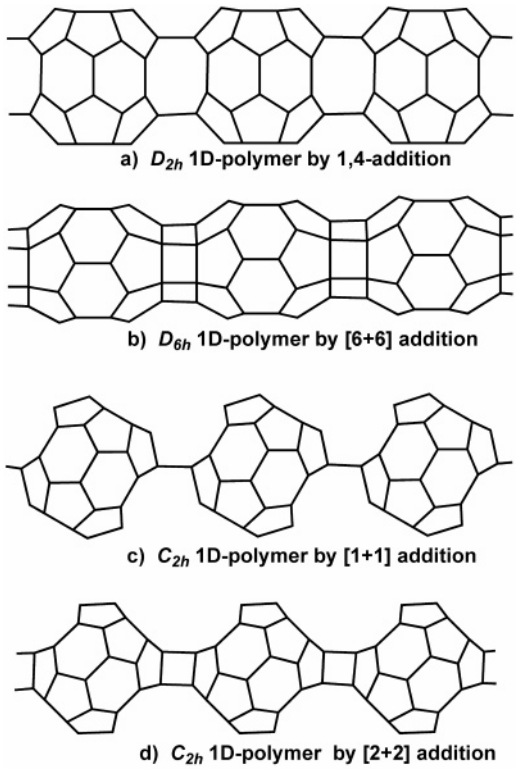

Figure 25. 1D polymers derived from D_{6h} C_{36} fullerenes.

kcal/mol per C_{36}. Besides this one, three more 1D polymers (Figure 25b–d) consisting of the D_{6h} C_{36} monomers were proposed in subsequent theoretical investigations by Huang et al.[111a–c] With the help of ab initio crystal orbital (SCF–CO) method (at the B3LYP/3-21G level), they predicted the following: (i) all four 1D-polymers are semiconductors with band gaps ranging from 0.55 to 2.04 eV, among which the D_{2h} 1D-polymer is the most stable with the largest band gap (2.04 eV); (ii) their negatively charged forms, $[C_{36}^{m-}]_\infty$ (m = 1, 2, 3, 4), are metallic even at very low temperatures.[111c]

In contrast to intensively investigated 1D polymers formed by D_{6h} C_{36} fullerenes, less attention has been paid to the 1D polymers derived from D_{2d} C_{36} fullerene. Huang et al.[111d] designed several 1D polymers based on D_{2d} C_{36} fullerene. However, only two of them (shown in Figure 26a,b) were found to be energetically favorable; they are semiconductive with a band gap of ~1.0 eV predicted by density functional SCF-CO calculations.

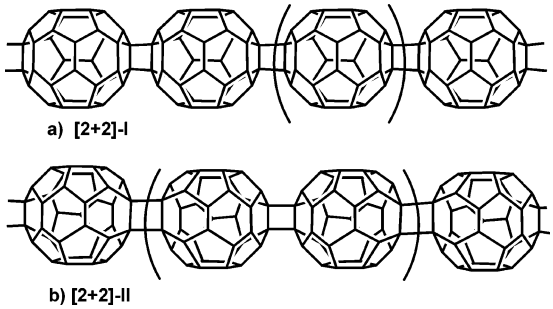

Figure 26. 1D polymers derived from D_{2d} C_{36} fullerenes. Unit cells are included in parentheses.

2D Polymer. Several 2D polymers of C_{36} have been supposed, derived exclusively from the highly symmetric D_{6h} C_{36} fullerene.[94a,110,112] Figure 27 depicts six 2D slabs proposed by Huang et al.[112b] The first one (**Slab-I** in Figure 27a) is a hexagonal "supergraphite";[94a] each C_{36} monomer is "hexavalent", i.e., forming six intercage C–C bonds with its nearest neighbors via the face-to-face 1,4-connection bonding mode (see Figure 21a for the definition). **Slab II** (Figure 27b) is derived from the "supergraphite" by putting one more C_{36} cage into the hexagonal hole. Accordingly, each monomer forms 12 intercage C–C bonds, whereas the cage–cage bonding mode is the same as that of **Slab-I**. **Slab-III** (Figure 27c) is an evolution of **Slab-II** by indroducing intercage [2+2] additions in one-dimension; there are in total 20 intercage bonds for each monomer. **Slab-IV** (Figure 27d) is topologically equivalent to **Slab-II** but adopts a different intercage bonding mode (i.e., intercage [2+2] addition). **Slab-V** (Figure 27e) and **Slab-VI** (Figure 27f) adopt tetragonal structures. All these 2D polymers were predicted to be semiconductors.[112b] However, only the supergraphitic **Slab-I** shows substantial stability relative to the free D_{6h} C_{36} fullerenes. The predicted intercage C–C bond length in the supergraphite is 1.60 ± 0.02 Å.[94a,112b] The predicted band gap for this 2D polymer depends substantially on the theoretical methods employed, ranging from 2.09 eV[94a] to 3.12 eV.[112b] Nevertheless, it can be safely concluded that the C_{36}-based supergraphite would be a semiconductor.

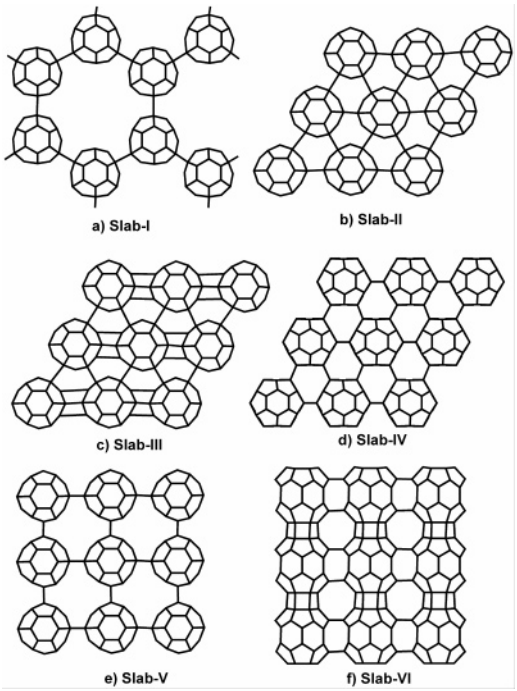

Figure 27. 2D polymeric slabs derived from D_{6h} C_{36} fullerenes. The number of atoms for each monomer to form intercage C–C bonds is 6 for **slab-I**, 12 for **slab-II**, 20 for **slab-III**, 12 for **slab-IV**, 8 for **slab-V**, and 16 for **slab-VI**.

Solids of C_{36}. The first C_{36}-based solid was proposed by Cote et al.[97c] As depicted in Figure 28a, this rhombohedral C_{36} solid is composed of layers of D_{6h} C_{36} cages in a ABC stacking sequence with no intralayer cage–cage bonding. Because of the formation of interlayer cage–cage bonding (optimal bond

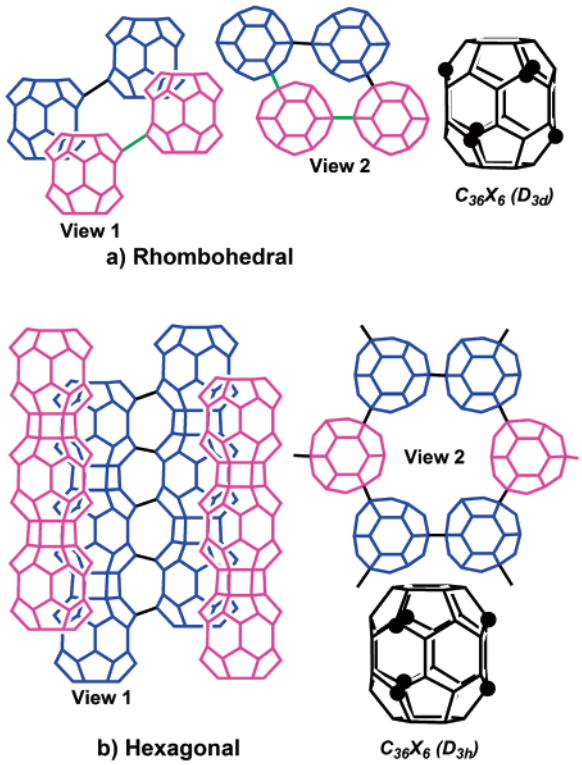

Figure 28. C_{36}-based solids without intralayer cage−cage bonding: (a) rhombohedral and (b) hexagonal structures.

length ~ 1.56 Å), each C_{36} cage has a local symmetry of D_{3d}, similar to the D_{3d} isomer of $C_{36}H_6$. Density functional calculation using the local-density approximation predicted this solid to be metallic with a binding energy of 2.2 eV/C_{36}.[97c] By simply altering the interlayer stacking mode to an AB sequence, a hexagonal crystal structure (Figure 28b) was found by Grossman et al.[113a] to be semiconductive and by ~3.4 eV/C_{36} more stable than the previously reported rhombohedral structure. Each C_{36} cage in this close-packed hexagonal form of C_{36} solid has a local symmetry similar to the D_{3h} isomer of $C_{36}H_6$. This solid was also predicted separately by Fowler et al. [94a]

Since C_{36} readily forms 2D-polymeric slab structures,[94,110,112] the possibility that C_{36}-based solids are constructed by stacking of 2D-polymeric slabs was investigated theoretically by Grossman et al,[113a] and Fowler et al.[94] Considering the unusual stability of 2D-polymeric "supergraphite" slab (cf. Figure 27a), Fowler et al. predicted that a solid constructed by 2D-polymeric "supergraphite" slabs with interlayer van der Waals interactions would have a *d*-spacing parameter of 6.78 Å,[94] in good agreement with the *d*-spacing (~6.8 Å) measured by TEM for the "C_{36} solid" synthesized by Zettl et al.[14a] Using a different 2D-polymeric slab (Figure 29a,b) as building blocks, Grossman et al,[113a] found two crystal structures (Figure 29c,d) with interslab covalent bonds that are energetically favorable and semiconductive. Among all the aforementioned solids, the AB-stacking crystal shown in Figure 29d is the most stable and has an optimal *d*-spacing parameter of 6.74 Å,[113a] also compatible with the TEM measurement.[14a]

In addition to the aforementioned solids built up solely with C_{36} cages, other C_{36}-based solids with

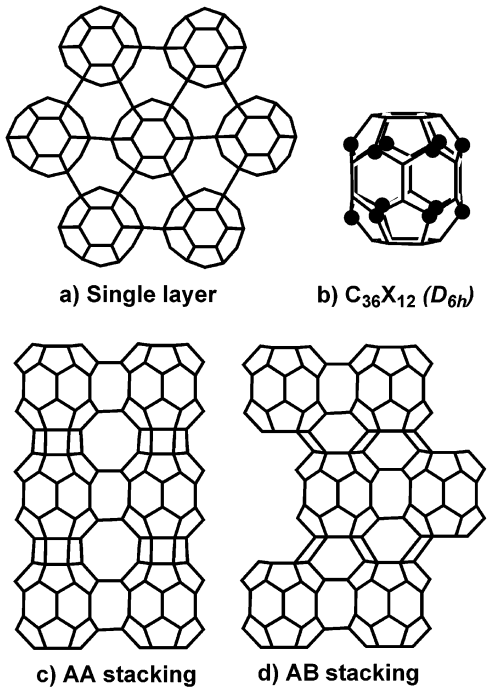

Figure 29. C_{36}-based solids with intralayer cage−cage bonding: (a) Structure of a single C_{36} layer, (b) local symmetry of C_{36} (black dots denote those carbon atoms to form intralayer cage−cage bonds), (c) crystal structure formed with the C_{36} layers in an AA-stacking sequence, and (d) crystal structure formed with the C_{36} layers in an AB-stacking sequence.

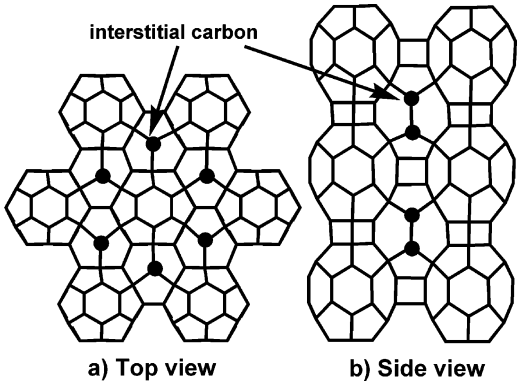

Figure 30. Clathrate structure formed by C_{36} cages and interstitial carbon atoms. All carbons are sp^3-hybridized.

clathrate structures[113e,f] (Figure 30) can be designed, for example, by introducing C_2 dimers into the interstitial region of a polymeric crystal of pure C_{36} solid. Owing to the presence of interstitial carbon atoms, all carbon atoms in the clathrate C_{36} solid are sp^3-hybridized. Yet, the C_{36}-based clathrate form of carbon solid is structurally different from the well-known carbon allotrope, diamond, although both consist of only sp^3-hybridized carbon atoms.

In short, the journey to search for C_{36} solids is full of surprises, e.g., with the findings of brand-new carbon allotropes such as the "supergraphite" solid[94,110] and the clathrate form of carbon[113e,f] and demonstrates that highly symmetric small fullerenes such as D_{6h} C_{36} fullerene can provide remarkable flexibility in the construction of various carbon allotropes

comprising of both sp^2- and sp^3-hybridized carbon atoms or solely of sp^3-hybridized carbon atoms.

2.5 C_{50} and Its Molecular and Solid Derivatives

2.5.1 Geometric and Electronic Structures of C_{50}

Fullerene C_{50} has a total of 50 π-electrons around its spherical carbon surface, fulfilling the spherical aromaticity rule.[23] Hence, it was believed to be synthetically approachable.[14b] In gas-phase experiments, C_{50} did show enhanced stability relative to its neighbors in the carbon cluster distribution (for examples see refs 1, 19, and 92).

Theoretical studies[18b,114,115] revealed several low-energy isomers of C_{50}; among them the D_3 isomer is the most stable (Figure 31), followed by the D_{5h}

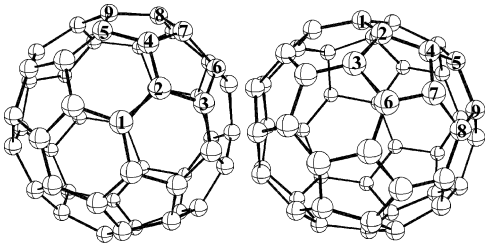

Figure 31. Geometry of C_{50} (D_3): (a) top view and (b) side view. The independent carbon atoms are numbered.

isomer (Figure 32) which is 2.3 kcal/mol[18b] higher in energy than the former. Note that D_3 and D_{5h} isomers are the only two C_{50} fullerene isomers without three pentagons directly or sequentially fused; they only have isolated and double pentagon configurations. There are six and five PP fusions within the D_3 and D_{5h} isomers, respectively.

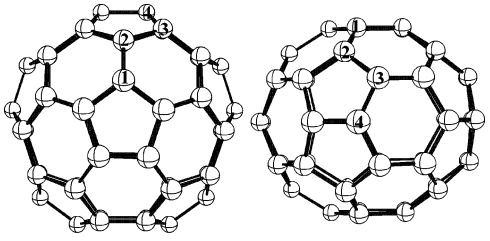

Figure 32. Geometry of C_{50} (D_{5h}) (a) top view, (b) side view. The independent carbon atoms are numbered.

As predicted by recent DFT calculations,[18b] the D_3 isomer has a singlet ground state (^{1}A). The ground state for the D_{5h} isomer, however, is a little more elusive. This isomer has three low-lying energy states, two singlet states (denoted as $^1A_1'$(A) and $^1A_1'$(B)), and a triplet state ($^3A_2'$); the lowest-energy state $^1A_1'$(B) is only 3.3 and 4.5 kcal/mol lower in energy than the $^1A_1'$(A) and $^3A_2'$ states, respectively. Both the HOMO and LUMO coefficients of C_{50} (D_{5h}) are distributed around the equatorial PP annulations, as shown schematically in Figure 33. The two $^1A_1'$ singlets of D_{5h} C_{50} differ in the occupancy of the frontier orbitals. In the $^1A_1'$ (A) state, the highest occupied molecular orbital (HOMO) is the $13a_1'$ MO; the lowest unoccupied molecular orbital (LUMO) is

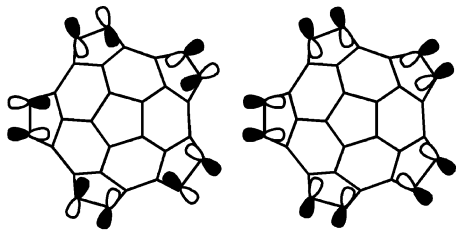

Figure 33. Schematic presentation of the frontier molecular orbitals of C_{50} (D_{5h}). (Top view along the C_5 axis).

$5a_2'$ (shown schematically in Figure 33). The HOMO and LUMO are reversed ($5a_2'$ and $13a_1'$, respectively) in the $^1A_1'$ (B) state. It was found that due to such an orbital-switching, the two singlet states differ substantially in geometry and global aromaticity:[18b]

(i) The $13a_1'$ MO is bonding, whereas the $5a'_2$ MO is antibonding for C−C bonds at the equatorial PP fusions. Accordingly, the equatorial pentaphenyl belt within C_{50} (D_{5h}) is quinoid-like (Scheme 1A) in the

Scheme 1

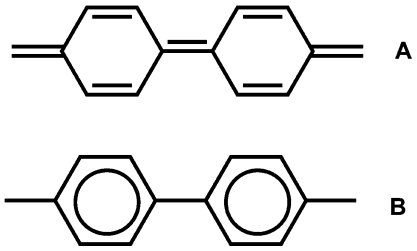

$^1A_1'$ (A) state and benzene-like (Scheme 1B) in the $^1A_1'$ (B) state. The C−C bonds at the PP fusions (∼1.40 Å) in the $^1A_1'$ (A) state are shorter than those (∼1.47 Å) in the $^1A_1'$ (B) state. The lower energy of $^1A_1'$ (B) over $^1A_1'$ (A) indicates that the double CC bonds at the equatorial pentagon−pentagon fusions are not favorable.

(ii) The NICS value at the C_{50} (D_{5h}) cage center is −32.4 ppm for the $^1A_1'$ (A) state and −2.7 ppm for the $^1A_1'$ (B) state. Hence, the $^1A_1'$ (A) state shows spherical aromaticity, but the more energetically favorable $^1A_1'$ (B) state is nonaromatic.

Note that $C_{50}(D_3)$ with six adjacent pentagons is lower in energy than $C_{50}(D_{5h})$ with only five adjacent pentagon. This violates the PAPR.[8] However, D_5 C_{50} has a more spherical shape[116] and is more aromatic (NICS −40.3 ppm) than D_{5h} C_{50}. (NICS −2.7 ppm at the cage center for electronic state B). The aromatic stabilization energy of D_3 isomer compensates its larger strain energy and results in the higher stability of $C_{50}(D_3)$. Most recently, the Gibbs energies of C_{50} isomers were computed to clarify the relative stabilities at elevated temperatures, and it was found that $C_{50}(D_3)$ is more stable thermodynamically than $C_{50}(D_{5h})$ within a wide temperature range related to fullerene formation.[117]

In addition to the predominant distribution of frontier orbitals around the pentalene-like fusions of D_{5h} C_{50}, these sites also have the largest curvature. Hence these sites are the most active sites for chemical reactions, such as addition reaction and dimerization etc.[18b,114b,115,118] This explains why the

Cl atoms in the synthesized $C_{50}Cl_{10}$ are bound to the equatorial PP fusions.[16] Indeed, full chlorination or hydrogenation of the PP fusions in the D_3 and D_{5h} isomers of C_{50} (eqs 4−7) was predicted to be highly exothermic, leading respectively to the formation of exohederal derivatives $C_{50}X_{12}$ and $C_{50}X_{10}$ (X = Cl, H).[18b]

$$C_{50}\,(D_{5h}) + 5Cl_2 \rightarrow C_{50}Cl_{10}\,(D_{5h})$$
$$\Delta H\,(per\ Cl_2) = -50.7\ \text{kcal/mol} \quad (4)$$

$$C_{50}\,(D_{5h}) + 5H_2 \rightarrow C_{50}H_{10}\,(D_{5h})$$
$$\Delta H\,(per\ H_2) = -50.9\ \text{kcal/mol} \quad (5)$$

$$C_{50}\,(D_3) + 6Cl_2 \rightarrow C_{50}Cl_{12}\,(D_3)$$
$$\Delta H\,(per\ Cl_2) = -37.5\ \text{kcal/mol} \quad (6)$$

$$C_{50}\,(D_3) + 6H_2 \rightarrow C_{50}H_{12}\,(D_3)$$
$$\Delta H\,(per\ H_2) = -35.2\ \text{kcal/mol} \quad (7)$$

Upon functionalization of the PP fusions, the large strain in the bare fullerenes can be drastically released. For example, a strain energy was estimated to be 529.4 kcal/mol for the bare D_{5h} C_{50} and to be 225.1 kcal/mol for $C_{50}H_{10}$ (D_{5h}) at the B3LYP/6-31G* level.[115]

C_{50} has a narrow HOMO−LUMO gap of ∼0.8 eV measured experimentally[92d] by XPS experiments. The predicted HOMO−LUMO gaps for the D_3 and D_{5h} isomers are 2.27 and 1.37 eV, respectively;[18b] both are higher than the experimental measurement. Nevertheless, the narrow HOMO−LUMO gap is indicative of its low kinetic stability. Reduction of C_{50} would increase its stability. At B3LYP/6-31G* level, the dianionic C_{50}^{2-} has a larger HOMO−LUMO gap (∼2.12 eV) than that of neutral D_{5h} C_{50} (1.37 eV).[18b]

C_{50} appears to be better electron acceptor than C_{60}. The experimental electron affinity (EA) of C_{50} (∼3.35 eV[92d]) is even higher than that of C_{60} (2.668 ± 0.008 eV[119]). In agreement with the experimental measurement, the predicted vertical electron affinities for the nearly isoenergetic D_3 and D_{5h} isomers of C_{50} are 2.97 and 3.40 eV at the B3LYP/6-31+G* theoretical level, respectively.[18b] This suggests that both isomers are probably attainable in the gas-phase experiments.

2.5.2 Exohedral Derivatives of C_{50}

Using a modified graphite arc-discharge method,[120] Xie et al. successfully prepared the first C_{50} derivative, decachlorofullerene[50] ($C_{50}Cl_{10}$), in milligram quantities.[16] By means of multiple staged mass spectrum (MS/MS), ^{13}C NMR, infrared (IR), Raman, ultraviolet−visible absorption (UV−Vis), and DFT calculations, it was demonstrated convincingly that this new compound has a D_{5h} fullerene[50] structure with 10 chlorine atoms attached to the equatorial PP fusions (Figure 34).[16,18] This finding, for the first time, provides evidence experimentally that small fullerenes can be remarkably stabilized and, hence, attainable in macro quantity by covalent functionalization of its active PP fusions.[17]

In the ^{13}C NMR spectrum of $C_{50}Cl_{10}$ (D_{5h}) measured in C_6D_6 solution, four peaks were observed at 143.2, 146.8, 161.5, and 88.7 ppm for C1, C2, C3, and C4

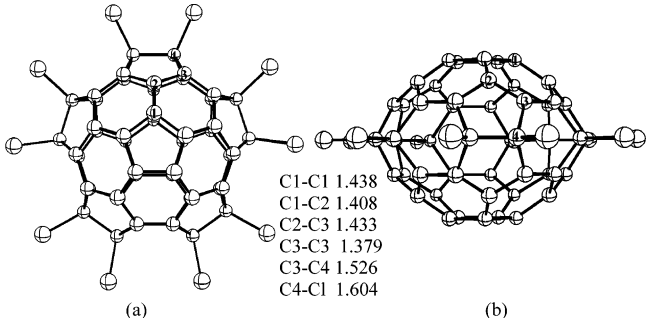

Figure 34. The B3LYP/6-31G* optimized geometry of $C_{50}Cl_{10}$ (D_{5h}) (a) top view, (b) side view.

atoms, respectively.[16] Such an assignment was confirmed by DFT calculations with the predicted ^{13}C chemical shifts at 141.5 (C1), 146.1(C2), 163.6(C3), and 87.5(C4) ppm. Its UV−Vis spectrum of $C_{50}Cl_{10}$ (D_{5h}) shows several absorption bands at 433.8, 356.5, 334.0, 322.0, and 238.5 nm. Subsequent TDDFT calculations[18b,121] reproduced the experimental spectrum and predicted an optical gap of 532.8 nm.

$C_{50}Cl_{10}$ (D_{5h}) appears to be highly electron affinitive. According to DFT calculations, its EA (3.04 eV) is ∼0.5 eV higher than that of C_{60}. Hence, like its large homologous $C_{60}X_n$ (X = F, Cl, Br),[122] $C_{50}Cl_{10}$ may work as a good electron acceptor with possible photonic/photovoltaic applications.

$C_{50}Cl_{10}$ (D_{5h}) also shows interesting solvo-chemistry in protic solvents. It was found that solvolysis of $C_{50}Cl_{10}$ in methanol solvent at room temperature leads to the formation of $C_{50}Cl_{10-x}(CH_3O)_x$ ($x = 1-5$).[16] Moreover, recent density functional studies showed that both the average static polarizability and the second hyperpolarizability of $C_{50}Cl_{10}$ are larger than those of C_{60}; thus, $C_{50}Cl_{10}$ was predicted to be a promising nonlinear optical material.[123]

In addition to the $C_{50}Cl_{10}$(D_{5h}), another chlorinated exohedral derivative of C_{50}, $C_{50}Cl_{12}$, was also produced by Xie et al., although isolation and characterization of this molecule is yet unsuccessful.[16] Actually, $C_{50}Cl_{12}$ is even more abundant than $C_{50}Cl_{10}$ in the HPLC chromatogram,[124] and thus a promising target for isolation. The D_3 symmetrical structure (Figure 35) was predicted for $C_{50}Cl_{12}$.[18b] Note that D_3

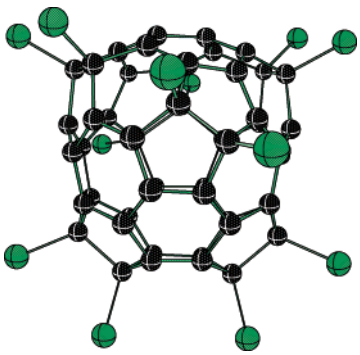

Figure 35. B3LYP/6-31G* optimized structure of $C_{50}Cl_{12}$ (D_3), in which the 12 Cl atoms are attached to the pentagon−pentagon fusions of C_{50} (D_3).

C_{50} is the ground state of C_{50} and has exactly 12 most strained sites for chlorine additions.

Most recently, $C_{50}(D_{5h})$ oxide, $C_{50}O$, was computed at B3LYP/3-21G level of theory.[125] Among a total of eight possible isomers, the structure (Figure 36)

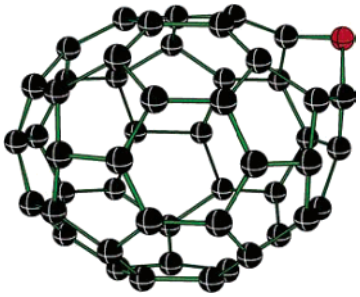

Figure 36. B3LYP/6-31G* optimized geometry of the most stable isomer of $C_{50}O$.

which as an annulene-like structure with oxygen bridging across a [5,6] type COC bond at the site between the pole and the equatorial belt, is found as the ground state. However, the unfavorable electronic state of D_{5h} C_{50} was used in the computation.

2.5.3 Endohedral Derivatives of C_{50}

In experiments to produce the first small metallofullerene $U@C_{28}$ by laser vaporization of a mixture of UO_2/graphite in a cluster FT-ICR apparatus, monocations of $U@C_{50}$ and $U_2@C_{50}$ were also observed as byproducts by Guo et al.[19] Preliminary XPS spectroscopic characterization indicated the encapsulated U atom in neutral $U@C_{50}$ and $U_2@C_{50}$ most probably adopts formal 4+ valence state. Using similar experimental techniques, a series of C_{50}-based endohedral metallofullerenes, $M@C_{50}$ (M = Sc, Y, La, and Ca), were observed in their cationic forms in the gas phase.[126]

The possibility of forming other endohedral derivatives of C_{50} such as $X@C_{50}$ (X = Mg, He, Ne, Ar) was recently sought by means of DFT calculations.[18b,42,127] The inclusion energies predicted for $He@C_{50}$ (D_{5h}), $Ne@C_{50}$ (D_{5h}), and $Ar@C_{50}$ (D_{5h}) are 2.12, 5.77, and 26.41 kcal/mol at the B3LYP/6-311G* theoretical level (plus basis set superposition error correction).[127] Accommodation of Mg in C_{50} was also predicted to be endothermic by 16.0 kcal/mol for the D_{5h} isomer and by 43.6 kcal/mol for the D_3 isomer.[18b] Hence, these endohedral fullerenes should be attainable in the gas phase. Note that a helium atom has been incorporated into the much smaller $C_{20}H_{20}$ (I_h) cage[81] and that the computed accommodation energy is 35.0 kcal/mol.[42]

2.5.4 Heterofullerenes of C_{50}

Disubstituted derivatives of the D_{5h} isomer of C_{50}, $C_{48}X_2$ (X = B, N), were investigated by means of semiempirical AM1 and MNDO methods.[128] Three low-energy isomers are schematically shown in Figure 37. It appears that the substitution occurs preferentially at the equatorial PP fusion sites. The lowest-energy Isomer-I (Figure 37a) adopts the 1,4-substitution pattern (at the equatorial pentalene belt). Most recently Xu et al.[129] studied the BN substituion pattern of C_{50} at semiempirical (AM1 and MNDO) and density functional (B3LYP/3-21G*) and

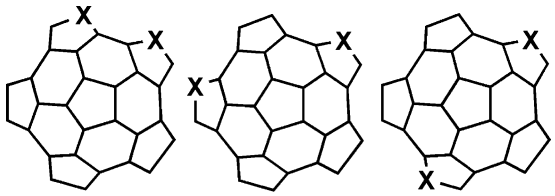

Figure 37. Three low-energy isomers (top view) of heterofullerene $C_{48}X_2$ (X = B,N).

found that the BN units prefer to stay together following "single-bond", "hexagon filling", and "continuity and equatorial belt" rules.

2.5.5 Oligomers of C_{50}

Dimers. It was predicted theoretically that dimerization of C_{50} (D_{5h}) can readily occur at its PP junctions. Four possible dimerization modes were proposed by Lu et al.,[18b] as depicted in Figure 38. The formal [2+2]-addition mode (Figure 38a) appears to be the most favorable, whereas the [4+2] and [4+4]-additions (Figure 38b,c) are also exothermic. The open-[2+2] mode (Figure 38d), which involves cleavage of the two formal C−C bonds of the closed dimer (Figure 38a) and the formation of two C=C bonds between two C_{50} cages, is thermoneutral. On the contrary, dimerization of the D_3 isomer of C_{50} (Figure 39) was predicted to be energetically unfavorable.

The aforementioned dimers of C_{50} (D_{5h}), although thermally favorable, still suffer kinetic instability from the rest of the PP fusions. Functionalization of or further oligomerization through these active sites gives rise to trimeric and oligomeric species with enhanced stability, as was predicted by Heine et al.[115] Figure 40 lists several stable dimeric and oligomeric species of C_{50} (D_{5h}), whose PP fusions were all saturated by H atoms. On the basis of these structures, it was concluded that formation of regular covalently bound C_{50} solids is impractical.[115]

2.6 Other Small Fullerenes and Their Derivatives

Except the aforementioned C_{20}, C_{28}, C_{36}, and C_{50}, other small fullerenes such as C_{24}, C_{32}, C_{40}, C_{44}, etc. have been seldom investigated either experimentally or theoretically.

2.6.1 C_{24} and Its Derivatives

The ground-state structure of C_{24} is the most elusive and under controversy, varying from polyacetylenic, dodecadehydrocoronenic, to fullerenic structures with the quantum chemical methods used.[130] Recent CCSD(T) calculations indicate the fullerene (D_6) structure (Figure 41a) with a singlet $^1A_1$ ground state is the most stable one.[131] This fullerenic structure can be regarded as a [12]trannulene[62b] capped with two benzene rings at both sides. Its optimized structure[42] is indeed affirmative of such a consideration with the uniform C−C bond length (1.423 Å) of the benzene-like rings, the localized C=C bond lengths of 1.365 Å and C−C bond lengths of 1.463 Å in the central [12]trannulenic ring, and the much longer C−C bond lengths of 1.531 Å between the six-

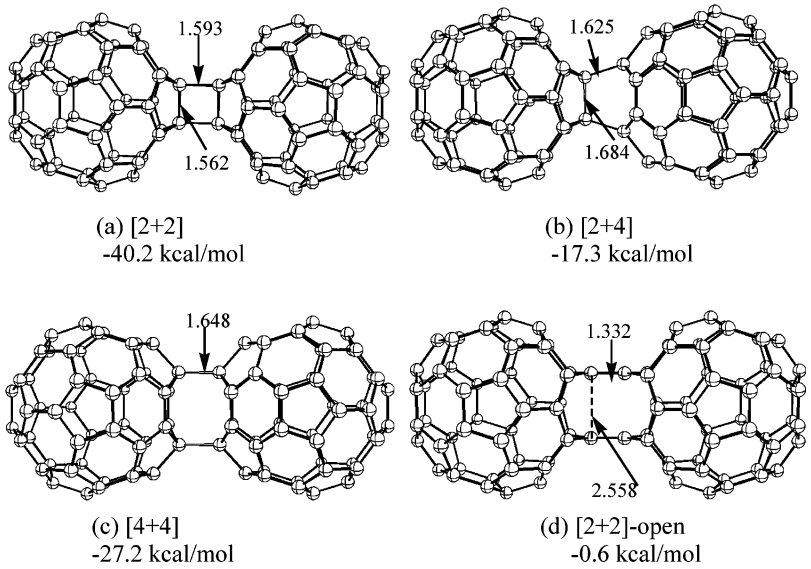

Figure 38. Four possible modes for the dimerization of C_{50} (D_{5h}). Key geometric parameters (bond lengths in angstroms) optimized at the B3LYP/6-31G* level; the dimerization energies are also given.

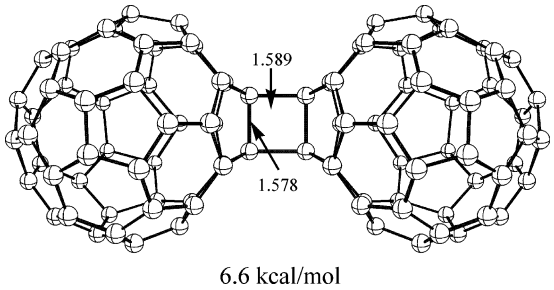

Figure 39. [2+2] dimer of C_{50} (D_3) (bond lengths in angstroms) and dimerization energy.

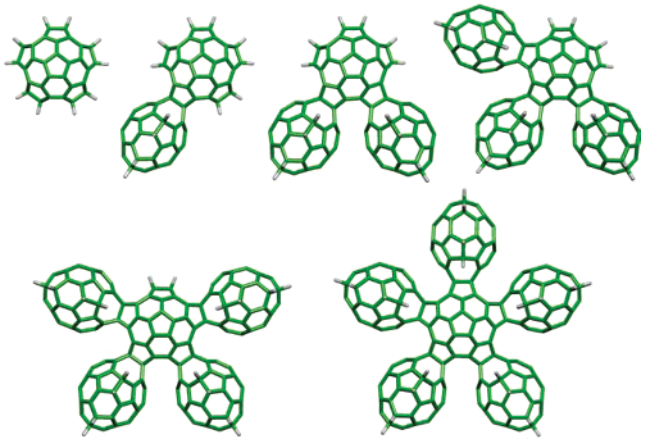

Figure 40. Minimal energy pathway from monomeric $C_{50}H_{10}$ to hexameric $C_{300}H_{40}$. All the oligomeric structures contain only the D4 intercage-bonding pattern (from ref 115).

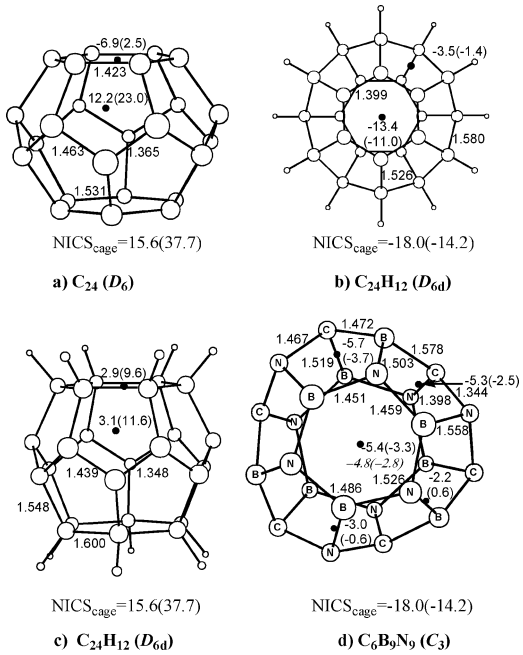

Figure 41. Structures of (a) the C_{24} (D_6) fullerene and its derivatives: (b) $C_{24}H_{12}$ (D_{6d}), (c) $C_{24}H_{12}$ (D_6), and (d) $C_6B_9N_9$ (C_3). B3LYP/6-31G* bond lengths (Å) and NICS values from GIAO-SCF/6-31G* (B3LYP/6-31G* in parentheses) are also given. The NICS values at the cage centers are given in bold below each structure, while those at individual ring centers are shown in the corresponding ring. Reprinted with permission from ref 42. Copyright 2001, Springer.

membered rings and the central [12]trannulenic ring. The local ring currents are diatropic within the six-membered rings and, in sharp contrast, paratropic within the [12]trannulenic ring. Compensation of these two local effects results in an NICS value of 15.6 ppm at the cage center,[42] which is much smaller compared to the [12]-trannulene value (35.7 ppm).[62b] So C_{24} fullerene is not aromatic at all.

The aromaticity of the C_{24} (D_6) cage can be tuned by chemical functionalization.[42] When all the [12]-trannulene-ring carbon atoms are attached with H atoms (Figure 41b), the resulting hydride $C_{24}H_{12}$ (D_{6d}) is aromatic with a highly negative NICS value (−18.0 ppm) at the cage center due predominantly to the local diatropic ring currents within the two benzene-like rings. On the contrary, another hydride $C_{24}H_{12}$ (D_6) with all the rim carbons being sp^3-hybridized (Figure 41c) is antiaromatic with a highly positive NICS value (11.6 ppm) at the cage center because of the antiaromatic [12]trannulene ring. So the exohedral derivative $C_{24}H_{12}$, if synthesized, should adopt the aromatic D_{6d} structure (Figure 41b).[132]

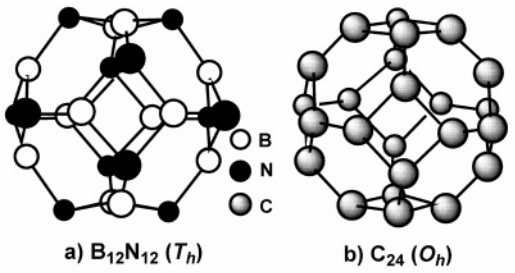

Figure 42. Structures of (a) $B_{12}N_{12}$ (T_h) and (b) the nonclassical O_h-symmetric C_{24} fullerene.

Two heterofullerenes of C_{24}, $C_6B_9N_9$ (Figure 41d) and $B_{12}N_{12}$ (Figure 42a), have been suggested by Chen et al.[42] and Strout,[133] respectively. The former was predicted to have a rather small NICS value (−6.7 ppm) at the cage center and, hence, to be nonaromatic.[42] The latter, though isoelectronic with the C_{24} (D_6) fullerene, was found to have a nonclassical fullerene structure with the presence of six four-membered rings. The analogous structure for C_{24} of O_h symmetry (Figure 42b) was found to be ~30 kcal/mol higher in energy than the D_6 isomer.[130c]

Although the nonclassical O_h C_{24} is less stable than its D_6 isomer, it has an octahedral distribution of four-membered rings, facilitating the construction of a cubic solid based on this nonclassical fullerene. The possibility of forming a cubic lattice from the C_{24} and $B_{12}N_{12}$ cages was predicted by Pokropivny et al.[134] Figure 43 shows the simple cubic lattice of a fullerite

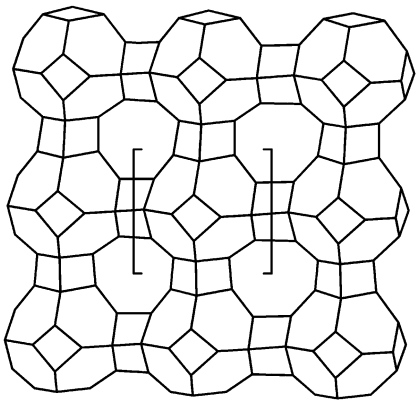

Figure 43. Local view of the simple cubic lattice of fullerite consisting of nonclassical O_h-symmetric C_{24} fullerene. Included in the bracket is a C_{24} cage.

consisting of the O_h C_{24} cages or the T_h $B_{12}N_{12}$ cages. This cubic fullerite and its analogues may serve as structural models for intermediate carbon phases, e.g., "cubic graphite", whose structures are elusive.[135] It is interesting to note that the simple cubic fullerite C_{24} (or $B_{12}N_{12}$) shown in Figure 43 has a two-dimensional lattice of cylindrical nanopores with a diameter of 0.41 nm, and, hence, may find its application as molecular sieves.[134]

2.6.2 C_{32} and Its Derivatives

C_{32} is such a remarkable magic-number carbon cluster that always shows very intensive signals in the gas-phase experiments.[1,92] PES studies[92d] revealed that the neutral C_{32} molecule has a large HOMO−LUMO gap (~1.3 eV), comparable to those of its larger, very stable homologues C_{70} and C_{60} (1.3 vs 1.6 eV). The experimental EA of C_{32} (~2.8 eV) is also comparable to those of C_{70} and C_{60} (~2.8 vs ~2.7 eV). The unusual stability of C_{32} (compared to its near neighbors) has been ascribed to its spherical aromaticity arising from its completely filled 32-π-electron valence shell.[23,24,42] Despite its high stability, bulk synthesis of C_{32} has never been accomplished yet.

The lowest-energy structure of C_{32} was predicted to be a D_3 fullerenic cage.[136] This cage has six unique carbon atoms and three unique ring centers (Figure 44). The computed NICS values at the ring and cage

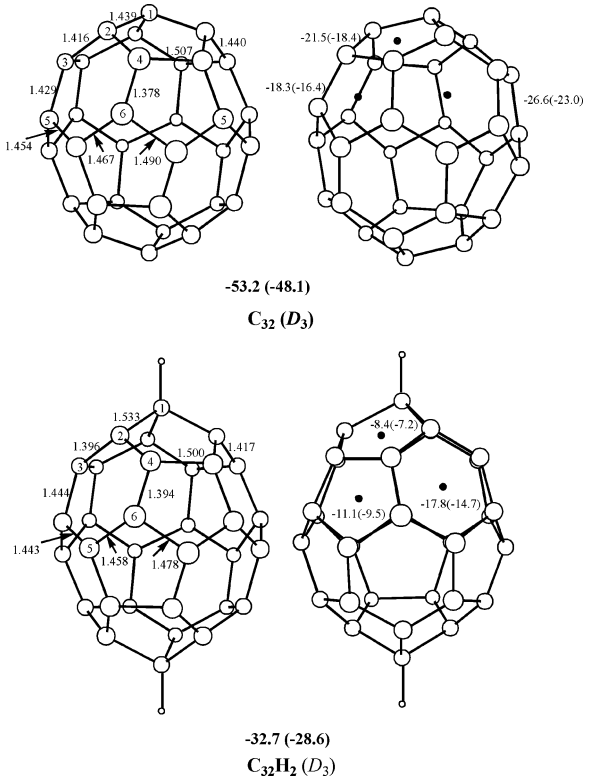

Figure 44. Structures of the C_{32} (D_3) fullerene and its derivative $C_{32}H_2$ (D_3). B3LYP/6-31G* bond lengths (Å) and NICS values from GIAO-SCF/6-31G* (B3LYP/6-31G* in parentheses) are also given. The NICS values at the cage centers are given in bold below each structure, while those at individual ring centers are shown in the corresponding ring. Reprinted with permission from ref 42. Copyright 2001, Springer.

centers are highly negative,[42,137] indicating that both the pentagons and the hexagons exhibit strong diatropic ring currents, which in turn result in a very large endohedral shielding of −53.2 ppm.[42] The very large endohedral shielding is indicative of the spherical aromaticity of C_{32} (D_3) cage.

Note that there are two pentagon−pentagon−pentagon (PPP) fusion apices in the C_{32} (D_3) cage. Saturation of these highly strained PPP sites with H atoms gives rise to the stable hydride, $C_{32}H_2$ (D_3), in which the remaining 15 double bonds are contained within three naphthalenic subunits (Figure 44).[136a,138] Because of the diatropic ring currents of the three aromatic naphthalenic subunits, this hydride also exhibits a large endohedral shielding of −32.7 ppm.

The possibility of encapsulating a metal atom M (M = Li, Na, K, and Be) or a small molecule (H_2) into

the C_{32} (D_3) cage were predicted by Sun et al.[136c] Their DFT calculations reveal that inclusion of a Li or Na atom is favorable, while encapsulation of K, Be, or H_2 is energetically unfavorable with inclusion energy ranging from 13 (for Be) to 24 kcal/mol (for H_2). Accommodation of a noble-gas atom such as He, Ne, or Ar is energy consuming too; the endothermicity was predicted to be 14.8, 42.7, and 154.2 kcal/mol for He, Ne, and Ar, respectively.[127] On the basis of the predicted inclusion energy, it appears that most of these concerned endohedral derivatives of C_{32} are viable, except Ar@C_{32}.

Inspired by the structure of the stable hydride $C_{32}H_2$, we further propose the following (Chart 9),

Chart 9

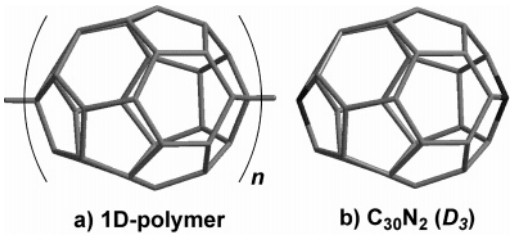

(i) A one-dimensional polymer consisting of the C_{32} (D_3) cage might be attainable upon chain reaction of C_{32} (D_3) monomers.

(ii) Heterofullerene $C_{30}N_2$ (D_3) would be stable, exhibiting similar endohedral shielding as does the hydride.

2.6.3 C_{40} and Its Derivatives

Gas-phase experiments showed that the neutral C_{40} cluster has an EA of ~2.8 eV and a HOMO−LUMO gap of ~0.7 eV.[92d] The much narrow HOMO−LUMO gap is indicative of its low kinetic stability.

To find the most stable structure of C_{40}, Albertazzi et al.[7] have searched through a total of 40 fullerene isomers of C_{40} with 12 theoretical methods varying from molecular mechanics to full ab initio SCF and DFT approaches. It was concluded that the most stable structure for C_{40} is the D_2 isomer, followed by the D_{5d} isomer (Figure 45).[7,139] Both isomers have the minimal number (10) of PP fusions; the energy difference between them is quite small, only 10.6 kcal/mol predicted at the B3LYP/6-31G* level.[42] Subsequent GIAO-SCF calculations[42] revealed that both isomers are nonaromatic with quite small positive NICS values (4.0 ppm for the D_2 isomer vs 2.8 ppm for the D_{5d} isomer) at their cage centers (cf. Figure 45). In detail, their hexagons show weak diatropic ring currents (aromatic) with negative NICS values at the ring centers, while pentagons have paratropic ring currents giving positive NICS values.

Apart from the D_2 and D_{5d} isomers, the T_d isomer (Figure 46) is of special interest. This isomer has a total of 12 PP fusions, with four triplet vertexes of pentagons (i.e., C1 atoms in Figure 46). Although not very stable,[140] this T_d C_{40} has a $^5A_2$ open-shell ground state with four singly occupied MOs, i.e., the $9a_1$ and $19t_2$ orbitals; the four dangling bonds are mainly localized at the C1 atoms which are vertices of a tetrahedron.[141] Hence, C_{40} (T_d) is highly reactive and

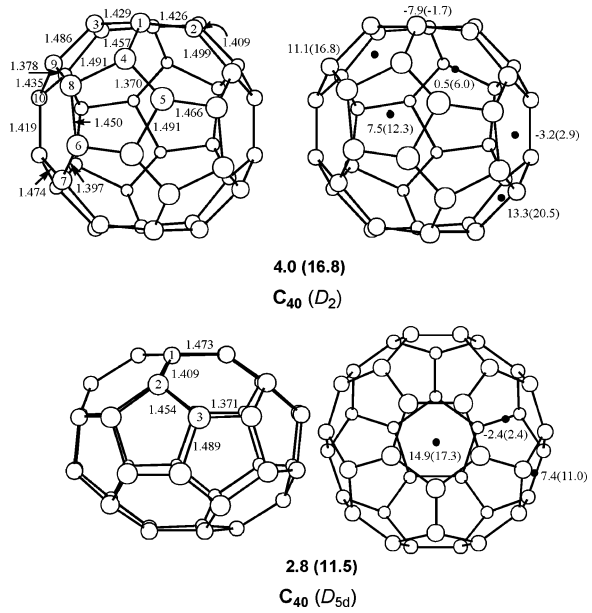

Figure 45. Structures of the D_2 and D_{5d} isomers of C_{40}. B3LYP/6-31G* bond lengths (Å) and NICS values from GIAO-SCF/6-31G* (B3LYP/6-31G* in parentheses) are also given. The NICS values at the cage centers are given in bold below each structure, while those at individual ring centers are shown in the corresponding ring. Reprinted with permission from ref 42. Copyright 2001, Springer.

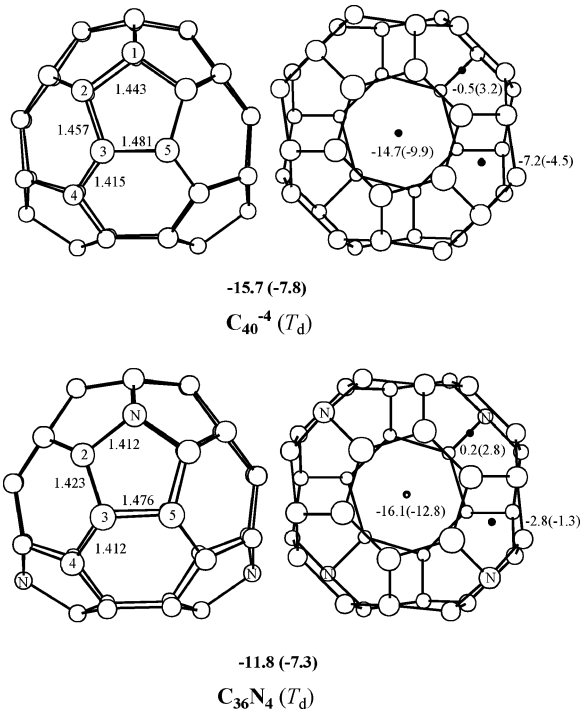

Figure 46. Structures of C_{40}^{4-} (T_d) and $C_{36}N_4$ (T_d). B3LYP/6-31G* bond lengths (Å) and NICS values from GIAO-SCF/6-31G* (B3LYP/6-31G* in parentheses) are also given. The NICS values at the cage centers are given in bold below each structure, while those at individual ring centers are shown in the corresponding ring. Reprinted with permission from ref 42. Copyright 2001 Springer.

could behave as a superatom of tetrahedral valence, analogous to C_{28} (T_d). It is inferable that the reactive neutral C_{40} (T_d) cage can be stabilized by covalent addition, reduction, and heterosubstitution to form correspondingly exohedral derivatives in the form of

$C_{40}X_4$ (X is a monovalent atom or group), tetraanion C_{40},$^{4-}$ and heterofullerenes $C_{36}Y_4$ (Y is a heteroatom such as P and N).[42,140−142]

The tetraanion C_{40}^{4-} (T_d) having a close-shell $^1A_1$ ground state[141] is globally aromatic.[42] As indicated by the computed negative NICS values at the rings and cage centers (Figure 46),[42] all pentagons and hexagons in C_{40}^{4-} (T_d) cage have diatropic ring currents, which cooperatively give rise to endohedral shielding. The isoelectronic heterofullerene $C_{36}N_4$ (Figure 46) exhibits similarly local and global aromaticity. On the contrary, the exohedral derivative $C_{40}H_4$ and two heterofullerenes $C_{36}Y_4$ (Y = B, P) (Figure 47) are nonaromatic with rather small NICS

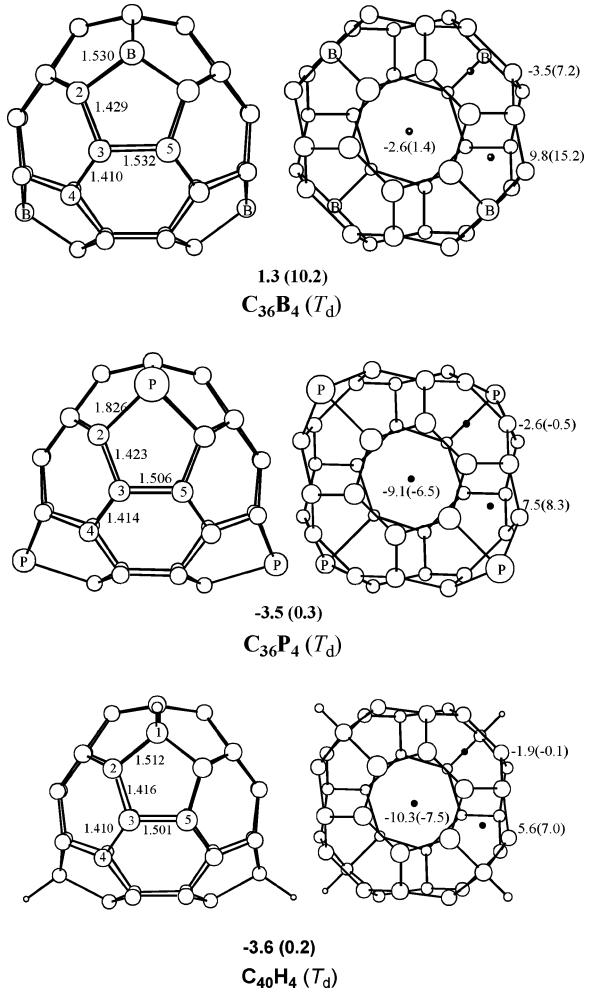

Figure 47. Structures of $C_{36}B_4$ (T_d), $C_{36}P_4$ (T_d), and $C_{40}H_4$ (T_d). B3LYP/6-31G* bond lengths (Å) and NICS values from GIAO-SCF/6-31G* (B3LYP/6-31G* in parentheses) are also given. The NICS values at the cage centers are given in bold below each structure, while those at individual ring centers are shown in the corresponding ring. Reprinted with permission from ref 42. Copyright 2001, Springer.

values at the cage centers.[42] Note that all these heterofullerenes as well as the exohedral hydride have a close-shell ground state with large HOMO−LUMO gaps, which are suggestive of their substantial kinetic stability.[141] Indeed, the semiempirical PM3 calculations by Lu et al.[142] demonstrated that the exohedral derivatives $C_{40}X_4$ (X = H, F, Cl, Br, I) have a stability similar to the known 1,3,5,7-tetrahaloadamantane molecules.

Apart from the heterofullerenes $C_{36}X_4$ (X = N, P, B), more surprising is the finding of cage-subsitituted fullerenes MC_{39}^+ (M = Nb, La) and its homologues in the gas phase by Jarrold et al.[143] because the metal atom in these metallofullerenes is networked, rather than encapsulated (for normal endohedral metallofullerenes), in the fullerene cage. By means of DFT calculations, Cui et al.[141] predicted a C_{3v}-symmetic cage structure (Figure 48) for NbC_{39}^+, which is

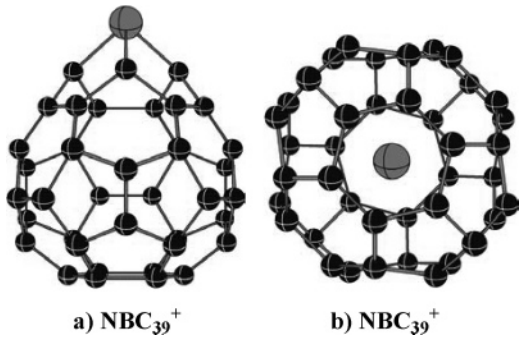

Figure 48. Geometries of (a) NbC_{39}^+ (C_{3v}) and (b) $Nb@C_{40}^+$ (T_d).

derived from the C_{40} (T_d) cage by substituting one of the PPP vertex with Nb atom. Because of the heteroatoms substitution, the NbC_{39}^+ cage adopts a C_{3v}-symmetric structure and a close-shell $^1A_1$ ground state with the $34(a_1^2)14(a_2^2)44(e^4)$ electronic configuration.[141] The predicted binding energies per atom for NbC_{39}^+ and the normal endohedral metallofullerene $Nb@C_{40}^+$ are 6.333 and 6.327 eV, respectively, implying that NbC_{39}^+ is thermodynamically favorable over $Nb@C_{40}^+$.[141]

In addition to $Nb@C_{40}^+$, other endohedral metallofullerenes composed of the C_{40} (T_d) cage and a tetravalent metal atom (e.g., Hf and Zr) were proposed by Fan et al.[144] These metallofullerenes should have a close-shell electronic configuration and be substantially stable.

Like C_{28} (T_d), the tetravalent C_{40} (T_d) cage may also serve as "superatomic" building block to construct "hyperdiamond" solids containing both sp^3- and sp^2-hybridized carbons. This deserves further theoretical investigations.

2.6.4 C_{44} and Its Derivatives

Under suitable conditions, C_{44}^- can show an enhanced abundance even higher than C_{60}^- in mass spectroscopy.[92d] It was estimated by PES experiments that neutral C_{44} molecule has a EA of ~3.3 eV and a HOMO−LUMO gap of 0.8 eV, quite similar to C_{50}.[92d]

C_{44} has in total 89 fullerene isomers.[6] The ground-state structure of C_{44} has been studied in various papers.[144,145] Early tight-binding molecular dynamics total energy calculations by Zhang et al.[145a] show C_{44} (75,D_2) (Figure 49) as the most stable. In a recent ab initio study, Lin et al.[145c] considered two D_{3h} and two D_{3d} isomers of C_{44} and found that C_{44} (72, D_{3h}) is the most stable. A similar suggestion was put forward by Fan et al.[144] However, a systematic computation on all possible isomers at the B3LYP/6-31G* level by Sun et al.[145e] shows that the C_{44}(75, D_2) is the most

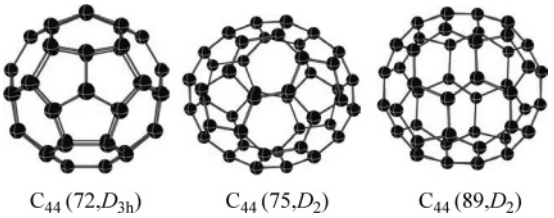

Figure 49. Structures of the most stable isomers of C_{44}.

stable isomer, closely followed by $C_{44}(89, D_2)$ (0.6 kcal/mol less stable), while $C_{44}(72, D_{3h})$ is the third lowest energy isomer, 8.0 kcal/mol higher in energy than C_{44}-(75, D_2). These two D_2 isomers have the lowest number (eight) of PP fusions, while the D_3 isomer has nine PP fusions, which suggests the instability of abutting pentagons for small fullerenes. Note that C_{44} has in total six D_2 isomers with only eight PP fusions (in contrast to only two as believed in ref 145d); thus counting the PP fusions can only give a qualitative answer for the stability of small fullerenes.

A series of endohedral metallofullerenes of C_{44}, M@C_{44} (M = Ca, Sc, Y,[126a] La,[88] and U[19]), were produced and observed in their cationic forms with remarkably intensive signals in the FT-ICR positive mass spectra from M-doped graphite disk. Notably, the monoanion of La@C_{44} was also found to be dominant in the FT-ICR negative mass spectra.[88] A structure model of M@C_{44} (M = Sc, Y, Ca, and La) was proposed that has a D_{3h}-symmetric C_{44} cage (Figure 50),[88,126a] but no theoretical calibration is yet available.

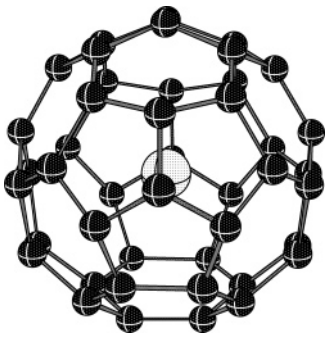

Figure 50. A structural model of M@C_{44} (M = Sc, Y, Ca) proposed by Kimura et al. (ref 126a).

2.6.5 C_{26}, C_{30}, C_{34}, C_{38}, C_{42}, C_{46}, C_{48}, C_{52}, C_{54}, C_{56}, C_{58}, and Their Derivatives

Neither these fullerenes nor their endohedral derivatives have been found to show highly remarkable signals in mass spectra. So these fullerenes have much lower kinetic stability than those magic-number clusters such as C_{32}, C_{36}, C_{44}, and C_{50}.[92]

C_{26}. Topologically C_{26} has only one fullerene structure and its highest possible symmetry of the fullerene cage is D_{3h}. The C_{26} cage has three hexagons and 12 pentagons with 21 PP fusions. This D_{3h} structure has a nondegenerate singlet ground state, and no first-order Jahn−Teller distortion is expected.[30x] However, early tight-binding molecular dynamics [145a] and recent diffusion quantum Monte Carlo calculations[84] both revealed that the stable structure for C_{26} is not ideally D_{3h}-symmetric but of C_{2v} symmetry (Figure 51). In contrast, B3LYP/6-31G* computations show

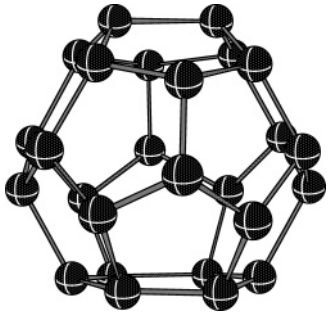

Figure 51. Structure of C_{26} (C_2/C_{2v}/D_{3h}) fullerene.

that both D_{3h} and C_{2v} isomers are higher saddle points (with three imaginary frequencies), and mode following of the first imaginary frequency leads to a C_2 local minimum. Moreover, the wave function of singlet C_{26} (C_2) has a RHF to UHF instability, and the triplet state is more stable.[146]

Nevertheless, the anion C_{26}^{4-} was predicted to have the D_{3h} symmetry with a large HOMO−LUMO gap (3.15 eV at B3LYP/6-31G*) and is highly aromatic (NICS value −25.9 ppm at the cage center at GIAO-B3LYP/6-31G*//B3LYP/6-31G*).[146] Accordingly, it was assumed that the heterofullerene $C_{22}N_4$ (C_{3v}) and endoheral metallofullerenes such as Ti@C_{26} are stable.[144]

C_{30}. For C_{30}, PES experiments revealed a EA of ∼3.5 eV and a HOMO−LUMO gap of ∼0.4 eV,[92d] indicative of its low kinetic stability. There are three fullerenic isomers of C_{30} consisting of 12 pentagons and 5 hexagons, i.e., one D_{5h} isomer and two C_{2v} isomers (Figure 52).[6] Because of the Jahn−Teller

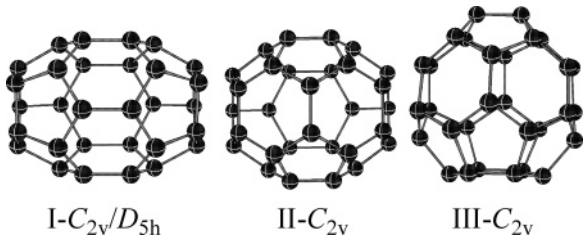

Figure 52. Structures of C_{30} fullerenes.

effect, the singlet state of I-D_{5h} distorts to C_{2v} symmetry (denoted as C_{2v}/D_{5h}). The I-C_{2v}/D_{5h} isomer has a total of 20 PP fusions, whereas the II-C_{2v} and III-C_{2v} isomers have 18 and 16 PP fusions, respectively. According to the PAPR,[8] the order of stability for these isomers should be III-C_{2v} > II-C_{2v} > I-C_{2v}/D_{5h}. Indeed, the III-C_{2v} isomer having minimal number of PP fusions is the most stable from tight-binding molecular dynamics[145] and density functional computations (the relative energies are 0.0, 4.0, 55.6, and 56.4 kcal/mol for III, II, I (singlet), and I (triplet) at the B3LYP/6-31G* level).[146b] Although it was considered that the instability of the highly symmetric I-D_{5h} isomer is related to its open-shell $^3A'$ ground state,[144] the D_{5h} triplet is 2.0 kcal/mol higher in energy than the I-C_{2v}/D_{5h} singlet at the B3LYP/6-31G* level.[146b]

The III-C_{2v} isomer appears to be aromatic with a negative NICS value (−11.4 ppm) at the cage center predicted at the GIAO-B3LYP/6-31G* level of theory.[146a] The dianions of these isomers having 32 π-electrons are expected to have more pronounced spherical aromaticity[23,24] and, hence, would show

higher kinetic stability than the neutral cages. B3LYP/6-31G* computations show that C_{30}^{2-} (III-C_{2v}) is the most stable among the dianions; its I-D_{5h} and II-C_{2v} isomers are 78.1 and 29.3 kcal/mol higher in energy. The lowest-energy isomer (III-C_{2v}) of C_{30}^{2-} has also the most significant aromaticity (NICS −41.2 ppm at GIAO-B3LYP/6-31G*//B3LYP/6-31G*), C_{30}^{2-}(II-C_{2v}) is also highly aromatic (NICS −29.3 ppm), while C_{30}^{2-}(I-D_{5h}) is weakly antiaromatic (NICS 9.9 ppm). As such, one can assume stable endohedral metallofullerenes such as M@C_{30} (II-C_{2v} and III-C_{2v}, M = Be, Mg, Ca, and Sc^+).

Theoretical studies of various possible structures of $C_{29}Si$ and $C_{28}Si$ have been performed. At the HF/3-21G level, the best structure of $C_{29}Si$ has a closed-cage structure with the silicon atom incorporated into the III-C_{2v} C_{30} cage.[89]

C_{34}. C_{34} has six fullerenic isomers, i.e., three C_2, two C_s, and one C_{3v} (Figure 53).[6] Interestingly, they

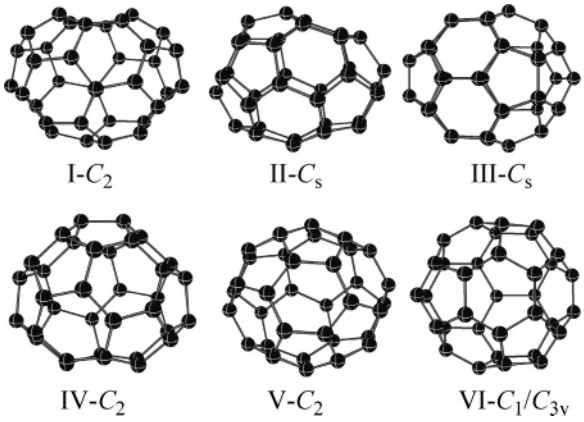

Figure 53. Structures of C_{34} fullerenes.

all have an equal number (15) of PP fusions. The C_{3v} symmetric cage has an open-shell triplet ground state,[144] and its singlet state structure distorts to C_1 symmetry (denoted as C_1/C_{3v}) due to the Jahn−Teller effect (the C_1 singlet is 2.8 kcal/mol higher in energy than the C_{3v} triplet).[146b] Such a C_1/C_{3v} structure was predicted to be the most stable among all the fullerene isomers of C_{34} by tight-binding molecular-dynamics calculations.[145a] However, B3LYP/6-31G* computations show that isomer **V** is the most stable, followed by **VI** (5.8 kcal/mol higher in energy), while the C_{3v} triplet is 22.7 kcal/mol less stable than V.[146a] GIAO−SCF/6-31G* computations revealed that all these isomers are aromatic with negative NICS values ranging from −16.9 ppm (isomer I-C_2) to −37.9 ppm (isomer V-C_2) at the cage centers.[146a] However, all of them have small HOMO−LUMO gaps and should have quite low kinetic stability. Indeed, PES experiments[92d] indicated a HOMO−LUMO gap of only ~0.3 eV for C_{34} cluster produced in the gas phase. Notably, the tetraanion of C_{34} (C_{3v}) was predicted to have a close-shell electronic configuration with a large HOMO−LUMO gap.[144] At the B3LYP/6-31G* level, C_{34}^{4-}(C_{3v}) has a 2.66 eV HOMO−LUMO gap and an NICS value of −19.9 ppm at the cage center (at GIAO−B3LYP/6-31G*),[146b] which indicates its high aromaticity.

C_{38}. In total, 17 conventional fullerene isomers can be constructed for C_{38}.[6] Among them, a C_2 isomer

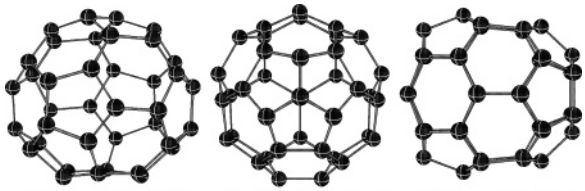

Figure 54. Structures of three isomers of C_{38}: (a) C_{38} (17,C_2), (b) C_{38} (16,C_{3v}), and (c) C_{38} (15,C_{2v}).

(Figure 54a) has the minimal number (10) of PP fusions, followed by the C_{3v} and C_{2v} isomers (Figure 54b,c) that have 12 and 13 PP fusions, respectively. Hence, the C_2 isomer can be expected to be the most stable, as was predicted by tight-binding molecular-dynamics[145a] and B3LYP/6-31G* computations.[145e] The rather small negative NICS value (−7.3 ppm) at the cage center (at the GIAO-SCF/6-31+G*// B3LYP/6-31G* level) [145e] indicates that the most stable C_2 isomer is nonaromatic or weakly aromatic. The low stability of C_{38} was evidenced by its relatively small HOMO−LUMO gap (~0.7 eV) estimated by PES experiments.[92d]

***C_{42}*.** C_{42} has a EA of ~ 3.0 eV and HOMO−LUMO gap of ~0.7 eV from PES experiments.[92d] Among its 45 fullerene isomers,[6] the (45,D_3) isomer shown in Figure 55 has the minimal number (9) of PP fusions

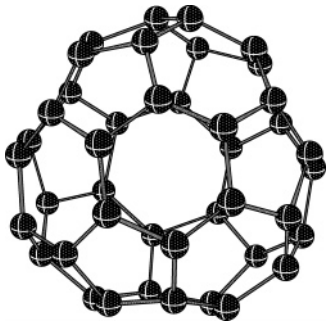

Figure 55. Structure of the C_{42} (45, D_3) fullerene.

and was predicted to be the most stable at the B3LYP/6-31G* level.[145e] The C_{42} (45, D_3) fullerene has a pseudo close-shell electronic structure and was assumed to form stable endohedral metallofullerenes by trapping a hexavalent metal such as W.[144] It is nonaromatic; the overall ring currents around the C_{42} cage is just weakly endohedral shielding with a small negative NICS value (−6.4 ppm) at the cage center.[145e]

C_{46}. There are 116 conventional fullerene isomers for C_{46}.[6] Most recently, 32 isomers, which have only isolated pentagons and pentagons fused with one or two other pentagons, have been computed at the B3LYP/6-31G* level. The computations show that C_{46}(109, C_2) is the most stable isomer, followed by (108,C_s), which is 1.9 kcal/mol higher in energy.[145e] These two isomers (Figure 56) have the minimal number (8) of PP fusions. The NICS values at the cage center are −11.4 and −14.2 ppm, respectively, for (109,C_2) and (108,C_s);[146] thus these two most stable C_{46} isomers are aromatic. The aromaticity of these C_{46} cages would be enhanced upon reduction to their tetraanions (C_{46}^{4-}) that fulfills the $2(N+1)^2$ rule of spherical aromaticity. For the same reason,

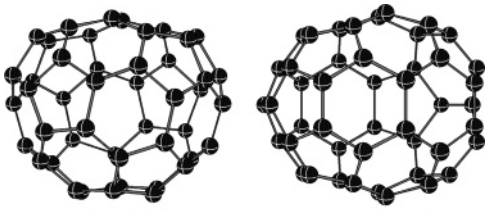

Figure 56. Structures of the most stable C_{46} fullerene cages.

these C_{46} cages would be stabilized by encapsulating a tetravalent metal atom such as Ti, Zr, and Hf to form endohedral metallofullerenes.

C_{48}. The structure of C_{48} has been the subject of a number of theoretical investigations with both conventional fullerene structures[145,147] and nonclassic fullerene structures[148] being considered. For example, Dunlap et al.[148b] proposed a nonclassic fullerene structure of C_{48} (Figure 57) consisting of 12 squares,

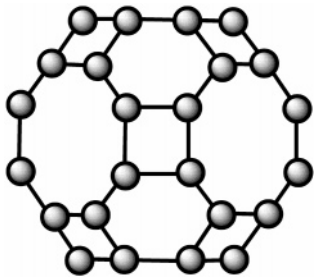

Figure 57. Nonclassic fullerene isomer of C_{48} in O_h symmetry.

8 hexagons and 6 octagons in O_h symmetry and predicted that all the carbon atoms in this nonclassic fullerene are equivalent. Another nonclassic fullerene isomer of C_{48} was suggested by Gao et al.[148a] to have 2 squares, 8 pentagons and 16 hexagons in D_{4d} symmetry. But these nonclassic fullerene isomers were proven to be less stable than some classic fullerene isomers.[147]

Topologically, there are 199 possible conventional fullerene isomers for C_{48}.[6] Figure 58 depicts the structures of four classic fullerene isomers that have the minimal number (7) of PP fusions (ref 147d miscounted the PP fusions of I-C_2 as six). According to the PAPR,[8] they are candidates for the most stable structure of C_{48}. Indeed, recent DFT calculations[147d] revealed that these four isomers are energetically favorable over other classic and nonclassic fullerene isomers and have very similar energies (difference within 5 kcal/mol) in the stability order: I−(171,C_2) > II−(199,C_2) > III−(196,C_1) > IV−(197,C_s). These four fullerene isomers are aromatic with the NICS values (cf. Figure 56) ranging from −17.3 (for isomer IV−(197,C_s)) to −37.4 ppm (for isomer I−(171,C_2)).[147d] The corresponding dianions possessing 50 π-electrons fulfill the $2(N+1)^2$ electron-counting rule of spherical aromaticity, and, accordingly, are expected to have enhanced spherical aromaticity. This is true for the isomers II−IV, whose dianions are more endohedral shielding (i.e., more negative NICS values) than the neutral cages, whereas the aromaticity of isomer I-C_2 decreases upon reduction to the dianionic form. The

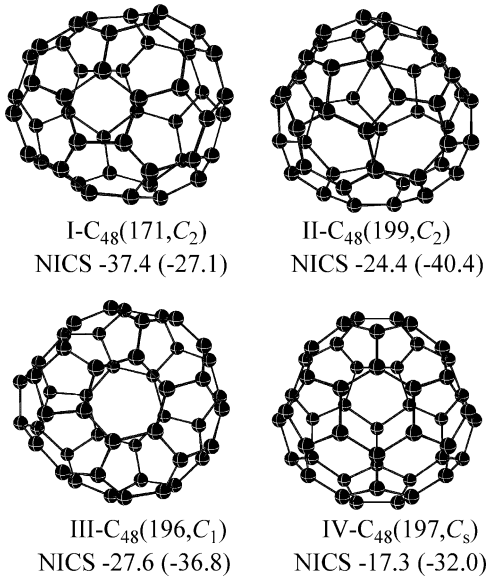

Figure 58. Structures of four most stable conventional fullerene isomers of C_{48} and NICS values at the cage centers that are computed at the HF/6-31+G*//B3LYP/6-31G* level of theory (from ref 147d). The NICS data for the dianions (C_{48}^{2-}) are given in parentheses.

predicted stability for the dianions of these isomers follows the order: II−(199,C_2) > III−(196,C_1) > I−(171,C_2) > IV−(197,C_s).[147d] Thus, the dianion of isomer II-C_2 is the most stable among dianion isomers. Note that C_{48}^{2-}(II-C_2) has a more spherical shape and is more aromatic than other isomers; its stronger aromatic stabilization energy makes C_{48}^{2-}(II-C_2) more stable than other isomers. Stable endohedral metallofullerenes M@C_{48} (M can be a divalent metal atom such as Mg, Ca) can be formed preferentially with the II-C_2 fullerene cage.

C_n (n = 52, 54, 56, 58). These near neighbors of C_{60} were observed in the gas phase with intensive mass signals in mass spectra.[92] Chlorine derivatives of C_{54} and C_{56} such as $C_{54}Cl_8$ and $C_{56}Cl_{10}$ were synthesized as byproducts in preparation of $C_{50}Cl_{10}$.[16] Theoretical investigations on the ground-state structures of this series of carbon clusters are scarce.[145a,149,150] Figure 59 depicts the conventional fullerene structures of these clusters predicted by tight-binding molecular-dynamics optimizations[145a] and first principles DFT calculations.[150a] These structures have the minimal numbers of PP fusions among possible fullerene isomers (in total 1205, 924, 580 and 437 fullerene isomers for C_{58}, C_{56}, C_{54} and C_{52}, respectively), i.e., three, four, four, and five PP fusions within C_{58}(1205, C_s/C_{3v}), C_{56}(916, D_2), C_{54}(540, C_{2v}), and C_{52}(422, C_2), respectively. However, it was also suggested that these clusters might have nonclassic fullerene structures as the most stable because they can be produced by laser-irradiation-induced fragmentation of C_{60}.[92b] For example, a nonclassic fullerene structure containing a seven-membered ring was proposed as the most stable structure of C_{58} (Figure 60),[149] which is derived by simply deleting a C_2 unit (a pentagon−hexagon fusion) from C_{60} (I_h). However, this nonclassic fullerene structure is 2.5 kcal/mol less stable than the conventional fullerene structure (Figure 59a) of C_{58} at B3LYP/6-31G* level.[146b] Sulfur-doped C_{58} cage was

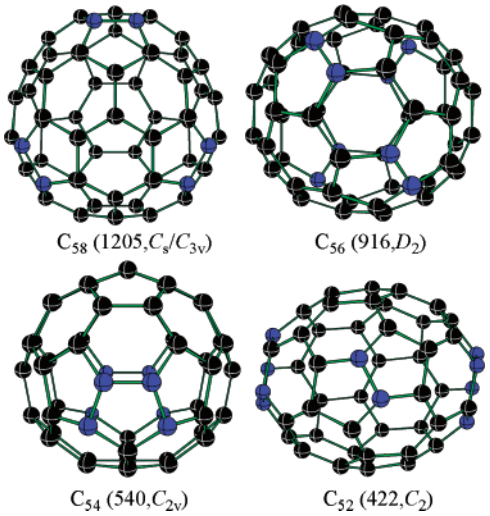

Figure 59. Conventional fullerene structures for C_{58}, C_{56}, C_{54}, and C_{52}, in which the pentagon−pentagon fusions are highlighted in blue.

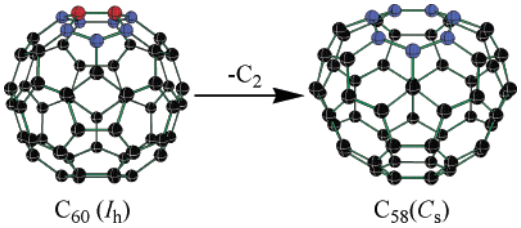

Figure 60. Nonclassic fullerene structure of C_{58} formed by deleting a C_2 unit (a pentagon−hexagon fusion, highlighted in red) from C_{60} (I_h).

studied at the DFT level: the most stable $C_{58}S$ represents an open cage structure with a nine-membered ring orifice, and a endohedral fullerene based on the nonclassic fullerene was also calculated.[151] Note that the S@C_{58} isomer considered in ref 151 is not the best one and is 8.7 kcal/mol less stable than that based on the conventional fullerene cage (Figure 59a) at the B3LYP/6-31G* level.[146b] Most recently, an intense beam of C_{58}^+ ions were produced by using electron-impact induced dissociation/ionization of C_{60} molecules,[152a] and solid C_{58} films were created in ultrahigh vacuum by utilizing the aggregation process of C_{58} molecules deposited onto highly oriented pyrolytic graphite from a mass selected low-energy ion beam comprising C_{58}^+.[152b] Because of significantly stronger cluster−cluster bonds, the C_{58} film created exhibit much higher thermal stability than the C_{60} solid phase.

Alcami et al.[150] carried out systematic investigations on the structures and electronic energies of neutral, mono-, and dications of fullerenes C_{50}−C_{58}. Interestingly, it was found that the most stable structure of C_{52}^{2+} is the (437,T) isomer (shown in Figure 61) having six adjacent pentagons, which contradicts the PAPR. The C_{52}^{2+}(437,T) is highly aromatic, as suggested by its remarkably negative NICS value (−46.2 ppm at GIAO-6-31G*//B3LYP/6-31G*); its high stability is a consequence of complete filling of the HOMO π shell and the near-perfect sphericity.

2.7 Small Metal-Substituted Metallofullerenes MC_n

While metallofullerenes with metal atoms either inside or outside the carbon cage have been widely

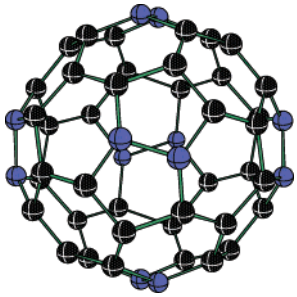

Figure 61. Structure of the C_{52}(437,T) isomer, in which the pentagon−pentagon fusions are highlighted.

studied and well-known,[19,76,126,153,154] metal-substituted fullerenes with metal atoms as part of the carbon cage framework are far less common and less understood.[143,155] Yet, mass spectroscopic and ion mobility studies have disclosed a number of heterofullerenic clusters with metallic heteroatoms incorporated into the carbon cage network.[143,155] The pioneering work by Jarrold et al. demonstrated that niobium-substituted small fullerenes NbC_n^+ (n is an odd number ranging from 29 to 49) could be generated by laser vaporization of graphite/NbC composites.[143a] Similar cage substituted metallofullerenes with such atoms as La,[126a,143b,c] Fe, Co, Ni, Rh,[155a,b] Pt, and Ir[155c,d] were also reported. Of particular interest is the chemistry of Ir- and Pt-containing hereofullerenes MC_x (M = Ir, Pt; $56 \le x \le 59$), among which both the odd- and even-numbered clusters adopt heterofullerene structures. It was demonstrated that the anions of Ir-series heterofullerenes, IrC_x^- ($56 \le x \le 59$), could bind simple alkenes such as 2-butene to form complexes $[IrC_x(2\text{-butene})]^-$, whereas the Pt-containing ones, except PtC_{59}^-, are unreactive toward simple alkenes under similar conditions.[155d]

Few theoretical investigations have been reported with regard to the geometric and electronic structures of these metal-substituted small fullerenes. HF calculations on a heterofullerenic structure of LaC_{29}^+ (Figure 62)[143b] revealed that the contribution of the

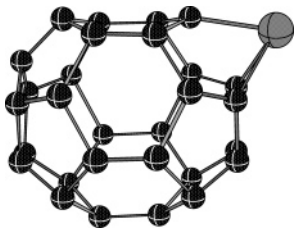

Figure 62. Structure of LaC_{29}^+ metallofullerene derived from D_{5h} C_{30} by substitution of a La atom for a carbon atom at a junction of three pentagons (ref 143b).

La atomic orbitals to the π-system of fullerene is trivial with the three-coordinated La atom protruding far away from the fullerene surface. Similar findings were made on some monosubstituted heterofullerenes such as NbC_{39}^+(cf. Figure 48a),[141] MC_{59} (M = Pt, Ir,[155d] Fe, Co, Ni, Rh[156]), and MC_{69} (M = Co, Rh, Ir).[157] However, the situation for the heterofullerenes MC_{58} (M = Pt, Ir) is a little more complicated. Recent DFT calculations[155d] showed that MC_{58} preferentially adopts a C_{2v}-symmetric structure (Figure 63a) formed by

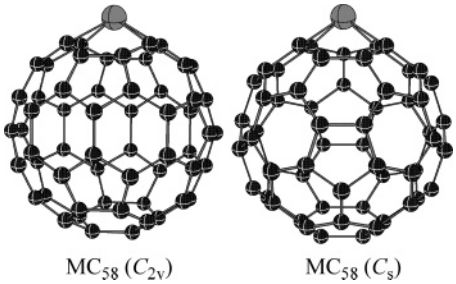

Figure 63. Optimized structures of MC_{58} (M = Pt, Ir) metallofullerenes (ref 155d).

substitution of a metal atom for a C_2 unit at a hexagon−hexagon junction in C_{60}, whereas a C_s-symmetric isomer (Figure 63b) resulted from substituting a C_2 unit at a pentagon−hexagon junction is energetically less favorable. The metal atom is four-coordinated in MC_{58} (C_{2v}) and does not protrude far away from the cage. Both the neutral PtC_{58} (C_{2v}) and anionic IrC_{58}^- (C_{2v}) have a close-shell singlet ground state, in which the M atomic orbitals are rather localized in the occupied states but contribute significantly to the delocalized unoccupied states.[155d] Accordingly, the extent of electron-delocalization within MC_{58} heterofullerenes can be reversibly tuned through redox reactions.

3. π-Conjugation in the Sidewalls of Single-Walled Carbon Nanotubes (SWCNTs) and the Related Sidewall Chemistry

3.1 Geometric and Electronic Structures of SWCNTs

A single-walled carbon nanotube (SWCNT) is a seamless graphene cylinder constructed by rolling-up a two-dimensional (2D) graphite layer in such a way that the end of the roll-up vector $\mathbf{C}_h$ is superimposed on its origin (see Figure 64).[3,4] As such, the

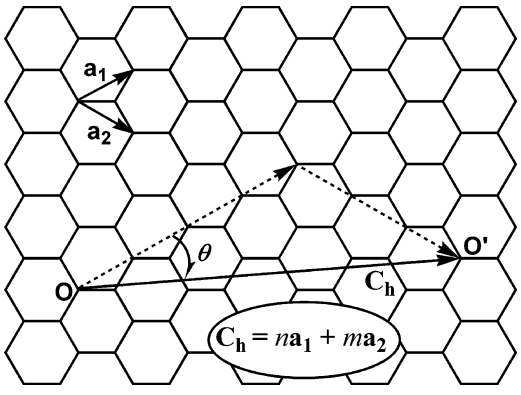

Figure 64. Roll-up vector $\mathbf{C}_h$ ($\mathbf{C}_h = n\mathbf{a}_1 + m\mathbf{a}_2$) and chiral angle θ for a (n,m) SWCNT (for this special case, $n = 5$, $m = 3$), where $\mathbf{a}_1$ and $\mathbf{a}_2$ are the primitive vectors of a graphene sheet.

structure of a SWCNT can be uniquely defined by the roll-up vector, $\mathbf{C}_h = n\mathbf{a}_1 + m\mathbf{a}_2$, and is simply designated by (n,m). By definition, three types of SWCNTs can be constructed, i.e., achiral armchair (n,n) SWCNTs, achiral zigzag (n,0) SWCNTs, and chiral (n,m) SWCNTs ($n > m$ and $m \neq 0$). For a chiral (n,m) SWCNT, the chiral angle, θ, is defined as the angle between the roll-up vector $\mathbf{C}_h$ and the (n,0) zigzag direction (Figure 64).

3.1.1 Zone-Folding Approximation

Because of the aforementioned structural similarity of SWCNTs and graphene sheets, the simplest model to describe the electronic band structure of SWCNTs is the *π-only band theory* that is derived from the band theory of graphite[158] by neglecting the effects of curvature-induced rehybridization (see its definition in subsection 2.1). This simplest model states that an infinite-length SWCNT adopts a one-dimensional band structure fulfilling the periodic boundary condition: $\boldsymbol{k}\bullet\mathbf{C}_h = 2\pi q$, where q is an integer and $\boldsymbol{k}$ is the wavevector quantized along the circumferential direction. Following this model, all infinite-length armchair (n,n) SWCNTs are metallic, whereas an infinite-length SWCNT either of zigzag (n,0) type or of chiral (n,m) type is metallic only if (n-m)/3 is an integer, and otherwise is a semiconductor with a band gap *depending inversely on its diameter*. Such simple predictions were confirmed by both π-only tight binding calculations[159,160] and low-temperature STM observations,[161] which demonstrate that the π-only model is capable of approaching the essential physics of SWCNT band structure. The above treatment is also called zone folding (or confinement) approximation and applies reasonably well for the larger diameter SWCNTs. However, other factors, such as finite curvature and intertube interactions also have significant influence on the electronic properties of SWCNTs.

3.1.2 Curvature Effects

The curvature effects become important for small diameter nanotubes, since their high curvature induces rehybridization of σ, σ^*, π, and π^* orbitals within its graphenic sidewall. Consequently, some narrow tubes that should be semiconducting in the curvature-less zone folding picture, such as (5,0) tubes, are metallic according to the first principles calculations,[162] while some small diameter tubes expected to be metallic have a small gap in the band structure (see below).

The severe curvature may open up a small band gap around its Fermi point, as indicated by full-valence tight binding calculations.[163] Such a consideration led to the development of *a Fermi-point shifting model* proposed independently by Ouyang et al.[164a,b] and Kleiner et al.[164c] The Fermi-point shifting model states that the finite curvature will induce shifts of the Fermi points of SWCNTs from "original Fermi points" (i.e., the Fermi points from simple π-only model). More interestingly, the direction of the Fermi-point shifting was found to be helicity-dependent, e.g., shifting along the circumference direction for "metallic" zigzag (n,0) SWCNTs and shifting along the tube axis for armchair (n,n) SWCNTs.[4c] Consequently, when the curvature effect is taken into account, infinite-length armchair (n,n) SWCNTs remain metallic; however, the (n−m)/3 zigzag and chiral nanotubes have a finite gap proportional to

$1/d^2$ (d is the tube diameter) and sin 3θ (θ is the chiral angle).[163,164d] The expected $1/d^2$ dependence of the $(n-m)/3$ zigzag SWCNT band gap and the zero-band gap of the armchair SWCNTs were confirmed by Ouyang's experiment.[164a]

3.1.3 Intertube Interactions in Nanotube Bundles

Although isolated armchair SWCNTs are metallic in nature, the existence of a small energy gap, namely, "pseudo gap", at the Fermi level was disclosed both theoretically[165] and experimentally[161c,164a] for armchair SWCNTs bundles. Such a phenomenon is attributed to the fact that the n-fold rotational symmetry of an armchair SWCNT is certainly broken upon the intertube interaction within a tightly packed bundle of armchair SWCNTs.

It can be concluded that the unique 1D electronic band structure of SWCNTs depends subtly upon helicity, carbon surface curvature (or diameter), and intertube interactions, and, hence, can be finely tuned by controlling these structural factors. An extreme case is that the electronic properties of SWCNTs can be modified by radial deformation upon external pressure or strain;[166] for example, the band gap of a semiconductive SWCNT can reduce and eventually vanish (e.g., metallization) with increasing applied radial strain.

3.2 Aromaticity of SWCNTs

3.2.1 Clar Valence Bond (VB) Model Description

A general relationship between the aromaticity and helicity (as well as conductivity) of infinite, defect-free SWCNTs has been established recently by Ormsby and King using the Clar aromatic sextet valence bond (VB) model.[167] The Clar VB model[168,169] employs both aromatic sextets (i.e., benzenoid six-electron π-cycles) and conventional two-electron π-bonds to describe the valence-bond structure of polycyclic aromatic hydrocarbons (PAHs). It has been demonstrated that for a large variety of PAHs, the VB structures with the largest number of aromatic sextets best model chemical reactivity, and that the *fully benzenoid* structures, i.e., possessing only aromatic sextets, have large HOMO−LUMO gaps and, of course, display unusual chemical stability.[168−170] For example, the Clar VB structures of four PAHs are depicted in Figure 65; among them only pyrene (Figure 65a) is not fully benzenoid. Indeed, the fully benzenoid dibenzopyrene (Figure 65b) does not show the reactivity of pyrene at all. The fully benzenoid triphenylene (Figure 65c) and hexabenzocoronene (Figure 65d) are also unusually unreactive.[168b] It should be added that Clar's rule on the extra stability of 6nπ-electron PAHs has a wider and more general applicability than the well-known Hückel 4n+2 rule, even though the former has received much less attention than the latter.[169]

Very recently, Ormsby and King applied the Clar VB model to describe the π-bonding (and aromaticity) in infinite-length and defect-free (n,m) SWCNTs.[167] They found that three variations exist, depending on the value of $R(n,m) = m - n$ modulo 3 (Figure 66).

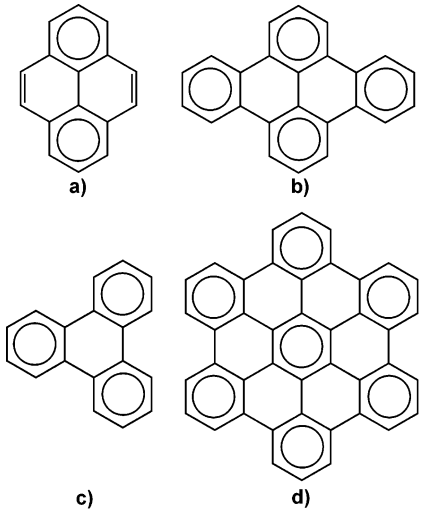

Figure 65. Clar VB representations of (a) pyrene ($C_{16}H_{10}$), (b) dibenzopyrene ($C_{24}H_{14}$), (c) triphenylene ($C_{18}H_{12}$) and (d) hexabenzocoronene ($C_{42}H_{18}$), where the aromatic sextets and the conventional two-electron π-bonds are represented by circles and lines, respectively.

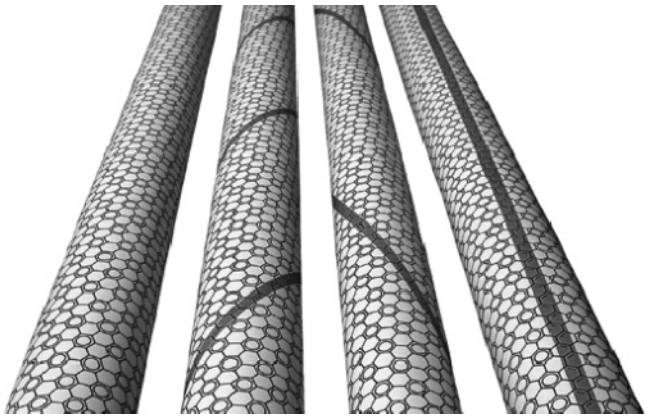

Figure 66. Clar VB representation of (12,9), (12,8), (12,7), and (19,0) SWCNTs (from ref 167).

For a potentially metallic (n,m) SWCNT with $R(n,m) = 0$ (e.g., (12,9)), all π-electrons can be represented by aromatic sextets, and the SWCNT is fully benzenoid; the converse is also true. Since $m - n = 3k$ is known to be a necessary criterion for conductivity in CNTs, only fully benzenoid CNTs are metallic, and only potentially metallic CNTs are fully benzenoid. This behavior is in sharp contrast with that of planar PAHs, among which the fully benzenoid structures always have quite large HOMO−LUMO gaps. This can be explained by the opposite operation of the leapfrog rule, which gives exactly the two disparate results for leapfrog fullerenes and nanotubes, i.e., leapfrog fullerenes have closed shells, and leapfrog infinite nanotubes are metallic in the Hückel model.[171] For a semiconductive SWNCT with $R(n,m) = 1$ or 2 (e.g., (12,8) and (12,7)), a seam of double bonds wraps about the otherwise fully benzenoid SWCNT. However, it is unexpected that for an achiral zigzag $(n,0)$ SWCNT with $R(n,0) = 1$ (e.g., (19,0)), an enatiomeric pair of chiral Clar VB structures can be constructed, each having a seam 60° offset from the tube axis. In this special case, an alternative Clar VB structure having an achiral quinoidal seam parallel to the tube

axis (Figure 66) can be constructed with the same double bond: aromatic sextet ratio as the chrial representations. To support these Clar VB models, Ormsby and King performed NICS calculations (HF/STO-3G//PM3) on a series of short, H-terminated chiral SWCNTs, including (12,9), (12,8), and (12,7) tubes. As demonstrated in Figure 67, the calculated NICS values of these short SWCNTs agree with the Clar VB model.

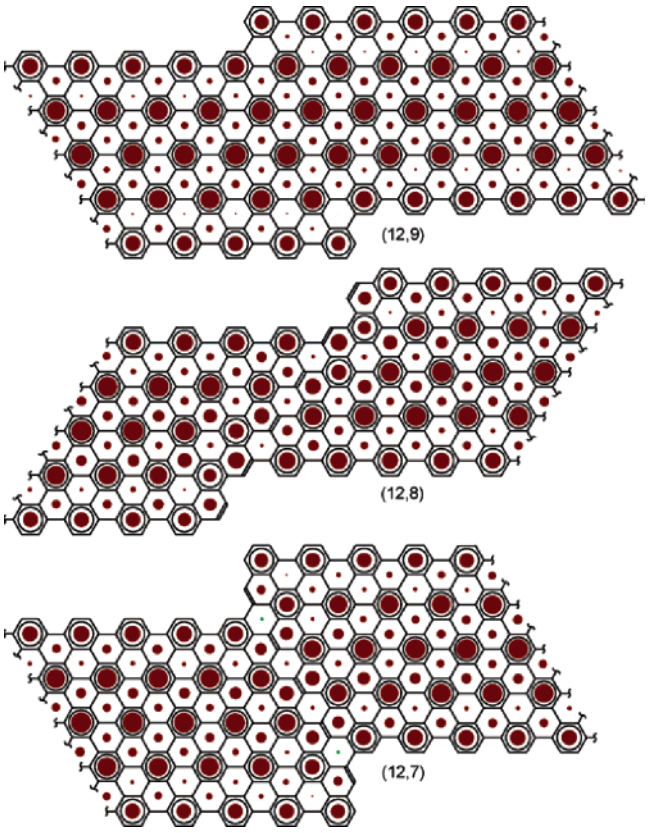

Figure 67. Planar representations of short (12, 9), (12, 8), and (12, 7) CNTs shown with the Clar VB structures. Filled circles represent the magnitude of the average of the NICS values inside and outside the CNT, with the radius normalized to the largest value. Red is negative, and green is positive (from ref 167).

The Clar VB model was also employed to understand the effect of tube length on the structures, aromaticity, and sidewall reactivity of finite-length SWCNTs.[172,173] Nakamura et al. found that the chemical structure of finite-length armchair (*n*,*n*) SWCNT (*n* = 5 or 6) depends on the length of the tube and falls into three different classes, i.e., Kekulé (Figure 68(i) and (iv)), incomplete Clar (Figure 68(ii) and (v)), and complete Clar (Figure 68(iii) and (vi)) structures.[172] More interesting is that the energy of the frontier orbitals and the HOMO−LUMO gap also oscillate periodically with increasing the tube lengths (Figure 69). As a result, the chemical reactivity of finite-length SWCNTs should change periodically as the tube length increases. Indeed, the DFT calculations by Bettinger on the addition of fluorine atom and methylene to the sidewalls of a series of armchair (5,5) SWCNT slabs with the formula, $C_{30+10n}H_{20}$ (*n* = 0, 1, 2, ... 18), confirmed such an inference. Figure 70 shows the oscillation of the calculated addition energy (for fluorine atom) with the increase of the tube length.

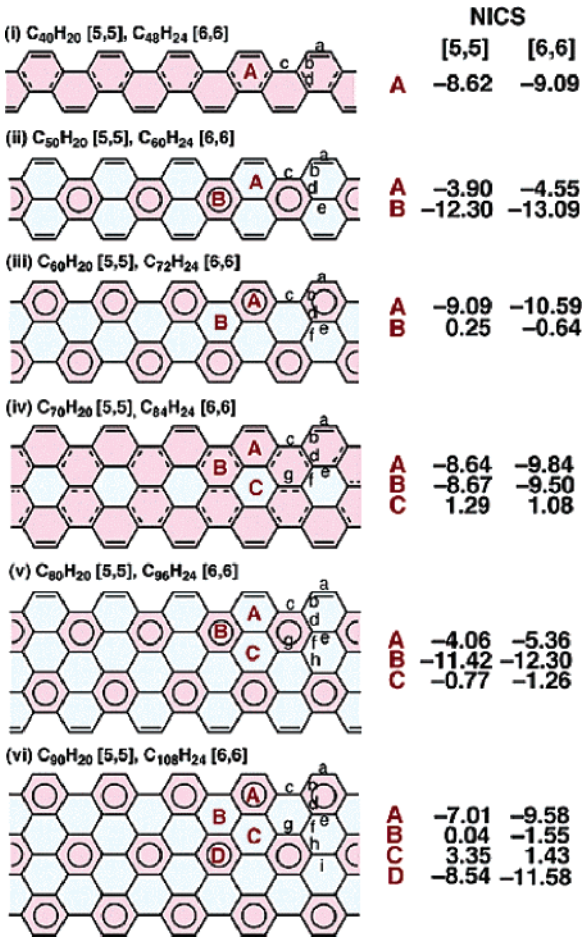

Figure 68. Schematic structures and color-coded NICS (ppm) maps of finite-length (*n*,*n*) SWCNTs (*n* = 5 and 6). Hydrogen atoms are omitted for clarity. Chemical bonds are schematically represented by using single-bond (solid single line; bond length > 1.43 Å), double-bond (solid double line; bond length < 1.38 Å), single-bond halfway to double-bond (solid-dashed line; 1.43 Å > bond length > 1.38 Å), and Clar structures (i.e., fully benzenoid). NICS coding: red, aromatic < −4.5 ppm; blue, nonaromatic > −4.5 ppm (from ref 172).

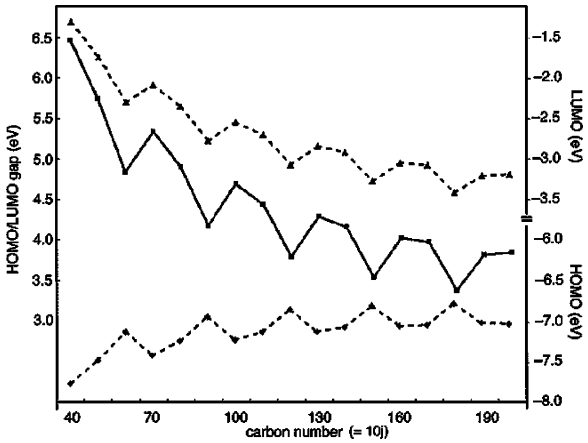

Figure 69. HOMO/LUMO levels and band gap oscillation of the finite-length (5,5) CNTs ($C_{10j}H_{20}$). The values were determined by PM3 level calculations, and the trend parallels the one observed in the B3LYP/6-31G* calculations (for $C_{40}H_{20}$ until $C_{120}H_{20}$) (from ref 172).

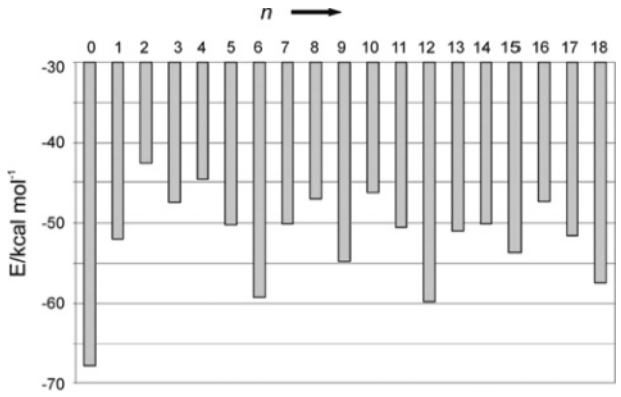

Figure 70. Reaction energies (in kcal mol^{-1}) for the addition of fluorine atom to (5,5) SWCNT models $C_{30+10n}H_{20}$ ($n = 0-18$) as computed at the (U)B3LYP/6-31G*//(U)PBE/3-21G level of theory (from ref 173).

3.2.2 Aromaticity and Chemical Reactivity: A Chemist's View

Carbon nanotubes can be regarded as quasi-1D cylindrical aromatic macromolecules. Aihara showed that both armchair and semiconducting carbon nanotubes have positive resonance energies, and nanotubes with realistic size are as highly aromatic as graphite,[174] although "metallic" nanotubes are slightly less aromatic than semiconducting ones,[175] which is contrast with the Clar VB model rationalization as given above.

Joselevich qualitatively correlated the aromaticity with the chemical reactivity of SWCNTs.[176] According to Joselevich, semiconducting nanotubes are analogous to aromatic [4n+2]annulenes, whereas metallic nanotubes are analogous to antiaromatic [4n]annulenes. Such reasoning explains well the high reactivity of metallic nanotubes over their semiconducting counterparts.[177] However, it is also important to note that a major practical difficulty with functionalization of nanotubes is actually their restricted solubility, which is essentially a matter of molecular size and overrides the steric and electronic factors mentioned above.

3.3 Curvature-Induced Pyramidalization and Misalignment of π-Orbitals

The extent of curvature-induced weakening of π-conjugation within SWCNT depends on the helicity and diameter of the tube, according to the POAV analyses.[4e] Besides the curvature-induced pyramidalization of π-orbitals of carbon atoms (similar to the fullerene case, see Figure 2), curvature also induces misalignment of π-orbitals of carbon atoms within a SWCNT (Figure 71).[4e] As a result, the sidewall of a SWCNT could be more reactive than a flat graphene sheet; a SWCNT of smaller diameter having larger π-orbital pyramidalization and misalignment angles suffers more severe curvature-induced weakening of π-conjugation and, hence, is more reactive. However, due to the different bending pattern, the nanotubes have less curvature compared with fullerenes with comparable diameters;[178] accordingly nanotubes are generally less reactive than fullerenes, and more critical experimental conditions are required to functionalize carbon nanotubes.

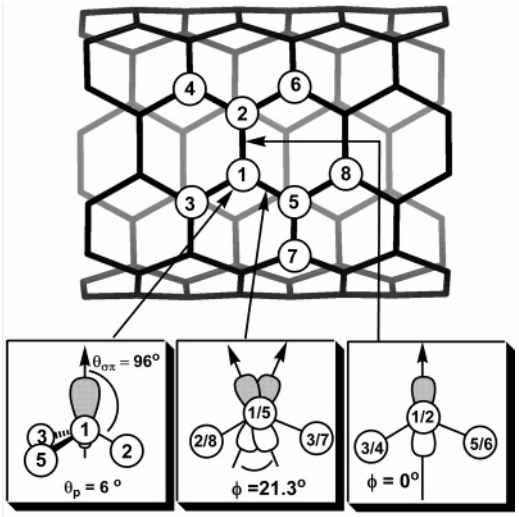

Figure 71. A schematic description of the π-orbital pyramidalization and misalignments in the sidewall of a (5,5) SWCNT. The π-orbital pyramidalization and misalignment angles are designated by θ_p and ϕ, respectively (ref 4e).

A computational analysis on the dependence of exohedral and endohedral sidewall reactivity of SWCNTs on the tube diameter (or sidewall curvature) was performed by Chen et al.[178] For the addition of a univalent X atom (X = H, F) to the sidewalls of a series of short, H-terminated armchair (n,n) SWCNTs ($n = 2-6$), their B3LYP/6-31G* calculations revealed the following effects of curvature on the sidewall reactivity:

(i) Exohedral addition is much more favorable over endohedral addition.

(ii) For the energetically favorable exohedral addition, the addition energy increases with decreases in tube diameter (or with the increase of the pyramidalization angle θ_p of the sidewall carbon atom) (Figure 72).

(ii) In sharp contrast to the inert concave surface of fullerenes.[179] the inside wall of normal SWCNTs is still reactive to hydrogen and fluorine radicals.

In addition to Chen's work on the single atom addition, theoretical work by Lu et al.[180] on the 1,3-dipolar cycloaddition (1,3-DC) of O_3 molecule to the sidewalls of a series of armchair (5,5) SWCNTs with n ranging from 5 to 10 (Figure 73), that by Park et al.[181] on the monovalent functional group additions and that by Zheng et al.[182] on the sidewall SWCNT additions of O/NH/CH_2 electrophiles predicted a similar trend.

Experimental evidence on the aforementioned dependence of sidewall reactivity on the tube diameter is scarce. Indirect evidence can be extracted from the experiments on the fluorination[183] of HiPCO−SWCNTs (produced by a high-pressure CO disproportionation process[184]) and L-SWCNTs (laser-ablated graphite-grown carbon nanotubes[185]). It was found that under the same fluorination condition more fluorine atom can be attached on the sidewalls of HiPCO−SWCNTs than on L-SWCNTs, while HiPCO−SWCNTs have smaller average tube diameters ($\sim$ 1 nm) than L-SWCNTs ($\sim$ 1.38 nm).[183]

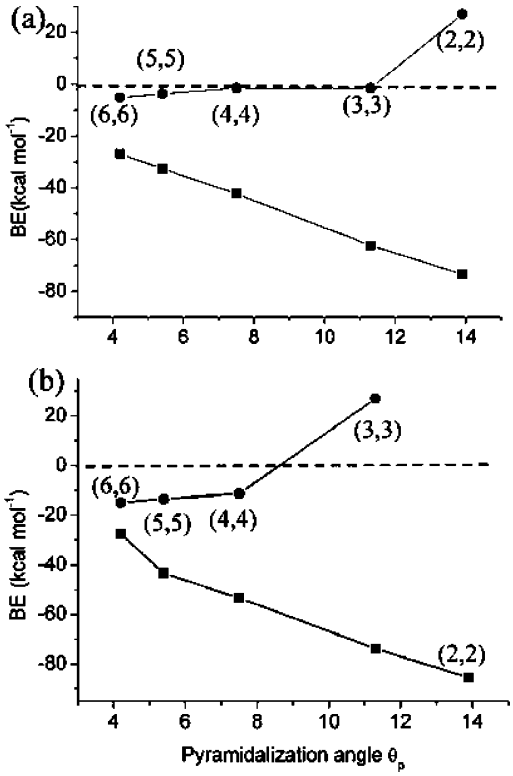

Figure 72. Dependence of exohedral (■) and endohedral (●) binding energies (B3LYP/6-31G*) on θ_p of (n,n) SWCNTs ($n = 2-6$). (a) Addition of H, (b) addition of F. Reprinted with permission from ref 178. Copyright 2003, VCH.

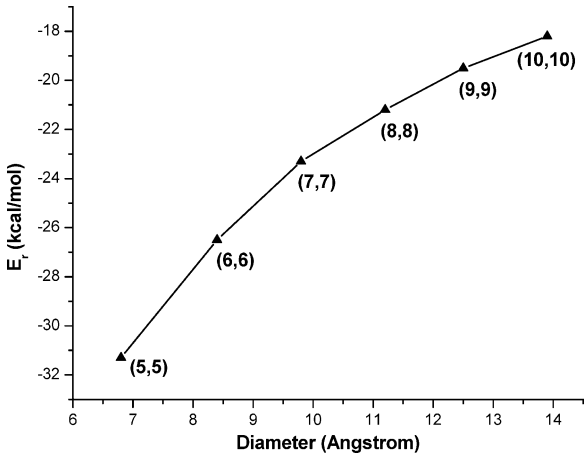

Figure 73. Predicted exothermicity (E_r) of the 1,3-DC reaction of ozone vs diameters of (n,n) SWNTs (from ref 180).

3.4 Sidewall Chemistry of SWCNTs Related to the Curved π-Conjugation and Aromaticity

Bearing a curved graphene-like structure, the sidewalls of carbon nanotubes were once believed to be chemically quite stable and, meanwhile, display notorious insolubility. This impedes the separation and manipulation of SWCNTs for various specific applications. Chemical modification of SWCNTs, although it appears to be a great challenge for chemists and material scientists, is highly desirable since it may provide a chemical means to circumvent such a hindrance and may furnish SWCNTs new physical and chemical properties (e.g., increased solubility, increased chemical reactivity, high bioactivity, and biocompatibility) for more specific applications. Indeed, efforts made in this field are remarkable within the past five years; successful approaches toward chemically functionalized SWCNTs reported so far can be generally divided into three categories, namely, defect functionalization, noncovalent (supramolecular) functionalization, and covalent functionlization of the sidewalls.[4e,186,187] Among these, covalent sidewall functionalization appears to be rather challenging, as a result of the rather high chemical stability of the graphene-like sidewalls of SWCNTs. Yet several experiments successfully approaching covalent sidewall-derivatization have been reported, which include fluorination,[183] addition of alkyl and phenyl radicals,[188,189] [2+1] cycloaddition,[188,190] birch reduction,[190a,191] electrochemical and solvent-free arylations,[177a,192] 1,3-dipolar cycloaddition (1,3- DC),[193,194] ozonolysis,[195] amination,[196] osmylation,[177b,197] and Diels−Alder (DA) reaction,[198] etc. In the meantime, a number of theoretical predictions have also been made on the viability of sidewall derivatization of SWCNTs by ozonization[199] and 1,3-dipolar cycladditions,[180,199] [4+2] cycloaddition (also known as Diels−Alder reaction),[200] osmylation,[201] hydroboration,[202] [2+1] cycloaddition,[203] and oxidation.[204] On one hand, these covalent sidewall-derivatizations were found to result in, for most cases reported,[186−198] a remarkable increase in the solubility of functionalized SWCNTs and, for some specific cases,[193] marvelous bioactivity and biocompatibility. On the other hand, these experimental and theoretical findings convincingly provide evidence for the curvature-induced higher chemical reactivity of nanotube sidewalls than that of flat graphenes,[4e,205] and constitute a brand-new topic of modern chemistry, namely, *covalent sidewall chemistry of carbon nanotubes*.[4e,187]

3.4.1 Fluorination

Fluorination is probably the first chemical means that was found for the chemical derivatization of carbon nanotubes.[183] In 1998, Margrave et al.[183b] found that F_2 can react with SWCNTs in the temperature range of 250−600 °C, giving rise to fluorinated SWCNTs (namely, F-SWCNTs). The reaction can be more efficient in the presence of HF (as catalyst). The saturated ratio could be as high as C/F = 2:1 for F-SWCNTs. Higher level of fluorination led to the collapse of the carbon skeleton of the CNTs.

The structures of F-SWCNTs have been actively investigated both experimentally and theoretically. Controversy exists regarding the favorable pattern of F addition onto the sidewalls of SWCNTs.[206] On the basis of scanning tunneling microscopic (STM) images and semiempirical CNDO and AM1 calculations, Kelly et al.[206a] proposed two possible addition patterns (Figure 74), i.e., 1,2-addition and 1,4-addition, and concluded that the 1,4-addition pattern is more stable. On the contrary, more sophisticated DFT calculations (PBE/3-21G and LSDA/3-21G) using periodic boundary conditions (PBC) on a fluorinated (10,10) SWCNT with a C/F ratio of 2:1 pre-

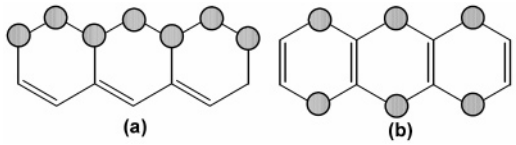

Figure 74. Two possible addition patterns of F atoms on the sidewalls of F-SWCNTs: (a) 1,2-addition and (b) 1,4-addition.

dicted that the 1,2-addition pattern is energetically favorable over the 1,4-addition one by about 4 kcal/mol per C_2F unit.[206b] Such a small energy difference between the two addition patterns implies that both types of F-SWCNTs probably coexist. Further PBC-PBE/3-21G calculations on a series of armchair F-SWCNTs (ranging from (3,3) to (12,12)) of C_2F stoichiometry[206c] revealed that the thermodynamic stability of these F-SWCNTs as well as the average C−F bond energy decreases with increase of tube diameter.

On the other hand, Bauschlicher[206d] investigated the addition of several fluorine atoms on a short, H-terminated zigzag (10,0) SWCNT by means of the ONIOM approach[207] and found that the F atoms tend to bond next to existing F atoms, accounting well for the STM observation that the fluorinated regions in a F-SWCNT appear to form bands around the tube.

F-SWCNTs display physical and chemical properties differing significantly from those of pristine SWCNTs, including solvation property, conductivity, and chemical reactivity. F-SWCNTs were shown to have much better solvation properties than pristine SWCNTs.[208] F-SWCNTs can form metastable solutions in several ordinary organic solvents such as DMF, THF, and alcohols after sonication but are insoluble in perfluorinated solvents and water.

In F-SWCNTs, the sidewall carbon atoms, on which F atoms are attached, are tetrahedrally coordinated and adopt sp^3 hybridization. This perturbs the periodicity of the pseudo 1D lattice and destroys the delocalized electronic band structure of the otherwise metallic or semiconductive SWCNTs. Hence, F-SWCNTs are insulating. DFT calculations[206b] revealed that both the bottom level of conduction band and the Fermi level of F-SWCNTs are drastically lowered in energy compared to that of pristine SWCNTs. As a result, F-SWCNTs are better electron acceptors and much more reactive toward nucleophilic reagents than are pristine SWCNT. Indeed, F-SWCNTs have been found to react with many nucleophilic reagents, e.g., organolithium compounds and Grignard reagents,[209,210] leading to a variety of new derivatives of SWCNTs. Some typical chemical reactions of F-SWCNTs are summarized as follows

(i) Reactions with Hydrazine and Diamines. F-SWCNTs react with hydrazine (N_2H_4) at room temperature, leading to defluorination of the F-SWCNTs with release of N_2 and HF.[183b] The balanced equation for this highly exothermic process is $4C_nF + N_2H_4 \rightarrow 4C_n + N_2 + 4HF$. This process can be useful for purification of SWCNTs and for production of partially fluorinated SWCNTs with controlled fluorine contents. On the other hand, the reaction of terminal diamines, $H_2N(CH_2)_nNH_2$ (n = 2, 3, 4, 6), with F-SWCNTs in the presence of a catalytic amount of pyridine was found to adopt a different mechanism (Scheme 2) that results in alkyldiaminated

Scheme 2

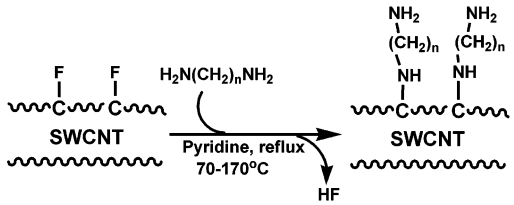

SWCNTs.[211] Because of the presence of terminal NH_2 groups, the as-obtained alkyldiaminated SWCNTs are soluble in dilute acids and water. More important, the known chemistry of primary amines can thus be employed to further functionalize such amino-functionalized SWCNTs, e.g., to bind amino acids and DNA to the sidewalls of SWCNTs for biochemistry applications.

(ii) Reactions with Organolithium Compounds and Grignard Reagents. Both reagents can actively react with F-SWCNTs, forming alkylated SWCNTs (Scheme 3).[209,210] The alkylated SWCNTs

Scheme 3

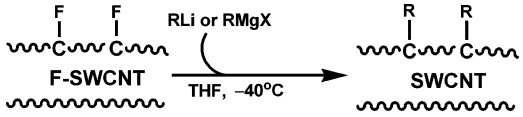

are soluble in common organic solvents such as THF and chloroform, and can be completely dealkylated upon heating at 500 °C in Ar with recovery of the pristine SWCNTs.

3.4.2 1,3-Dipolar Cycloadditions: A Facile Way to Sidewall Functionalization

1,3-Dipolar cycloaddition (1,3-DC) is the union of a 1,3-dipolar molecule with a multiple bond system (a dipolarophile) to form a five-membered ring.[212] The 1,3-dipole is a triad of atoms that has a four-electron π system and can be represented by a zwitterionic octet resonance structure.[212a,213] The great majority of 1,3-dipoles are isoelectronic with either 16-valence-electron (e.g., nitrile ylide and diazomethane) or 18-valence-electron (e.g., azomethine ylide and ozone) compounds. The dipolarophiles are usually olefins or acetylenes, but other multiple bonds, such as the C=N bond of imines and the C=O bond of aldehyde, also can act as dipolarophiles.[212−214] The 1,3-DC process can be understood in terms of the orbital symmetry and frontier molecular orbital (FMO) theory[213] or in terms of the configuration mixing model.[215] Scheme 4 depicts the relevant FMOs of a 1,3-dipolar molecule and a dipolarophile (e.g., ethylene) involved in a 1,3-DC reaction. Because either 1,3-dipoles or dipolarophiles may contain one or more heteroatoms (N,O and S, etc.), the 1,3-DC process is one of the most useful methods for the synthesis of five-membered ring heterocycles and has been widely exploited in synthetic organic chemistry and pharmaceutical chemistry.[212a] A very important extension of 1,3-DC is its recent applications in the chemical

Scheme 4

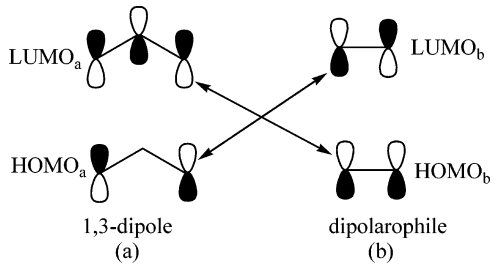

functionalization of highly π-conjugated carbon allotropes, fullerenes,[216,217] and SWCNTs.[180,193,194,199] Unfortunately, due to the chemical stability of SWCNTs, only most active 1,3-dipoles such as ozone, azomethine ylide, and nitrile imine have been found experimentally to react with the sidewalls of SWCNTs. These brand new 1,3-DC processes on the sidewalls of SWCNTs are summarized in the following subsections.

3.4.2.1 1,3-DC of Ozone − Ozonization of SWCNTs. Ozone (O_3) is a highly reactive, 18-valence-electron 1,3-dipole that readily undergoes 1,3-dipolar cycloaddition (1,3-DC) reaction with olefins followed by complicated decomposition/isomerization of the thus-formed primary ozonide (POZ).[218] Such an ozonolysis process follows the Criegee's mechanism (Scheme 5).[218a] The first step, i.e., the ozonization of

Scheme 5

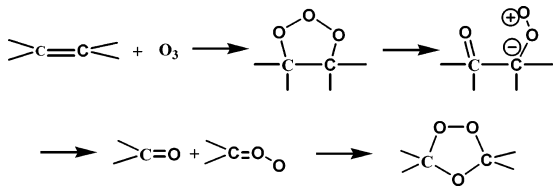

olefin, is the 1,3-DC of O_3 onto the alkenic group. Similar ozonization process has been found to occur on the highly π-conjugated C_{60}, producing fullerene ozonide ($C_{60}O_3$) followed by the formation of $C_{60}O$.[217] It is these chemical precedents that stimulated the recent theoretical exploration of the viability of sidewall-ozonization of SWCNTs,[180,199a] which was soon exploited experimentally.[195,219]

In early 2002, Lu et al.[199a] conducted the first theoretical investigation regarding the sidewall-ozonization of an armchair (5,5) SWNT by means of a two-layered ONIOM(B3LYP/6-31G*:AM1) approach [207] using a short, H-terminated tube model ($C_{90}H_{20}$). The calculations revealed that the 1,3-DC of O_3 onto the tube wall is exothermic and somewhat site-selective, i.e., the addition onto the 1,2-pair site is much more favorable over the addition onto the 2,3-pair site (see Figure 75a for definitions of the sites), preferentially yielding the primary SWCNT-ozonide (Figure 75b). Thermolysis of the as-formed sidewall-ozonides was predicted to preferentially lead to desorption of ozone rather than to the formation of sidewall-epoxides with elimination of O_2. An exothermicity of ~20.2 kcal/mol and an activation barrier of 2.9 kcal/mol for the formation the primary SWCNT-ozonide were predicted by cluster model calculations (B3LYP/6-31G*) using a larger model ($C_{130}H_{20}$).[199d]

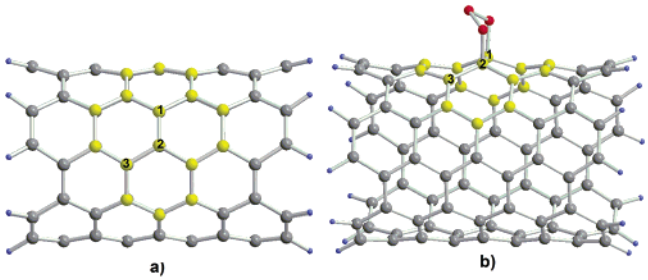

Figure 75. (a) A short, H-terminated tube model of (5,5) SWCNT; (b) geometry of the primary SWCNT-ozonide by 1,3-DC of O_3 to the 1,2-bond.

Note that a (5,5) nanotube is among those of the smallest SWCNTs that can be experimentally synthesized;[220] the theoretical prediction based on the (5,5) tube should be considered to be only an upper boundary of the reactivity of realistic samples. Subsequent theoretical effort[180] was made to explore the viability of the 1,3-DC of ozone on the sidewalls of a series of armchair (n,n) SWCNTs ($n = 6-10$) modeled by $C_{26n}H_{4n}$ tubes and, meanwhile, to unravel the dependence of the 1,3-DC reactivity of the nanotube sidewalls on their diameters. The ONIOM calculations showed that the 1,3-DCs of O_3 to the sidewalls of these larger SWCNTs are also plausible and that *the bigger the pyramidalization angles of the tube wall carbon atoms are*, *the higher reactivity the tube wall carbon atoms display in the addition reaction* (cf. Figure 73). (Caution should be paid when applying the ONIOM approach and short tube models for the study of sidewall chemistry of SWCNTs, as was discussed in refs 172, 173, 199b,c, 203b,c,d and section 3.4.5.3 and section 5) The theoretical finding[199a] demonstrates, for the first time, the viability of functionalizing the sidewalls of SWCNTs by means of 1,3-dipolar cycloadditions of 1,3-dipolar molecules.

The theoretically predicted sidewall-ozonization of SWCNTs was then confirmed and exploited experimentally by Wong et al.[195,219] in the purification and organic functionalization of SWCNTs. In the experiments, ozonolysis of HiPCO SWNTs dispersed in methanol was carried out on a commercial Welsbach ozonolysis apparatus at −78 °C, affording primary SWCNT-ozonides. The as-generated primary SWCNT-ozonides were subject to cleavage by independent chemical treatment with various "cleaving" agents such as hydrogen peroxide (H_2O_2), dimethyl sulfide (DMS), and sodium borohydride ($NaBH_4$), yielding a high proportion of carboxylic acid/ester, ketone/aldehyde, and alcohol groups on the nanotube surfaces.[195a] Such a process led to purified nanotubes by removing amorphous carbon and metal impurities from raw HiPCO nanotubes, broadening the chemical processability and reactivity of SWCNTs by introducing a large number of oxygenated functional group on the sidewalls of SWCNTs.[195,219]

3.4.2.2 1,3-DC of Azomethine Ylides (the Prato Reaction). Prato et al.[193a] reported the first experiment of the 1,3-DC on SWCNTs in early 2002. The 1,3-diplolar molecules used in their experiment were a series of azomethine ylides generated in-situ by condensation of an α-amino acid and an aldehyde (Scheme 6). An analogous synthetic strategy was

Scheme 6

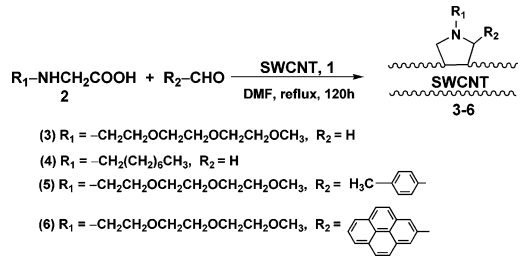

widely applied to the organic functionalization of C_{60} fullerene.[216] Prato et al. found that this protocol is capable of functionalizing different types of carbon nanotubes, including long purified SWCNTs, short oxidized SWCNTs, and purified MWCNTs obtained from Bucky USA as well as HiPCO SWCNTs obtained from Carbon Nanotechnologies, Inc. The heterogeneous reactions (Scheme 6) were performed at 130 °C for 5 days, yielding functionalized SWCNTs (**3**−**6**) with five-membered pyrrolidine adducts on their sidewalls. The abundance of pyrrolidine adducts (about one pyrrolidine adduct corresponding to about 95 carbon atoms of SWNTs) on the tube walls largely improves the solubility of SWNTs; the thus-functionalized nanotubes were found to be remarkably soluble in most organic solvents and even in water. For example, the modified SWCNT **3** ($R_1 = -CH_2CH_2OCH_2CH_2OCH_2CH_2OCH_3$, $R_2 = H$) could reach a solubility of 50 mg/mL in $CHCl_3$ without sonication.[193a]

A theoretical investigation of the 1,3-DC of azomethine ylide ($H_2CN(H)CH_2$) onto the sidewall of an armchair (5,5) SWCNT was performed by Lu et al.[180] using a two-layered ONIOM approach. In accordance with the experimental finding, the ONIOM(B3LYP/6-31G*:AM1) calculations predicted that the heterogeneous 1,3-DC reaction is exothermic by 39.3 kcal/mol with an readily accessible activation energy of 3.4 kcal/mol. This heterogeneous 1,3-DC reaction is by 17.3 kcal/mol less exothermic than its molecular analogue, the gas-phase reaction of $H_2CN(H)CH_2$ with ethylene (C_2H_4). The lower exothermicity of the reaction on the tube wall can be ascribed to the rather high π-conjugation within the nanotube sidewall. As a result, the pyrrolidine adducts on the tube wall can be easily detached upon thermal treatment, facilitating the purification of SWCNTs.

An immediate application of the Prato reaction is the purification of carbon nanotubes.[193b] Raw sample of HiPCO SWCNTs always contains metal particles as a result of using transition metal catalysts in the synthesis of SWCNTs. Organic functionalization of such raw sample by means of the 1,3-DC protocol resulted in the greatly enhanced solubilization of SWCNTs but left metal impurities insoluble. The organic groups covalently attached on the sidewalls of SWCNTs can be removed simply by heating at 350 °C, leaving carbon nanotubes intact and purified. As a result, the missing electronic properties in the functionalized carbon nanotubes can be fully recovered in the purified carbon nanotubes.[193b] Such derivatization-enhanced solubilization and purification of SWCNTs provide a high flexibility in routine manipulation of SWCNTs.

Further applications of the Prato reaction are the peptide[193c] and amino acid[193d] functionalization of carbon nanotubes, a stepping stone to biological applications of carbon nanotubes. The amino acid functionalization of SWCNTs was achieved by following the synthetic processes shown in Scheme 7.

Scheme 7

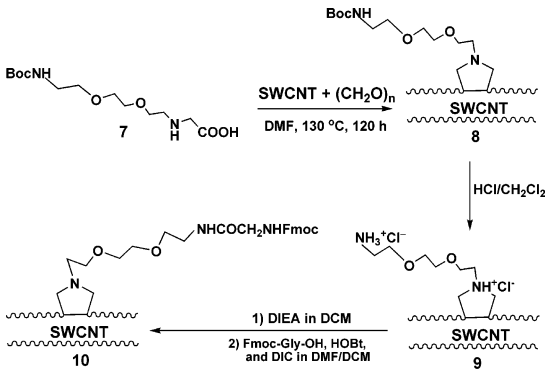

The first step is the 1,3-DC of an azomethine ylide (generated by condensation of amino acid **7** and paraformaldehyde) onto the sidewalls of SWCNTs, yielding N-protected amine functionalized SWNTs **8**. Subsequent chemical treatment of the amine functionalized SWCNTs **8** solution (in dichloromethane) by gaseous HCl could remove the N-*tert*-butoxycarbonyl (Boc) protecting group at the chain-end, producing amine functionalized SWCNTs **9**. **9** are highly water-soluble (a solution made of 20 mg of **9** in 1 mL of water can be stable for more than one month with no precipitation). The high water-solubility of **9** is of critical importance to extend the applications of CNTs to medicinal chemistry. The free amino group at the chain-end of the modified SWCNTs **9** can be easily derivatized with N-terminal protected amino acid, affording the N-terminal amino acid functionalized SWCNTs **10**.[193d] Moreover, the amine functionalized and water-soluble SWCNTs **9** can be a starting point for the covalent attachment of bioactive peptides onto SWCNTs.[193c] This target can be approached by two different methods: (i) the fragment of condensation of fully protected peptides[221] and (ii) selective chemical ligation.[222] Significantly, it was found that the as-produced peptide-SWCNT conjugate is "immunogenic, eliciting of antibody response of the right specificity". Thus, the peptide−SWCNT conjugates could be potentially useful in disease diagnosis and vaccine delivery.[193c]

The high versatility of the Prato reaction is also beneficial to the development of novel SWCNT-based nanohybrids for nanotechnological applications.[194] For example, amidoferrocenyl-functionalized SWCNTs **12** were prepared by following the Prato's protocol (Scheme 8). Upon photoexcitation with visible light, such a novel ferrocene−SWCNT nanohybrid displays fascinating "intramolecular" electron transfer between the attached ferrocene (Fc) and SWCNT, producing long-lived $SWCNT^{\bullet-}$-$Fc^{\bullet+}$ species.[193e] It was also found that **12** can work as an efficient exoreceptor for the redox recognition of $H_2PO_4^-$,[193f] owing to the presence of the amidoferrocenyl group.[223]

Scheme 8

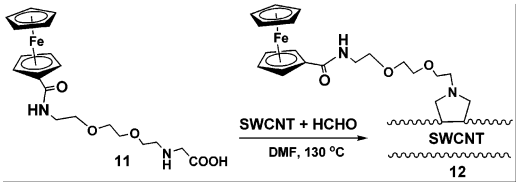

3.4.2.3 Addition of Other 1,3-Dipoles. Besides the most reactive 1,3-dipoles, ozone and azomethine ylide, the viability to covalently attach other 1,3-dipolar molecules (e.g., nitrile ylide and nitrile imine) on the sidewall of an armchair (5,5) SWCNT by 1,3-DC reaction were examined theoretically using a two-layered ONIOM approach.[180] The 1,3-dipoles concerned include five 16-valence-electron (16VE) 1,3-dipoles, i.e., nitrile ylide ($HCNCH_2$), nitrile imine (HCNNH), nitrile oxide (HCNO), diazomethane (H_2CN_2), and methyl azide (CH_3N_3), and an 18-valence-electron (18VE) 1,3-dipole, i.e., nitrone ($H_2CN(H)O$). The predicted reaction heats and activation energies for the 1,3-DCs of these 1,3-dipoles to the sidewall of an armchair (5,5) SWCNT and to ethylene are listed in Table 4.[180] These theoretical data suggest that the 16VE nitrile ylide and nitrile imine are reactive enough to react with the tube wall. Hence, these two 1,3-dipoles are the best candidates for experimentalists to try, in addition to the most reactive azomethine ylides and ozone.

Following the theoretical prediction, the 1,3-DC of nitrile imine to SWCNTs was recently realized and exploited to synthesize photoactive derivatives of SWCNTs **18** (Scheme 9).[193g] The whole synthetic process starts from acid-purified HiPCO SWNCTs **13** containing carboxylic acid groups at their open ends. Esterification of **13** results in the ester-modified SWCNTs **14**. The nitrile imine **17** is generated in-situ from its molecular precursor **16**. The 1,3-DC addition of nitrile imine **17** to the sidewalls of ester-modified SWCNTs **14** produces the pyrazoline-modified SWCNTs **18**, which are photoactive.

Scheme 9

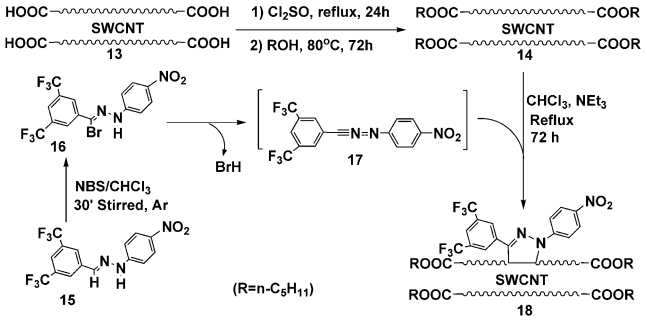

3.4.3 Diels-Alder Cycloaddition

Generally, a DA reaction occurs between a 1,3-diene (e.g., 1,3-butadiene) and a dienophile (e.g., ethylene), involving four π-electrons of the 1,3-diene and two π-electrons of the dienophile. Accordingly, a DA reaction resembles a 1,3-DC reaction mechanistically and both types of reaction have been referred to as $[4\pi+2\pi]$ cycloaddition.[225,226] Such a mechanistic resemblance inspired one of us to investigate the viability of DA reactions on the sidewalls of SWNTs.[200] The ONIOM(B3LYP/6-31G*:AM1) calculations[200] revealed that among the three dienes (**19**, **20**, and **21**) concerned, the latter two dienes (i.e., *o*-quinodimethanes **20** and **21**) can be attached to the sidewall of a (5,5) SWCNT by following the DA mechanism with substantial exothermicity, whereas the DA addition of the prototype diene, 1,3-butadiene (**19**), onto the tube wall is nearly thermoneutral and kinetically unfavorable. The much higher reactivity of the *o*-quinodimethanes than that of butadiene can be definitely ascribed to the much stronger aromatic stabilization at the transition states and products in the DA reactions of *o*-quinodimethanes.[200,227] Note that similar effects have been shown to be advantageous to the chemical functionalization of fullerenes.[227,228]

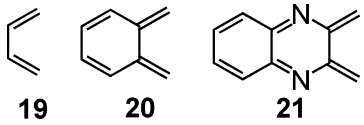

Experimental verification of such aromaticity-facilitated DA reactions on the sidewalls of SWCNTs was reported very recently by Delgado et al.[198] The DA functionalization of the ester-functionalized SWCNT **14** was performed with *o*-quinodimethane (generated in situ from 4,5-benzo-1,2-oxathiin-2-oxide **22**) under microwave irradiation (Scheme 10). The product, modified SWCNT **23**, was characterized by ^{1}H NMR, UV−Vis, FT-IR, FT-Raman, and surface force microscopy (SFM).

Table 4. Calculated Reaction Energies (E_r, in kcal/mol) and Barrier Heights (E_a, in kcal/mol) for the Cycloadditions of a Series of 1,3-Dipoles to the 1,2-Pair Site on the Sidewall of a (5,5) SWNT and to Ethylene (C_2H_4)[a]

		16VE 1,3-dipoles					18VE 1,3-dipoles		
		$HCNCH_2$	HCNNH	HCNO	H_2CN_2	CH_3N_3	$H_2CN(H)CH_2$	$H_2CN(H)O$	O_3
(5,5) SWNT[b]	E_r	−38.5	−28.6	−13.2	−3.2	6.1	−39.3	−5.0	−31.3
	E_a	13.7	15.3	20.6	22.1	29.2	3.4	15.5	2.8
	E_a^{retro}	52.2	43.9	33.8	25.3	23.1	42.7	20.5	34.1
C_2H_4[c]	E_r	−63.2	−55.2	−38.7	−30.0	−22.9	−56.0	−23.2	−56.6
	E_a	8.7	8.0	13.0	16.1	17.7	5.9	16.6	−1.8
	E_a^{retro}	71.9	63.2	51.7	46.1	40.6	61.9	39.8	56.6

[a] The barrier heights (E_a^{retro} in kcal/mol) of the retro-1,3-DC reactions are also given (from ref 180). [b] Data obtained by two-layered ONIOM(B3LYP/6-31G*:AM1) calculations. [c] Data obtained at the B3LYP/6-31+G* level of theory (see ref 224).

Scheme 10

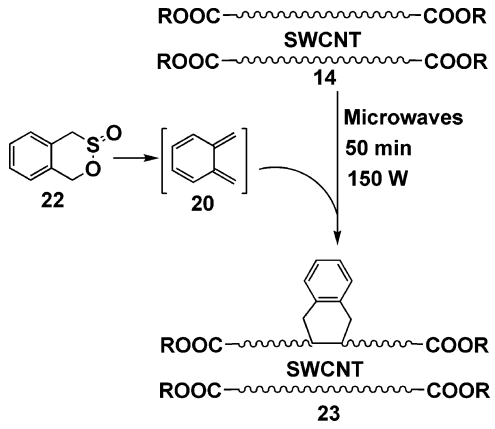

3.4.4 Sidewall Osmylation: Base-Catalyzed and Photo-Promoted Reactions

Transition metal oxides such as OsO_4 and MnO_4^- containing metal-oxo groups were long known to be powerful oxidants in the oxidation of alkenes.[229] OsO_4 is among the most powerful ones; the base-catalyzed [3+2] cycloaddition of OsO_4 with alkenes (i.e., osmylation) occurs readily at low temperatures (Scheme 11), forming osmate esters that can be further

Scheme 11

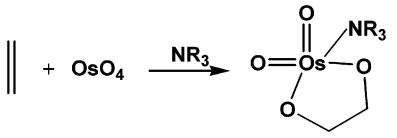

hydrated to give rise to diols.[229,230] An interesting extension of this reaction is the osmylation of fullerens, which gave birth to the first exohedral fullerene-metal complex single crystal.[231]

In light of these chemical precedents, it was proposed that analogous process could be viable on the sidewalls of SWTNs.[201] The inference was supported by QM/MM calculations on the [3+2] cycloaddition of OsO_4 on the sidewall of an armchair (5,5) SWNT.[201] The calculations predicted that the heterogeneous [3+2] cycloaddition of OsO_4 could be viably catalyzed by organic base, giving rise to osmylated SWCNT **24** (Scheme 12).

Scheme 12

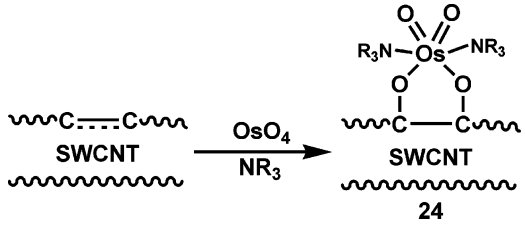

Although this theoretical prediction has not been confirmed experimentally, it was reported by Cui et al.[197a] that sidewall-osmylation of SWCNTs with the use of OsO_4 vapor could be approached by UV irradiation in the presence of O_2, which immediately brought about an increase in resistance for the carbon nanotube. Without UV irradiation, the resistance of the as-osmylated nanotube did not show any further change. After the removal of OsO_4 vapor, the original resistance could be slowly recovered by UV irradiation in a vacuum or in the O_2 atmosphere.[197a] By analogy with the photostimulated osmylation of arenes,[232] they proposed that the following mechanism to account for the UV-photostimulated sidewall-osmylation of carbon nanotube (Scheme 13): the first

Scheme 13

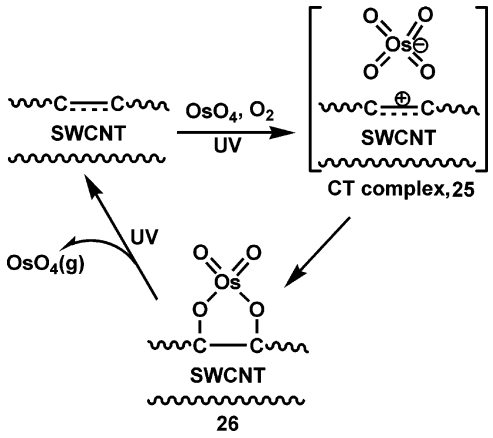

step, which is rate-limiting, is a photoinduced charge transfer from nanotube to OsO_4, yielding a metastable charge-transfer (CT) OsO_4/nanotube complex **25**; the second step is the quick formation of the osmyl ester adduct **26**. It was speculated that oxygen plays a role to assist the photoinduced charge transfer.[197a] This speculation is not convincing, given the fact that oxygen is indispensable for the photosimulated sidewall-osmylation but was not needed in the osmylation of arenes at all. This proposed reaction mechanism was also not supported by our ONIOM prediction that the simple osmyl ester adduct **26** is thermally unstable (or, more exactly, metastable).[201,233] Hence, further investigation is still desired to elucidate the reaction mechanism.

Very recently, a comprehensive experimental investigation was conducted by Wong et al. to understand the photopromoted (OsO_4 + SWCNT) reaction in solution phase.[197b] They showed that such a solution-phase photoreaction occurs selectively with metallic SWCNTs in the presence of O_2 and UV irradiation at 254 nm, leading predominantly to thickly coated SWCNTs that are densely covered with OsO_2. A reaction mechanism analogous to the photoactivated osmylation reactions of benzenoid hydrocarbons (Scheme 14)[232] was proposed to account for

Scheme 14

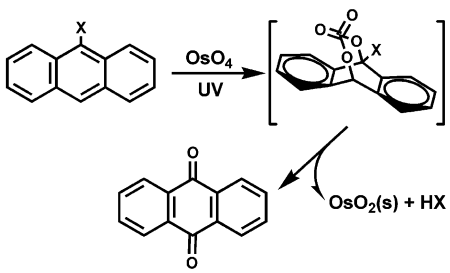

the selectivity. Under UV irradiation at 254 nm, OsO_4 is photoactivated from its A_1 ground state to

the T_2 excited state, which is more oxidizing. Note that the ionization potentials of metallic SWCNTs (e.g., ~6.4 eV for (5,5) SWCNT[234] and 6.0 eV for (4,4) SWCNT[235]) are lower than those of common arenes (9.23 eV for benzene and 7.11 eV for the electron-rich 9,10-dimethylanthracene[236]). Thus, the higher electrophilicity of the excited OsO_4 triggers electron transfer from SWCNTs to the oxide, leading to the formation of a short-lived charge-transfer (CT) complex, $[SWCNT]^+[OsO_4]^-$. This is followed by subsequent formation of covalently bonded complex intermediate (similar to the one shown in Scheme 14 for anthracene oxidation to anthraquinone[232a]). The final step is the oxidation of SWCNTs with precipitation of OsO_2. Within the whole process, the formation of the CT complex is of critical importance. Hence, oxidation of metallic SWCNTs should be favored over that of semiconductive SWCNTs, since semiconductive SWCNTs are much less electron-donative than metallic SWCNTs.[237]

3.4.5 [2+1] Cycloadditions

3.4.5.1 Addition of Carbene. The [2+1] cycloaddition of dichlorocarbene (CCl_2) was reported for the first time by Haddon et al.[190a−d] The synthetical protocol is presented in Scheme 15. In 2001, the

Scheme 15

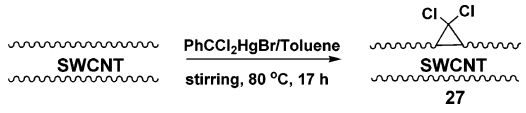

presence of Cl in the as-prepared [Cl_2C<SWCNT] **27** was estimated to be ~2 atomic% using energy-dispersive X-ray spectroscopy.[238] A very high modification ratio (varied between 12 and 23%)[190c,d] was achieved in 2003. (The dichlorocarbene functionalization ratio is based on the number of Cl atoms on CCl_2 groups and the number of C atoms on the tube sidewall, as used in the original experimental papers.[190c,d]) It was found that over 90% of the far-infrared (FIR) intensity is removed by 16% CCl_2 functionalization, and it was estimated that 25% functionalization would disrupt the SWCNT band structure completely. Such covalent chemistry exerts the largest effects on the electronic band structures of metallic SWCNTs by rapidly opening a gap at their Fermi levels, i.e., changing a metal to a semiconductor.[190c]

Scheme 16

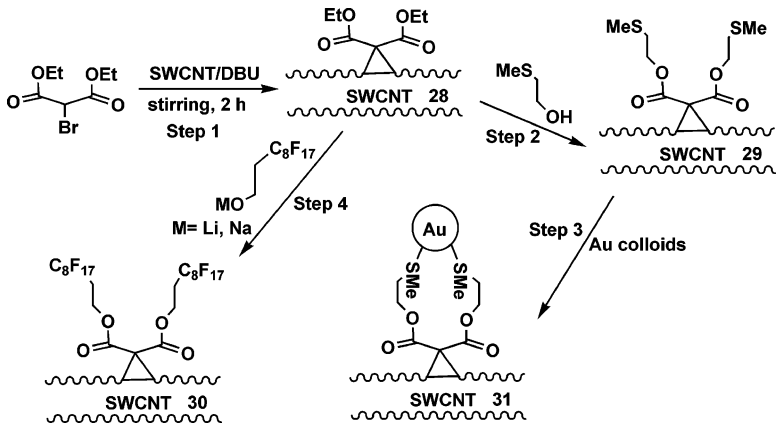

In addition to the [2+1] cycloaddition of dichlorocarbene, another [2+1] cycloaddition reaction of carbene, the Bingel reaction,[239] was recently exploited for the organic functionalization of SWCNTs under more moderate conditions (Scheme 16).[190e] In the Bingel reaction (step 1 in Scheme 16), diethyl bromomalonate works as the precursor of carbene. The [2+1] addition to SWCNTs dispersed in 1,8-diazobicyclo[5,4,0]undecene (DBU) affords the modified SWCNTs, [$(COOEt)_2C$<SWCNT] **28**. Subsequent reaction of the Bingel-SWCNTs **28** with an excess of 2-(methylthio)ethanol (step 2 in Scheme 16) results in [$(COOCH_2CH_2SMe)_2C$<SWCNT] **29**. The added organic functional groups in **29** could be "tagged" using ~5 nm gold colloids (step 3 in Scheme 16). The as-tagged modified SWCNTs **30** can be readily observed in AFM. On the other hand, transesterification of a suspension of the Bingel-SWCNTs **28** with the sodium (or lithium) salt of 1*H*,1*H*,2*H*,2*H*-perfluorodecan-1-ol were found to afford [$(COOCH_2CH_2C_8F_{17})_2C$<SWNT] **31**, which can be readily characterized by ^{19}F NMR and XPS spectroscopy. The degree of functionalization by Bingel reaction was estimated to be ~2%.[190e]

3.4.5.2 Addition of Nitrenes. Using alkyl azidoformate as nitrene precursor, Hirsch et al. obtained (R)-oxycarbonylnitrene-functionalized SWCNTs (Scheme 17).[188,190f] The first step of their synthetical protocol is the thermal decomposition of the organic azide **32**, which gives rise to (*R*)-oxycarbonylnitrene **33** with elimination of N_2; the second step is the [2+1] cycloaddition of **33** to the sidewalls of SWCNTs, affording the (*R*)-oxycarbonylaziridino SWCNTs **34**. Such a synthetical protocol allows for the covalent bonding of different functional groups onto the sidewalls of SWCNTs by the reaction with different (*R*)-oxycarbonylnitrenes generated from the corresponding azidocarbonates. A variety of organic functional groups such as alkyl chains, aromatic groups, crown ethers, dendrimers, and oligoethylene glycol units were successfully attached to SWNTs, leading to a considerable increase in the solubility in organic solvents such as DMSO, 1,1,2,2-tetrachloroethane (TCE), and 1,2-dichlorobenzene (ODCB) and allowing for their separation from insoluble contaminants such as starting SWCNTs and metal impurities.[190f] More interestingly, it was found that the modified SWCNTs containing chelating donor groups in the addends are

Scheme 17

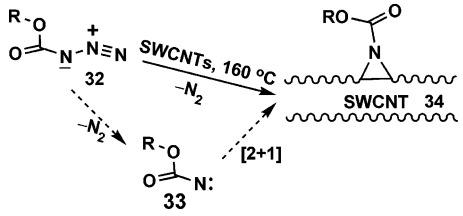

subject to complexation of metal cations such as Cu^{2+} and Cd^{2+}.[190f] As such, the [2+1] addition of (*R*)-oxycarbonylnitrenes onto the sidewalls of SWCNTs offers a flexible route to expand the chemistry of carbon nanotubes.

3.4.5.3 Structures and Energetics of the [2+1] Cycloadditions. One of the greatest difficulties in the study of the sidewall chemistry of SWCNTs is the lack of suitable physical chemical techniques for a stratifying structure characterization of the functionalized SWCNTs. Consequently, the detailed information regarding the structures of the attached functional group as well as the local structures of the SWCNTs, where the addends are attached, remain unclear and are the subject of controversy. A pertinent case is the SWCNTs functionalized by the [2+1] cycloadditions of carbenes and nitrenes.

A number of quantum chemical investigations have been performed to elucidate the local structure of the [2+1] product. Two possible structures have been proposed, as depicted in Figure 76. One is a bisnor-

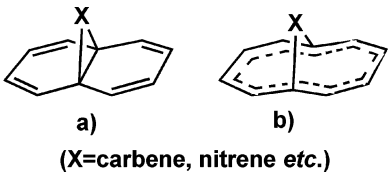

Figure 76. Two possible local geometries for the product of [2+1] cycloaddition to the sidewall of a SWCNT: (a) bisnorcaradiene-like structure with a three-membered ring; (b) delocalized annulenic structure with the substrate C−C bond opened.

caradienic structure with a three-membered ring (Figure 76a) and another with a bridged annulenic structure. While the two-layered ONIOM(B3LYP/6-31G*:AM1) calculations using a 16-C-atom inner shell in a (5,5) tube model preferred the former as the most stable geometry for the [2+1] products formed by additions of carbene, nitrene, germylene, and silylene to the armchair SWCNTs,[203a] the latter was favored by more sophisticated DFT calculations using either finite-length tube models (Figure 77a)[173,199d,203b,c,d] or infinite tube model (with periodic boundary conditions).[203d] Moreover, the diagonal CC bonds in (8,0) zigzag SWCNTs, rather than CC bonds parallel to the axis, are the favorable sites for chemical modification (Figure 77b). In contrast to previous experimental expectations, both armchair and zigzag SWCNTs with carbene and nitrene addends favor opened structures rather than three-membered rings.[203b−d] The computed band structure using PBC calculations also revealed the metallic-semiconducting transformation with increasing the dichlocarbene functionalization ratio,[203d] which agrees

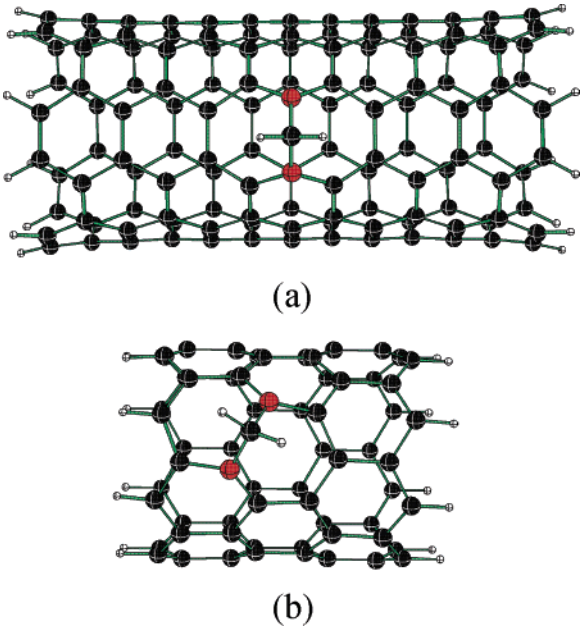

Figure 77. The B3LYP/6-31G* optimized CH_2 adduct of the finite model of (a) (5,5) SWCNT and (b) (8,0) SWCNT. The carbon atoms attached to the CH_2 addends are given in red for clarity; their distances are 2.186 and 2.190 Å, respectively.

well with the experiments,[190c] which shows that the electronic properties of SWCNTs can be engineered by chemical functionalization. The energetically favorable C−C bond breakage upon [2+1] cycloaddition can be ascribed to the strain energy release of the otherwise available three-memberred ring and to the aromatic stabilization of homoconjugation in the open structure.[173,199d,203b] Similar structural features have been well-known for the bridged 1,6-X-[10]annulenes[240] and the methylene adducts at the 6−5 junctions of fullerenes.[60]

Interestingly, based on DFT computations Lu et al.[241] found that the [2+1] cycloaddition derivatives of armchair SWCNTs evolve from open structures to closed three-membered ring structures with increasing the tube diameter, and the diameter upper limit of the opening of the sidewall of SWCNTs upon [2+1] cycloaddition is predicted to be 15 Å ((11,11) tube). It can be understood that the energy cost to push away the two addend-bridged six-membered rings increases in larger diameter tubes (one may consider the extreme, a graphite sheet model). Note that the reactivity of SWCNTs decreases with increasing tube diameters, and the SWCNTs used in the chemical modifications are mainly HiPCO tubes with small diameters (7−14 Å).[184] Thus, it is safe to characterize the experimentally synthesized [2+1] cycloaddition derivatives as open structures. Lu et al.'s result[241] showed the importance of the curvature effect (size-dependence) in the SWCNTs, but was rather artificial.

Theoretically it was predicted that the [2+1] cycloadditions of carbenes and nitrenes to the sidewalls of armchair SWCNTs are highly exothermic[173,199d] with small or no activation barrier at all,[203a,c] whereas the addition of silylene (SiH_2) is moderately exothermic.[203a,c] Nevertheless, this latter prediction suggests the viable functionalization of SWCNTs by

[2+1] cycloaddition of silylenes. In practice, silylenes can be generated, for example, by photolyzing trisilanes.[242]

3.4.6 [2+2] Cycloaddition of Singlet O_2 and Sidewall Oxidation

The intensive interest in the interaction of O_2 with the sidewalls of SWCNTs[243,244] was invoked by the serendipitous finding that the electronic properties of SWCNTs are sensitive to air exposure, e.g., a semiconductive SWCNT can be reversibly converted to a conductor by a small dose of adsorbed oxygen.[243a] It has been shown both experimentally[243a−i] and theoretically[244a−d] that O_2 in its triplet ground state ($^3\Sigma_g^-$) can only be physisorbed on the sidewalls of SWCNTs. The experimentally measured adsorption energy (E_{ads}) of O_2 ($^3\Sigma_g^-$) to CNT bundles is ~0.19 eV,[243e,f] whereas the theoretically predicted E_{ads} varies from ~0.1 to ~0.6 eV, depending on the theoretical methods and models employed.[244a−d] More recent experiments have even shown that the so-called "oxygen-sensitivity" of SWCNTs has nothing to do with the weak interaction between the physisorbed O_2 ($^3\Sigma_g^-$) and the tube walls but is artifical and likely due either to the residual chemical contaminants in the CNT bundles[243g] or to modification of the barriers at the metal−semiconductor contacts induced by oxygen.[243h,i]

While the thermal oxidation of CNTs in air (by O_2) occurs at high temperature (>700 °C),[245] facile photoinduced oxidation of CNTs can proceed by exposing CNTs concomitantly to UV light and oxygen.[243j] The accelerated oxidation of CNTs by UV light implies the involvement of the highly reactive singlet O_2 ($^1\Delta_g$) generated by photoexcitation. Further evidence on the chemical reaction of singlet O_2 with SWCNTs comes from the experiments that demonstrated the reversible surface oxidation and efficient luminescence quenching in semiconductor SWCNTs upon reacting with O_2 ($^1\Delta_g$) at low pH. [243k]

A number of theoretical investigations have been performed concerning the mechanism of singlet O_2 reaction with the sidewalls of SWCNTs.[243k,244d−l] The following remarks can be drawn:

(i) Singlet O_2 ($^1\Delta_g$) can be covalently bonded to the sidewalls of SWCNTs. As shown in Figure 78, the

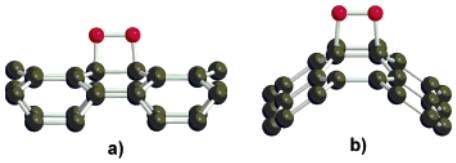

Figure 78. Predicted local geometries for the [2+2]-cycloaddition products of singlet O_2 to the sidewalls of (a) a zigzag (8,0) SWCNT and (b) an armchair (6,6) SWCNT.

most favorable bonding mode for singlet O_2 ($^1\Delta_g$) to a tube wall is the [2+2]-addition mode, i.e., forming a 1,2-dioxitane surface species.

(ii) The predicted activation energy for the [2+2]-addition to (8,0) SWCNT ranges from 0.6 to 0.8 eV for different substrate C−C sites.[244k]

(iii) Upon thermal activation, the [2+2] adducts (i.e., the 1,2-dioxitane surface species) can readily undergo O−O bond cleavage, giving rise to epoxide surface species.

3.4.7 Sidewall Epoxidation or Sidewall Opening by Oxidation

No experiments have been reported regarding the sidewall epoxidation of SWCNTs. It was proposed that sidewall epoxidation of SWCNTs might be approached by photolysis of sidewall ozonides formed by 1,3-dipolar cycloaddition of ozone with SWCNTs[199a] or by direct epoxidized by dioxiranes[204] on the basis of the ONIOM(B3LYP/6-31G*:AM1) method.

However, sophisticated DFT computations show that the epoxide of SWCNTs will not exist; in contrast, the sidewall can be opened by the oxidation.[203b]

3.4.8 Sidewall Hydrogenation

Hydrogen storage in carbon nanotubes once was a very hot topic.[246] However, this has little to do with the hydrogenation of carbon nanotubes. Quantum chemical calculations revealed that the dissociative chemisorption of H_2 on SWCNTs is endothermic, i.e., thermodynamically unfavorable.[247] Nevertheless, sidewall hydrogenation of SWCNTs was found to be plausible by a modified Birch reduction method[190a,191] and by atomic hydrogen generated from a glow discharge.[248]

Birch reduction was widely applied for the partial hydrogenation of conjugated systems and carboneous materials such as fullerenes and graphites. For example, a modified Birch reduction that was performed with metal Li and methanol dissolved in liquid ammonia (Scheme 18) leads to the hydrogena-

Scheme 18. Birch Reduction of SWCNTs

$$Li + n\,NH_3 \longrightarrow Li^+ + e^-(NH_3)_n \quad (a)$$

$$e^-(NH_3)_n + C \longrightarrow n\,NH_3 + C^- \quad (b)$$

$$C^- + CH_3OH \longrightarrow CH + CH_3O^- \quad (c)$$

tion of fullerenes.[249] A similar mechanism holds true in the reaction of C_8K graphite intercalated compound with weak protic acids in THF suspension that produces partially hydrogenated graphite with the stoichiometry of C_8H.[250] The Birch reduction of MWCNTs, SWCNTs, and graphites (Scheme 19) was

Scheme 19

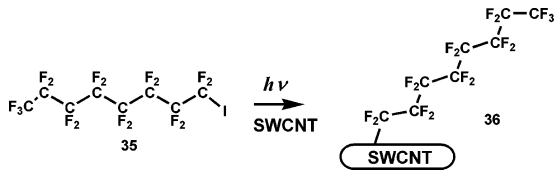

recently investigated by Pekker et al.[191] By means of thermogravimetry-mass spectroscopy (TG-MS) analysis, the hydrogenated CNTs (MWCNTs or SWCNTs) from Birch reduction were found to have a stoichiometry of $C_{11}H$, whereas a higher C:H ratio (~5:1) was reached for the Birch reduction of graphites. Desorption of H_2 from the hydrogenated CNTs

takes place by heating at the temperature range of 400−600 °C and eventually results in pristine CNTs.

Sidewall hydrogenation of SWCNTs by direct addition of atomic hydrogen generated in a cold plasma was attempted by Khare et al.[248] The as-prepared hydrogen-functionalized SWCNTs were characterized by FTIR with an intensive band around 2924 cm^{-1} for the stretching mode of sidewall C−H bonds.

3.4.9 Addition of Radicals

3.4.9.1 Addition of Alkyl Radicals. Besides the reactions of fluorinated SWCNTs with the Grignard reagents or with organolithium compounds,[209,210] sidewall alkylation of SWCNTs can also be approached by direct addition of free alkyl radicals.[188,189] By photolyzing the heptadecafluorooctyl iodide **35** with a medium-pressure mercury lamp, perfluorooctyl radicals can be generated and attached to the sidewalls of SWCNTs (Scheme 19).[188]

As shown in Scheme 20, free radicals can also be generated by the thermolysis benzoyl peroxide. The

Scheme 20

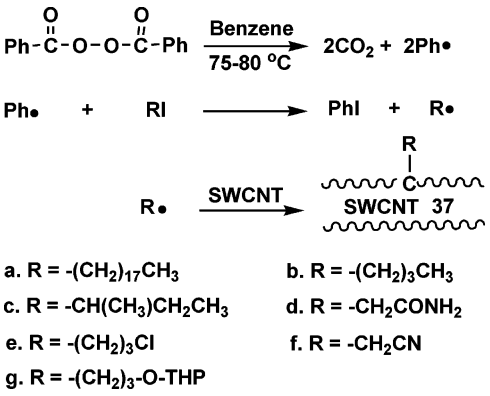

reaction of phenyl radicals with alkyl iodides produces free alkyl radicals, which react with SWCNTs to form alkylated SWCNTs **37**.[189] Phenylated SWCNTs were also formed as a byproduct.

3.4.9.2 Addition of Aryl Radicals. Tour et al. reported that the electrochemical reduction (Scheme 21) or thermal treatment (Schemes 22 and 23) of aryl

Scheme 21. Electrochemical Arylation of SWCNTs

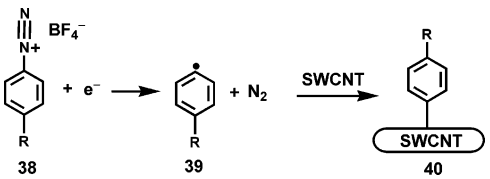

diazonium compounds with SWCNTs results in the radical-involving arylation of SWCNTs.[192] Aryl diazonium salts have been widely used as arylating agents in the arylation of olefins,[251] aromatic com-

Scheme 22. Self-Catalyzed Selective Arylation of Metallic SWCNTs.

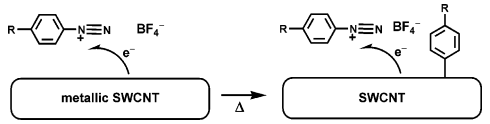

Scheme 23. Solvent-Free Arylation of SWCNTs

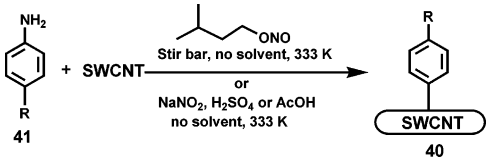

pounds,[252] and graphites.[253] As shown in Scheme 22, electrochemical reduction of the aryl diazonium salts **38** produces aryl radicals **39**, whose addition to small-diameter SWCNT sidewalls gives rise to the arylated SWCNTs **40**.[192a] The functionalization ratio was estimated to be 5% (one out of 20 carbon atoms in the CNTs bearing a aryl group). The aryl−SWCNT bonding is apparently covalent in nature, as thermal dearylation of the derivatized SWCNTs requires a high temperature (∼500 °C in an argon atmosphere). Following this pioneering work, Tour et al. disclosed that even without electrochemical reduction, the arylation can proceed selectively with metallic SWCNTs (Scheme 22).[192b] Underlying this marvelous finding is a self-catalyzing reaction mechanism, i.e., the reaction of the aryl diazonium salts is catalyzed by the more electron-donative metallic SWCNTs. The electron transfer from the metallic SWCNTs to the aryl diazonium salts triggers the formation of aryl radicals. The metallic SWCNTs were converted to semiconductors (arylated SWCNTs) upon such a selective arylation.

While the aforementioned arylations were performed with commercially available aryl diazonium salts and require SWCNTs diluted in solvents,[192a,b] arylations using in-situ generated aryl diazonium compounds were also studied,[192c−h] leading to the discovery of a solvent-free protocol[192d] for the arylation of SWCNTs (Scheme 23).

3.4.10 Chemical Reactivity of Sidewall Defects

While perfect infinite SWCNTs ideally have curved graphenic hexagon networks with strong, pseudo 1D π-conjugations, the presence of a variety of imperfections, such as vacancies, SW defects,[99] pentagons, heptagons, and dopants, is unavoidable in pristine SWCNTs.[254] These defects can be inevitably formed during the growth of CNTs or introduced by post-processing (e.g., ultrasonication and oxidative cleaning). It has been shown that these defects play a pivotal role in tailoring the physical[4c,254] and chemical properties[186b,244j,255,256] of SWCNTs. For example, defects have been shown to be of critical importance in the chemical etching and shortening of CNTs.[186b,256a,c] Owing to the importance of defects in the chemistry of SWCNTs, a number of theoretical investigations have been conducted recently, mainly focusing on the chemical reactivities of the following four types of defects: vacancies, dopants (e.g., B, N, Si, etc.), ad-dimers and SW defects.

3.4.10.1 Vacancies. Vacancies with unsaturated dangling bonds are of course highly reactive and can readily form covalent bonds with adsorbed species. For instance, recent temperature-programmed desorption (TPD) experiments by Chakrapani et al.[255b] showed that acetones can be chemisorbed on HiPCO−SWCNTs, and at least five chemisorption states were

formed with measured activation energies of acetone desorption ranging from 24.5 to 59.5 kcal/mol. Further theoretical calculations using hybrid quantum mechanical and semiempirical methods and short zigzag tube models revealed that the most stable chemisorption states are due to acetones covalently bonded to atomic vacancies, while those weaker ones are attributed to the [2+2]-cycloaddition adducts of actones on the SW defects.

3.4.10.2 Dopants. Doping the sidewalls of SWCNTs with heteroatoms such as B and N[257] modifies their electronic structures and chemical properties. Recent first-principles DFT calculations by Peng et al.[258a] predicted the following properties for the B- or/and N-doped zigzag (8,0) SWCNTs:

(i) Small polar molecules such as CO and H_2O that have electron-donative lone pair(s) can be chemisorbed onto the B sites of the B-doped and BN-doped CNTs, whereas physisorption occurs only on the intrinsic CNTs.

(ii) The B-doping drastically enhances the charge-transfer capability of the CNTs. Consequently, electron transfer from the chemisorbed CO or H_2O on the B-doped and BN-doped CNTs is also enhanced as compared to the CO/CNT and H_2O/CNT physisorption systems.

(iii) B-doped CNTs are good sensors of CO and water molecules.

Moreover, DFT computations of Nevidomskyy et al.[258b] showed that nitrogen substitutional impurities have different effects on metallic armchair and semiconducting zigzag nanotubes: at low concentration, the defect in a semiconducting tube creates a spatially localized state, which makes the impurity site chemically and electronically active, while the impurity in armchair nanotubes is totally delocalized.

Because of its electron deficiency, boron atoms doped in SWCNTs have a strong propensity to accept electrons from lithium energetically; thus, boron doping is expected to improve the Li absorption in SWNTs.[259] The electron-deficient boron doped SWCNTs, especially BC_3 nanotubes,[260] are computed to absorb lithium very favorably and exhibit superior Li absorption capabilities than the pure carbon nanotubes.

3.4.10.3 Stone-Wales Defect (5−7−7−5 Defect). The SW defect (an assembly of 5−7−7−5 rings) is a very important topological defect in the science of CNTs and graphites. By definition, an SW defect can be generated topologically by rotating one of the C−C bonds in a hexagonal network by 90° (Scheme 24).[99]

Scheme 24. Formation of a Stone-Wales Defect

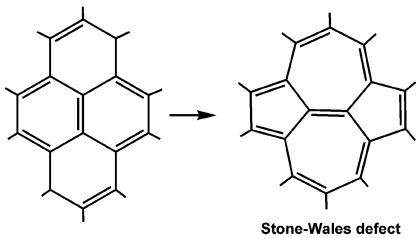

Recently, the presence of SW defects in carbon and boron nitride nanotubes was identified experimentally by combining resonant photoabsorption and vibration spectroscopy with scanning tunneling microscopy.[261]

Recent theoretical investigations showed that the central C−C bond (i.e., the 7−7 ring fusion) in the SW defective sites has a bond length with a range of 1.32−1.38 Å, shorter than that of an ordinary C−C bond (around 1.42 Å) in a defect-free SWCNT.[199d,244j,262] This implies the central C−C bond in an SW defect can be considered as a double bond with highly localized π-electron density. Consequently, the central C−C bond in an SW defect should be more reactive than the ordinary C−C bonds of a defect-free SWCNT. This is true for most of the cases concerned so far.[244j,255b,262] For instance, acetone was found to undergo exothermic [2+2]-cycloaddition with the central C=C bond of a SW defect in the sidewall of a zigzag (10,0) tube but does not react with a defect-free tube at all.[255b] A similar trend was predicted for the [2+2]-additions of singlet O_2[244j] and [2+1] cycloaddition of methylene[262a] to the sidewalls of the defective and defect-free (10,0) tube.

However, an exception exists: recent DFT computations show that the central C−C bond of an SW defect in an armchair (5,5) SWNT is chemically less reactive than perfect sites (Figure 79).[199d] Note that

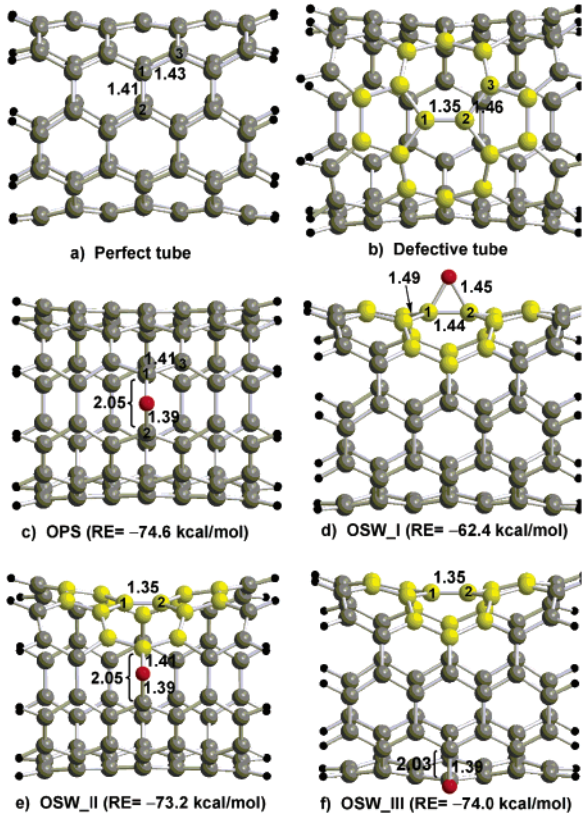

Figure 79. (a) Seven-layered defect-free (5,5) tube model ($C_{70}H_{20}$); (b) seven-layered defective (5,5) tube model containing an SW defect (colored yellow); (c) optimized O adduct of a defect-free (5,5) tube model; (d) Optimized O adduct at the SW defect of defective (5,5) tube model; (e) optimized O adduct at a 6−6 ring fusion near the SW defect of defective (5,5) tube model; (f) Optimized O adduct on a 6−6 ring fusion far away from the SW defect of defective (5,5) tube model. The reaction energies (RE) for the additions of O were predicted at the B3LYP/6-31G* level of theory (bond length in angstroms) (from ref 199d).

the local carbon skeleton at the 5−7−7−5 ring fusion of the SW defect is nearly planar with a curvature-induced pyramidalization angle of only ~0.3° at the C1 and C2 atoms, whereas the pyramidalization angle (~5.3°) at the C atoms of a defect-free tube is much larger. Clearly, the local curvature of the SW defect is far less severe than that of a perfect site. The much lower chemical reactivity at the defective 7−7 ring fusion can be ascribed to the constraints of its planar local structure. On the contrary, its peripheral C−C bonds (e.g., the 5−6 and 6−7 ring fusions) were predicted to be more reactive than an ordinary 6−6 ring fusion in the tube wall due to the much severe local curvatures at these sites.[199d,262] Thus, the local curvature introduced by the topological defect affects subtly the chemical reactivity of the sites in its vicinity.

3.4.10.4 Ad-Dimer Defect (7−5−5−7 Defect). In addition to the SW defect, another type of defect that also contains 5−7 ring pairs is the 7−5−5−7 defect (Scheme 25) generated by adding a C_2 dimer to bridge

Scheme 25. Ad-Dimer Induced Formation of a 7−5−5−7 Defect.

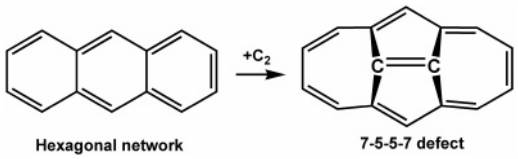

two parallel C−C bonds of a hexagon of the SWCNT sidewall with concomitant cleavage of the substrate C−C bonds. Ad-dimers, i.e., the central 5−5 ring fusion in the 7−5−5−7 defect, appear to have large pyramidalization angles (severe local curvature) and a short C=C bond. DFT calculations by Grujicic et al.[244j] showed that the ad-dimers on the sidewalls of both a zigzag (10,0) SWCNT and an armchair (5,5) SWCNT are much more reactive than the ordinary C−C bonds of the corresponding defect-free tubes, and the chemisorption of singlet O_2 on an ad-dimer is quite strong.

3.5 Hybrid Materials Consisting of Small Fullerenes and Single-Wall Carbon Nanotubes: Peapods

SWCNT-based hybrid materials are a quite recent research field. So far various atoms or molecules have been filled into the hollow core of SWCNT.[263] Among which, peapods, i.e., SWCNTs containing a self-assembled chain of fullerenes (exemplified by C_{60}@SWNCTs, Figure 80), represent a class of nanoscale materials with tunable properties.

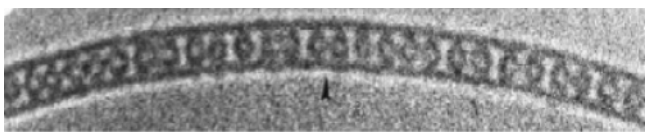

Figure 80. High-resolution TEM image of one of the first C_{60}@SWNTs (peapod) ever observed. The carbon nanotube diameter is that of a regular (10,10) SWNT (14 Å). Reprinted with permission from ref 264. Copyright 1999, Elsevier.

Peapod C_{60}@SWNCTs were first discovered serendipitously by Smith, Monthioux, and Luzzi in 1998;[265] such "endotubular fullerenes" formed spontaneously—and unexpectedly—during the purification and annealing treatments on raw SWNT materials produced by a pulsed laser vaporization method. In 2000, a high-yield production method was developed,[266] in which opened SWCNTs and fullerenes were heated simultaneously in a vacuum. This vapor phase reaction based method is applicable to various materials for doping inside individual SWCNTs. So far, higher fullerenes such as C_{70},[267] C_{78}, C_{80}, C_{82} and C_{84},[267a] endohedral fullerenes such as Cd@C_{82},[266a,267a,268] Dy@C_{82},[269] Sc@C_{82},[270] Ce@C_{82},[271] La@C_{82},[267a] La_2@C_{80},[272] Sc_2@C_{84},[267a] Cd_2@C_{92},[273] and exohedral fullerene derivatives such as $C_{61}(COOEt)_2$[274] and $C_{60}O$[275] have also been successfully inserted into SWCNTs. Although the detailed formation mechanism is still not known, it is assumed that after the nanotubes are synthesized, at high temperatures free fullerenes enter the nanotubes through the open ends or more possibly through defects in the tube wall[276] by surface diffusion and gas transportation.

In the C_{60} peapods, fullerenes are aligned in a necklace-like chain, with an average interval distance of ca. 10 Å (9.7 Å estimated by electron diffraction analysis,[267] 9.9 Å nm measured by scanning tunneling microscopy[277]). Such a C_{60}−C_{60} distance is about 3% shorter than that (10 Å) in C_{60} crystals, which indicates that the interaction between the C_{60} molecules was influenced by the SWNT walls (perhaps associated with the small amount of electron transfer from the fullerene cage to SWCNTs). The fullerene−SWCNT interaction also results in a selectivity of the fullerene−SWCNT diameter match, i.e., the exo- or endothermicity of the encapsulation reaction depends decisively on the space between the nanotubes and the encapsulated fullerenes.[278] The experimentally measured fullerene−nanotube spacing (3 Å) corresponds to the interplanar van der Waals distance in graphite.[265,266] Local density approximation (LDA) computations revealed a theoretical critical value of 12.8 Å, as is (10,10) SWCNT, for an energetically favorable C_{60} encapsulation, while other peapods with a smaller diameter such as (8,8) and (9,9) are endothermic.[278a] Once inserted into the interior space, the C_{60} molecules remain mostly unchanged up to ~800 °C in the SWCNT without dedoping under a high vacuum.[279]

Because of the fullerene−fullerene and fullerene−SWCT interactions, the electronic structure of the peapods is not a simple sum of those fullerenes and nanotubes, and novel nanoelectronic devices might be constructed. Fullerenes can modify the local electronic structure of the SWCNTs, mixing its orbitals with the nanotube's electronic band.[278a] Electronic measurements of C_{60} peapods using a scanning tunneling microscope demonstrate that the encapsulated C_{60} molecules modify the local electronic structure of the nanotubes. The experiments and calculations show that a periodic array of C_{60} molecules gives rise to a hybrid electronic band, which derives its character from both the nanotube states and the C_{60} molecular orbitals.[277] Theoretical

studies show that the electron states near the Fermi level depend crucially on the innerwall spacing between fullerenes and nanotubes, and the size and shape of the encapsulated fullerenes add important variety to the electronic structures of the peapods. In this sense, it is possible to engineer the Fermi level of the peapods by controlling the space in the tube and the species of the encapsulated fullerenes.[280] On the other hand, the inherent nanometric inner cavity of SWCNTs serves as a highly confining reaction vessel, which can modify the reactivity of the encapsulated molecules. Most recently, researchers have polymerized $C_{60}O$ in SWCNTs to form a linear, unbranched polymer that has never been observed before.[275] The technique may allow other unprecedented linear polymers to be synthesized.

However, small fullerenes have not been encapsulated in the SWCNTs experimentally so far, due to the infancy of small fullerene science. Once encapsulated in nanotubes, small fullerenes may spontaneously form a one-dimensional polymer by covalent bonds, due to their rather high strain energies. When C_{60} peapods are heated to 1000−1200°C, the C_{60} molecules coalesce and change into a new SWNT, and this results in a double-wall carbon nanotube (DWCNT).[279] Similarly, a small fullerene peapod may transform to a DWCNT with a much smaller inner diameter when heated (most likely under lower temperature than C_{60} peapods).

Few theoretical studies have been performed on small fullerene peapods.[281,282] The smallest nanotube diameter for encasing a single C_{20} exothermically was computed. However, using the same generalized gradient-corrected approximation (GGA) by Perdew, Burke, and Ernzerhof,[283] different critical values were obtained: ca. 9.53 Å (that of a (7,7) tube) by Liu et al,[281a] and ca. 10.64 Å (that of a (8,8) tube) by Lu et al,[281b] which correspond to a tube−fullerene distance of 2.83 and 3.22 Å, respectively. Note that the tube−fullerene spacing of 2.83 Å obtained by Liu is less than the interlayer separation in graphite. Lu et al[281b] also found that when C_{20} forms a double-bonded chain inside the (8,8) and (9,9) tubes two carrier channels exist, each of which distributes along either the nanotube or the C_{20} chain. Thus, when properly doped with electrons, the peapod with encapsulated double bonded C_{20} chain might have a higher T_c than that of $C_{60}K_3$. But the one-dimensional chain of C_{20}, most likely, adopts the open [2+2] structure, instead of the close [2+2] one as in ref 281b (Figure 81). Moreover, several Met-Car (M_8C_{12}, where M is Sc, Ti, or V) peapods were investigated theoretically, and it is found that modification of the chemical composition of the Met-Cars may be an effective way to control the electronic properties of such peapods.[282]

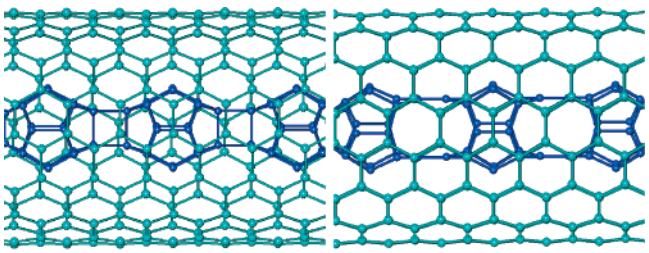

Figure 81. Schematic presentation of C_{20} peapod geometries (a) C_{20} forms a close [2+2] chain as in ref 281b; (b) C_{20} forms a open [2+2] chain in a (8,8) SWCNT

4. Pros and Cons of Different Approaches in Computational Nanotube Chemistry

Because of the large size of nanotubes, carefully chosen truncated models, appropriate for the problem being investigated, are required. There are basically three approaches: the finite cluster model, the ONIOM technique, and the periodic boundary conditions (PBC) method.

Using small finite nanotube models to simulate a full nanotube, we can carry out computations at a relatively high level.[178,284] The finite model is powerful in local bonding; however, it is not able to examine the electronic band structures and the results depend on the model used. For example, Bettinger[173] showed that the energy for addition of fluorine to the nanotube sidewall depends strongly on the length of the nanotube and pointed out that "the pronounced length dependence needs to be taken into account when probing the viability of sidewall functionalization computationally. As the infinite-length armchair nanotubes have zero band gaps, we suggest focusing on fully benzenoid slabs when the binding energy of a radical to an armchair tube is of interest." In light of the oscillating periodicity of the HOMO−LUMO gap of the finite armchair tubes,[172,173] we recommend that at least finite nanotube models with lengths covering one periodicity should be investigated.

The other approach uses the ONIOM technique,[207] which treats part of the system at a high theoretical level but the rest of the system at a lower level. This strategy allows larger systems to be simulated at a practical computational cost. However, ONIOM has the following drawbacks. First, partitioning the full system to high and low level regions, or the choice of the size of the higher level, is still something of art, and a careful selection of layers is crucial. Second, the combinations of the chosen computational methods in different layers are also critical for application. For example, the well-employed ONIOM(B3LYP/6-31G*/AM1) using pyrene in the higher theoretical region failed to get the open structure of the methylene and nitrene adducts of armchair nanotubes.[203b,d] With regard to this concern, Kar et al.[199b] recommended the "same level different basis set" protocol for studying SWCNTs. Instead, Irle et al.[285] stressed the importance of circumferential π-conjugation in the high level model system and recommended the ONIOM rings approach for carbon nanotube chemistry. Third, using ONIOM to simulate carbon nanotubes violates a golden rule: the high−low level boundary should not cut across double, triple, or aromatic bonds; if so, the model system in the high level cannot be properly terminated. However, using ONIOM in nanotube systems unavoidably cuts the aromatic C−C bonds, which leads to the inevitable technical limitation of ONIOM in computational nanotube chemistry. As a compensation, a rather large high level region is desired so that the active site is far from the boundary and the improper

termination will not result in significant effects on the site of interest (which will sacrifice the efficiency of the ONIOM method to some extent). In general, the ONIOM method is not a "black box" at all; careful validation of the ONIOM approach for any given application (such as the S-value test as recommended by Morokuma)[286] is highly desired. Unfortunately, such an evaluation has rarely been performed in computational nanotube chemistry in the literature. Like the finite cluster model, the ONIOM method is not capable of computing the band structures and other bulk properties.

The third approach is the periodic boundary conditions (PBC) method, which is a well-established method in solid-state physics and is becoming popular in computational chemistry. PBC is a clever approach to make a simulation that consists of only a relatively small number of atoms (as in a supercell) to behave as if it was infinite in size. Using a finite model, the system size would have to be extremely large to ensure that the boundary has only a small influence on the bulk properties, which usually makes the model too large to simulate. The PBC method removes the severe artifacts of the boundary effect in the finite models without increasing computational effort and thus allows simulation of the bulk properties (such as band structure, electronic transport, and elastic properties, etc.) using a reasonable CPU cost (note that it is important to choose a suitable supercell in PBC computations). However, when dealing with local bonding site (such as defects, molecule functionalization, or adsorption), PBC creates periodic local bonding sites and the coupling between each other might lead to some fictitious effects. PBC is also not so powerful in locating the transition state in the investigations of the reaction mechanism, which may be improved technically with better implementation.

In summary, every approach used in computational nanotube chemistry has its own advantages and disadvantages, and using combined approaches, if possible, may be the best choice. Moreover, it may be recommended that the effects of chirality and the electronic structures of the nanotubes are considered in computations. This means that at least three types of tube models should be taken into account: metallic armchair tubes such as (6,6), metallic zigzag tubes such as (9,0), and semiconductor zigzag tubes such as (10,0).

5. Concluding Remarks

In his recent book, Hirsch[3d] concluded, "Although comparatively young, fullerene chemistry is already a mature discipline." This is true for fullerenes exemplified by C_{60} but generally not true for small fullerenes (the smaller counterparts of C_{60}) and nanotubes (elongated giant fullerenes). Although the general principles established in fullerene chemistry can be extended to small fullerenes and nanotubes to some extent, small fullerene and nanotube chemistry is still in its infancy, a research field full of challenges and opportunities to both experimentalists and theoreticians.

Small fullerenes are very reactive due to their highly strained cage structures; thus, it is impossible or extremely difficult to isolate them in the pure molecular form. However, their exohedral and endohedral derivatives are good targets for preparation and isolation. The recent isolation of $C_{50}Cl_{10}$ in macroscopic amounts gave us momentous encouragement and confidence. Using efficient instruments (such as multistage HPLC) and given enough patience, the bulk synthesis of small fullerene derivatives using the modified graphite arc-discharge method are expected to be a routine in the lab. Another possible way to get stable small fullerene derivatives is by losing carbon atoms in C_{60} adducts, as was just achieved by Taylor et al.[287] In Taylor's landmark experiment, two seven-memberred ring C_{58} fullerene derivatives, $C_{58}F_{17}CF_3$ and $C_{58}F_{18}$ (Figure 82) were

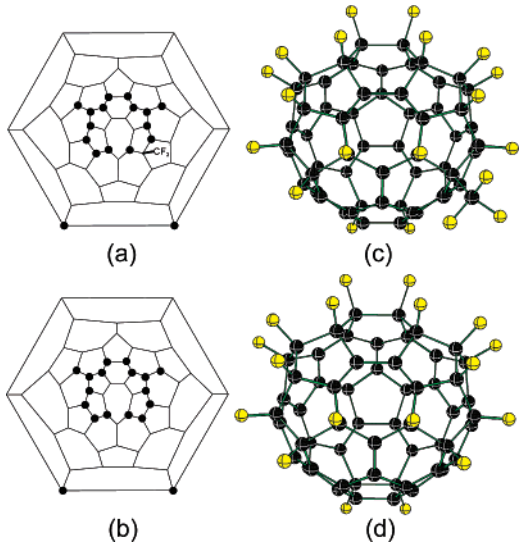

Figure 82. Schlegel diagrams for $C_{58}F_{17}CF_3$ (a) and $C_{58}F_{18}$ (b) (● = F), and the semiempirical AM1 optimized structures for $C_{58}F_{17}CF_3$ (c) and $C_{58}F_{18}$ (d).

produced in milligram quantities by fluorinating C_{60} at 550 °C using a fluorinating agent based on a cesium lead oxyfluoride salt. It is suggested that the strain that has hindered past attempts to prepare smaller quasi-fullerenes is mitigated because fluorine addition changes the hybridization of some of the pentagon carbons from sp^2 to sp^3. Hopefully small fullerene derivatives can be generally available, and routine investigations of the properties and applications of small fullerenes will become possible in the very near future.

Carbon nanotubes, discovered in 1991,[2] have an even shorter history than fullerenes (discovered in 1985),[1] and the SWCNT chemical modification began only around 7 years ago. Because of the less curved surface, the reactivity of the common SWCNTs are much lower than that for fullerenes, and generally very reactive addends and more critical reaction conditions are required to functionalize SWCNTs. Nevertheless, great progress has been achieved in nanotube functionalization. However, the production and separation according to diameter, length, and chirality of SWCNTs is still far from being achieved, and the purification and characterization of SWCNT derivatives are still not satisfactory. Hopefully these two major problems can be solved in next few years.

Afterward, SWCNTs will serve as standard building blocks in organic synthesis, and the potential of the unprecedented properties of SWCNTs will be fully unleashed for practical applications. Recent achievements are rather encouraging: using a water-assisted chemical vapor deposition (CVD) method, impurity-free SWCNTs can be synthesized with high efficiency;[288] moreover, now it is possible to separate the metallic and semiconducting SWCNTs,[289] and the large-scale separtion is especially remarkable.[290]

The interplay between theory and experiment has played such an important role in fullerene chemistry that this field has reached a mature stage as a teenager (only 15 years old). Definitely, the healthy development, especially of our dreamed precocity of small fullerene and nanotube chemistry, will also heavily depend on the synergy of theoretical and experimental investigations from many different disciplines.

6. Acknowledgment

This work was sponsored by NSF of China (Grants No. 20021002, 20425312, 20203013, 90206038, and 20423002), MOE of China (Grant No. 20010384005), Fok Ying-Tung Education Foundation, NSF of Fujian Province (Grants No. E0210001 and 2002F010), and MOST of China (Grant No. 2002CCA01600), and by NSF USA Grant CHE 0209857. Z.C. thanks Alexander von Humboldt foundation for supporting the 2004 summer visit in Germany.

7. Notes Added in Proof

During the acceptance and proof of this review, several papers pertinent to this review appeared. They are briefly summarized below.

Two hypothetical C_{28} crystalline phases, namely hyperdiamond and hyperlonsdaleit, were studied by Seifert et al.[291] at the density-functional based tight-binding level. It is found that both solid phases of C_{28} have very similar characteristics, which are compared with those of crystals of other small fullerenes, C_{20} and C_{36}; moreover, the π component of the C−C bonds (the sp^2 hybridized atoms) in the lattice changes considerably the mechanical and electronic properties.

Billups et al.[292] found that SWCNT can be reduced by lithium in liquid ammonia and the resulting nanotube salts can be treated with aryl iodides to yield debundled, functionalized SWCNTs (Scheme 26). Furthermore, the Billups group[293] found that

Scheme 26.

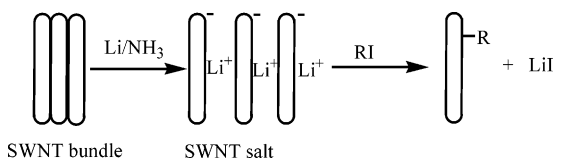

alkylation of nanotube salts prepared using lithium, sodium, or potassium in liquid ammonia can yield highly functionalized nanotubes that are soluble in organic solvents. The SWCNT derivatives from different alkali metals have radically different thermal behavior during detachment of the alkyl groups, which may indicate differences in the relative amounts of 1,2- and 1,4-addition of the alkyl groups.

A recent exciting finding is that carbon nanotubes can be used to kill cancer cells. Dai et al.[294] showed that carbon nanotubes solubilized in the aqueous phase by noncovalent functionalizations can be selectively directed to cancer cells and kill them by the excessive local heating of SWCNTs in vitro with near-infrared radiation. However, along with the disintegration of the cancer cells, the nanotubes aggregate and give rise to insoluble materials. To overcome this, Prato[295] pointed out that "for biological uses, covalently functionalized and fully soluble carbon nanotubes would probably be more tolerated".

8. References and Notes

(1) (a) Kroto, H. W.; Heath, J. R.; O'Brien, S. C.; Curl, R. F.; Smalley, R. E. *Nature* **1985**, *318*, 162. (b) Krätschmer, W.; Lamb, L. D.; Fostiropoulos, K.; Huffman, D. R. *Nature* **1990**, *347*, 354.

(2) (a) Iijima, S. *Nature*, **1991**, *354*, 56. (b) Iijima, S.; Ichihashi, T. *Nature* **1993**, *363*, 603. (c) "Hollow core or central tube" structures, essentially nanotubes, were observed as early as 1976, although the structure clarification was only done by Iijima in 1991; see Oberlin, A.; Endo, M.; Koyama, T. *J. Cryst. Growth* **1976**, *32*, 335.

(3) (a) Dresselhaus, M. S.; Dresselhaus, G.; Eklund, P. C. *Science of Fullerenes and Carbon Nanotubes*; Academic Press: San Diego, 1996; pp 1−985. (b) Saito, R.; Dresselhaus, G.; Dresselhaus, M. S. *Physical Properties of Carbon Nanotubes*; Imperial College Press: London, 1998. (c) Reich, S.; Thomsen, C.; Maultzsch, J. *Carbon Nanotubes-Basic Concepts and Physical Properties*; Wiley-VCH: Weinheim, 2004. (d) Hirsch, A.; Brettreich, M. *Fullerenes - Chemistry and Reactions*; Wiley-VCH: Weinheim, 2005.

(4) For recent reviews, see (a) Dekker, C. *Phys. Today* **1999**, *52*, 22. (b) Dai, H. *Phys. World* **2000**, *13*, 43. (c) Ouyang, M.; Huang, J.-L.; Lieber, C. M. *Acc. Chem. Res.* **2002**, *35*, 1018. (d) Avouris Ph. *Acc. Chem. Res.* **2002**, *35*, 1026. (e) Niyogi, S.; Hamon, M. A.; Hu, H.; Zhao, B.; Bhowmik, P.; Sen, R.; Itkis, M. E.; Haddon, R. C. *Acc. Chem. Res.* **2002**, *35*, 1105. (f) Rao, C. N. R.; Satishkumar, B. C.; Govindaraj, A.; Nath, M. *ChemPhysChem* **2001**, *2*, 78. (g) Rao, C. N. R.; Satishkumar, B. C.; Govindaraj, A.; Nath, M. *ChemPhysChem* **2001**, *2*, 78. (h) Baughman, R. H.; Zakhidov, A. A.; de Heer, W. A. *Science* **2002**, *297*, 787. (i) Dai, L.; Patil, A.; Gong, X.; Guo, Z.; Liu, L.; Liu, Y.; Zhu, D. *ChemPhysChem* **2003**, *4*, 1150. (j) Lin, T.; Bajpai, V.; Ji, T.; Dai, L. *Aust. J. Chem.* **2003**, *56*, 635. (k) Davis, J. J.; Coleman, K. S.; Azamian, B. R.; Bagshaw, C. B.; Green, M. L. H. *Chem. Eur. J.* **2003**, *9*, 3732. (l) Ciraci, S.; Dag, S. Yildirim, T.; Gülseren, Senger, R. T. *J. Phys.: Condens. Matter.* **2004**, *16*, R901. (m) Steinhart, M.; Wehrspohn, R. B.; Gosele, U.; Wendorff, J. H. *Angew. Chem., Int. Ed.* **2004**, *43*, 1334. (n) Guldi, D. M.; Prato, M. *Chem. Commun.* **2004**, 2517. (o) Katz, E.; Willner, I. *ChemPhysChem* **2004**, *5*, 1084. (p) Kuzmany, H.; Kukovecz, A.; Simon, F.; Holzweber, M.; Kramberger, Ch.; Pichler, T. *Synth. Met.* **2004**, *141*, 113. (q) Kukovecz, A.; Kónya, Z.; Kiricsi, I. In *Encyclopedia of Nanoscience and Nanotechnology*; Nalwa, H. S, Eds.; Stevenson Ranch, Calif.: American Scientific Publishers, 2004; Vol. 9, p 923. (r) White, C. T.; Mintmire, J. W. *J. Phys. Chem. B* **2005**, *109*, 52.

(5) Kroto, H. W. *Nature* **1987**, *329*, 529.

(6) Fowler, P. W.; Manolopoulos, D. E. *An Atlas of Fullerenes*; Clarendon, Oxford, 1995.

(7) Albertazzi, E.; Domene, C.; Fowler, P. W.; Heine, T.; Deifert, G.; Van Alsenoy, G.; Zerbetto, F. *Phys. Chem. Chem. Phys.* **1999**, *1*, 2913.

(8) Campbell, E. E. B.; Fowler, P. W.; Mitchell, D.; Zerbetto, F. *Chem. Phys. Lett.* **1996**, *250*, 544.

(9) Kobayashi, K.; Nagase, S.; Yoshida, M.; Osawa, E. *J. Am. Chem. Soc.* **1997**, *119*, 12693.

(10) (a) Wang, C.-R.; Kai, T.; Tomiyama, T.; Yoshida, T.; Kobayashi, Y.; Nishibori, E.; Takata, M.; Sakata, M.; Shinohara, H. *Nature* **2001**, *408*, 426. (b) Takata, M.; Nishibori, E.; Wang, C. R.; Sakata, M.; Shinohara, H. *Chem. Phys. Lett.* **2003**, *372*, 512.

(11) (a) Stevenson, S.; Fowler, P. W.; Heine, T.; Duchamp, J. C.; Rice, G.; Glass, T.; Harich, K.; Hajdu, E.; Bible, R.; Dorn, H. C. *Nature* **2001**, *408*, 428. (b) Olmstead, M. M.; Lee, H. M.; Duchamp, J. C.; Stevenson, S.; Marciu, D.; Dorn, H. C.; Balch, A. L. *Angew. Chem., Int. Ed.* **2003**, *42*, 900.

(12) Kato, H.; Taninaka, A.; Sugai, T.; Shinohara, H. *J. Am. Chem. Soc.* **2003**, *125*, 7782.

(13) Kadish, K. M., Ruoff, R. S., Eds. *Fullerene: Chemistry, Physics and Technology*; John Wiley & Sons: New York, 2002.

(14) (a) Piskoti, C.; Yarger, J.; Zettl, A. *Nature* **1998**, *393*, 771. (b) Heath, J. R. *Nature* **1998**, *393*, 730. (c) Koshio, A.; Inakuma, M.; Sugai, T.; Shinohara, H. *J. Am. Chem. Soc.* **2000**, *122*, 398. (d) Koshio, A.; Inakuma, M.; Wang, Z. W.; Sugai, T.; Shinohara, H. *J. Phys. Chem. B* **2000**, *104*, 7908.

(15) Handschuh, H.; Ganteföf, G.; Kessler, B.; Bechthold, P. S.; Eberhardt, W. *Phys. Rev. Lett.* **1995**, *74*, 1095.

(16) Xie, S. Y.; Gao, F.; Lu, X.; Huang, R. B.; Wang, C. R.; Zhang, X.; Liu, M. L.; Deng, S. L.; Zheng, L. S. *Science* **2004**, *304*, 699.

(17) Fowler, P. W.; Heine, T. *J. Chem. Soc., Perkin Trans. 2* **2001**, 487.

(18) (a) Chen, Z. F., *Angew Chem, Int. Ed.* **2004**, *43*, 4690. (b) Lu, X.; Chen, Z. F.; Thiel, W.; Schleyer, P. v. R.; Huang, R. B.; Zheng, L. S. *J. Am. Chem. Soc.* **2004**, *126*, 14871.

(19) Guo, T.; Diener, M. D.; Chai, Y.; Alford, M. J.; Haufler, R. E.; McClure, S. M.; Ohno, T.; Weaver, J. H.; Scuseria, G. E.; Smalley, R. E. *Science* **1992**, *257*, 1661.

(20) Prinzbach, H.; Weller, A.; Landenberger, P.; Wahl, F.; Worth, J.; Scott, L. T.; Gelmont, M.; Olevano, D.; Issendorff, B. *Nature* **2000**, *407*, 60.

(21) (a) Prinzbach, H. *Angew. Chem., Int. Ed. Engl.* **1993**, *32*, 1722. (b) Prinzbach, H.; Weber, K. *Angew. Chem., Int. Ed. Engl.* **1994**, *33*, 2239. (c) Bertau, M.; Wahl, F.; Weiler, A.; Scheumann, K.; Wörth, J. Keller, M.; Prinzbach, H. *Tetrahedron* **1997**, *53*, 10029.

(22) (a) Haddon, R. C.; Scott, L. *Pure Appl. Chem.* **1986**, *58*, 137. (b) Haddon, R. C. *Science* **1993**, *261*, 1545.

(23) Hirsch, A.; Chen, Z.; Jiao, H. *Angew. Chem, Int. Ed.* **2000**, *39*, 3915.

(24) Chen, Z.; Jiao, H.; Hirsch, A.; Thiel, W. *J. Mol. Model.* **2001**, *7*, 161.

(25) (a) Hultman, L.; Stafström, S.; Czigány, Z.; Neidhardt, J.; Hellgren, N.; Brunell IF.; Suenaga, K.; Colliex, C. *Phys. Rev. Lett.* **2001**, *87*, 225503. (b) Stafström, S.; Hultman, L.; Hellgren, N. *Chem. Phys. Lett.* **2001**, *340*, 227. (c) Manaa, M. R.; Sprehn, D. W.; Ichord, H. A.; *J. Am. Chem. Soc.* **2002**, *124*, 13990. (d) Chen, Z.; Jiao, H.; Moran, D.; Hirsch, A.; Thiel, W.; Schleyer, P. v. R. *J. Phys. Org. Chem.* **2003**, *16*, 726.

(26) Chen, Z.; King, R. B. *Chem. Rev.* **2005**, *105*, 3613.

(27) Ceulemans, A.; Compernolle, S.; Lijnen, E. *Phys. Chem. Chem. Phys.* **2004**, *6*, 238.

(28) (a) Schleyer, P. v. R.; Maerker, C.; Dransfeld, A.; Jiao, H. J.; Hommes, N. J. r. V. E. *J. Am. Chem. Soc.* **1996**, *118*, 6317. (b) Schleyer, P. v. R.; Jiao, H.; Hommes, N. J. R. v. E.; Malkin, V. G.; Malkina, O. L. *J. Am. Chem. Soc.* **1997**, *119*, 12669.

(29) Chen, Z.; Wannere,C. S.; Corminboeuf, C.; Puchta, R.; Schleyer, P. v. R. *Chem. Rev.* **2005**, *105*, 3842.

(30) (a) Parasuk, V.; Almlöf, J. *Chem. Phys. Lett.* **1991**, *184*, 187. (b) Brabec, C. J.; Anderson, E. B.; Davidson, B. N.; Kajihara, S. A.; Zhang, Q.-M.; Bernholc, J.; Tomanek, D. *Phys. Rev. B* **1992**, *46*, 7326. (c) Slanina, Z.; Adamowicz, L. *Thermochim. Acta* **1992**, *23*, 299. (d) Raghavachari, K.; Strout, D. L.; Odom, G. K.; Scuseria, G. E.; Pople, J. A.; Johnson, B. G.; Gill, P. M. W. *Chem. Phys. Lett.* **1993**, *214*, 357. (e) Slanina, Z.; Adamowicz, L. *Fullerene Sci. Technol.* **1993**, *1*, 1. (f) Sawtarie, M.; Menon, M.; Subbaswamy, K. R. *Phys. Rev. B* **1994**, *49*, 7739. (g) Taylor, P. R.; Bylaska, E.; Weare, J. H.; Kawai, R. *Chem. Phys. Lett.* **1995**, *235*, 558. (h) Grossman, J. C.; Mitas, L.; Raghavachari, K. *Phys. Rev. Lett.* **1995**, *75*, 3870. (i) Wang, Z.; Day, P.; Pachter, R. *Chem. Phys. Lett.* **1996**, *248*, 121. (j) Martin, J. M. L.; El-Yazal, J.; Francois, J.-P. *Chem. Phys. Lett.* **1996**, *248*, 345. (k) Bylaska, E. J.; Taylor, P. R.; Kawai, R.; Weare, J. H. *J. Phys. Chem.* **1996**, *100*, 6966. (l) Jones, R. O.; Seifert, G. *Phys. Rev. Lett.* **1997**, *79*, 443. (m) Murphy, R. B.; Friesner, R. A. *Chem. Phys. Lett.* **1998**, *288*, 403. (n) Sokolova, S.; Lüchow, A.; Anderson, J. B. *Chem. Phys. Lett.* **2000**, *323*, 229. (o) Grimme, S.; Mück-Lichtenfeld, C. *ChemPhysChem* **2002**, *3*, 207. (p) Saito, M.; Miyamoto, Y. *Phys. Rev. B* **2002**, *65*, 165434. (q) Beran, K. A.; Greene, K. R. *J. Comput. Chem.* **2002**, *23*, 938. (r) Beran, K. A. *J. Comput. Chem.* **2003**, *24*, 1287. (s) Saito, M.; Miyamoto, Y. *Phys. Rev. Lett.* **2001**, *87*, 035503. (t) Lu, J.; Re, S.; Choe, Y.; Nagase, S.; Zhou, Y.; Han, R.; Peng, L.; Zhang, X.; Zhao, X. *Phys. Rev. B* **2003**, *67*, 125415. (u) Gianturco, F. A.; Kashenock, G. Y.; Lucchese, R. R.; Sanna, N. *J. Chem. Phys.* **2002**, *116*, 2811. (v) Castro, A.; Marques, M. A. L.; Alonso, J. A.; Bertsch, G. F.; Yabana, K.; Rubio, A. *J. Chem. Phys.* **2002**, *116*, 1930. (w) Romero, A. H.; Sebastiani, D.; Ramírez, R.; Kiwi, M. *Chem. Phys. Lett.* **2002**, *366*, 134. (x) Paulus, B. *Phys. Chem. Chem. Phys.* **2003**, *5*, 3364. (y) Luo, J.; Peng, L. M.; Xue, Z. Q.; Wu, J. L. *J. Chem. Phys.* **2004**, *120*, 7998.

(31) Chen, Z.; Heine, T.; Jiao, H.; Hirsch, A.; Thiel, W.; Schleyer, P. v. R. *Chem. Eur. J.* **2004**, *10*, 963.

(32) (a) Helden, G. V.; Hsu, M. T.; Gotts, N. G.; Kemper, P. R.; Bowers, M. T. *Chem. Phys. Lett.* **1993**, *204*, 15. (b) Hunter, J. N.; Fey, J. L.; Jarrold, M. F. *J. Phys. Chem.* **1993**, *97*, 3460. (c) Hunter, J. N.; Fey, J. L.; Jarrold, M. F. *Science* **1993**, *260*, 784. (d) Yang, S.; Taylor, K. J.; Craycraft, M. J.; Conceicao, J.; Pettiette, C. L.; Cheshnovsky, O.; Smalley, R. E. *Chem. Phys. Lett.* **1988**, *144*, 431. (e) Handschuh, H.; Ganteför, G.; Kessler, B.; Bechthold, P. S.; Eberhardt, W. *Phys. Rev. Lett.* **1995**, *74*, 1095.

(33) Ott, A. K.; Rechtsteiner, G. A.; Felix, C.; Hampe, O.; Jarrold, M. F.; Duyne, R. P. V.; Raghavachari, K. *J. Chem. Phys.* **1998**, *109*, 9652.

(34) Domene, M. C.; Fowler, P. W.; Mitchell, D.; Seifert, G.; Zerbetto, F. *J. Phys. Chem. A* **1997**, *101*, 8339.

(35) Galli, G.; Gygi, F.; Golaz, J. C. *Phys. Rev. B* **1998**, *57*, 1860.

(36) Ehlich, R.; Landenberger, P.; Prinzbach, H. *J. Chem. Phys.* **2001**, *115*, 5830.

(37) Choi, C. H.; Lee, H. I. *Chem. Phys. Lett.* **2002**, *359*, 446.

(38) Wang, Z.; Ke, X.; Zhu, Z.; Zhu, F.; Ruan, M.; Chen, H.; Huang, R.; Zheng, L. *Phys. Lett. A* **2001**, *280*, 351.

(39) (a) Miyamoto, Y.; Saito, M. *Phys. Rev. B* **2001**, *63*, 161401. (b) Okada, S.; Miyamoto, Y.; Saito, M. *Phys. Rev. B* **2001**, *64*, 245405;

(40) (a) Iqbal, Z.; Zhang, Y.; Grebel, H.; Vijayalakshmi, S.; Lahamer, A.; Benedek, G.; Bernasconi, M.; Cariboni, J.; Spagnolatti, I.; Sharma, R.; Owens, F. J.; Kozlov, M. E.; Rao, K. V.; Muhammed, M. *Eur. J. Phys.* **2003**, *31*, 509. (b) Spagnolatti, I.; Mussi, A.; Bernasconi, M.; Benedek, G. *Eur. J. Phys.* **2004**, *37*, 143. (c) Spagnolatti, I.; Bernasconi, M.; Benedek, G. *Eur. Phys. Lett.* **2002**, *59*, 572.

(41) Fowler, P. W.; Woolrich, J. *Chem. Phys. Lett.* **1986**, *127*, 78.

(42) Chen, Z.; Jiao, H.; Bühl, M.; Hirsch, A.; Thiel, W. *Theor. Chem. Acc.* **2001**, *106*, 352.

(43) Chistyakov, A. L.; Stankevich, I. V.; Korlyukov, A. A. *Phys. Solid State* **2005**, *47*, 191.

(44) (a) Plato, *Timaios*; *Sämtliche Werke*, *Bd. 5*, Grassi, E., Ed.; Rowohlt: Hamburg, 1959; (b) Heilbronner, E.; Dunitz, J. D. *Reflections on Symmetry*; VCH Verlag Helvetica Chimica Acta: Basel, 1993; p 12.

(45) (a) Mehta, G. *J. Sci. Ind. Res.* **1978**, *37*, 256. (b) Eaton, P. E. *Tetrahedron* **1979**, *35*, 2189 and references therein.

(46) (a) Paquette, L. A.; Ternansky, R. J.; Balogh, D. W. *J. Am. Chem. Soc.* **1982**, *104*, 4502. (b) Ternansky, R. J.; Balogh, D. W.; Paquette, L. A. *J. Am. Chem. Soc.* **1982**, *104*, 4503. (c) Paquette, L. A.; Ternansky, R. J.; Balogh, D. W.; Kentgen, G. *J. Am. Chem. Soc.* **1983**, *105*, 5446. (d) Paquette, L. A. *Chem. Rev.* **1989**, *89*, 1051. (e) Paquette, L. A. In *Cage Hydrocarbons*; Olah, G. A., Ed.; Wiley: New York, 1990; pp 313−352.

(47) (a) Prinzbach, H. In *Alkane Activation and Cage Compounds (A-37)*; Yurchenko, A. G., Ed.; Kiew, 1998. (b) Bertau, M.; Leonhardt, J.; Weiler, A.; Weber, K.; Prinzbach, H. *Chem. Eur. J.* **1996**, *2*, 570. (c) Fessner, W. D.; Prinzbach, H. In *Cage Hydrocarbons*; Olah, G. A., Ed.; Wiley: New York, 1990; pp 353−405. (d) Scheumann, K.; Sackers, E.; Bertau, M.; Leonhardt, J.; Hunkler, D. Fritz, H.; Wörth, J.; Prinzbach, H. *J. Chem. Soc., Perkin Trans. 2* **1998**, 1195. (e) Melder, J. P.; Weber, K.; Weiler, A.; Sackers, E.; Fritz, H.; Hunkler, D.; Prinzbach, H. *Res. Chem. Intermed.* **1996**, *22*, 667.

(48) (a) Beckhaus, H. D.; Ruchardt, C.; Lagerwall, D. R.; Paquette, L. A.; Wahl, F.; Prinzbach, H. *J. Am. Chem. Soc.* **1994**, *116*, 11775. (b) Beckhaus, H. D.; Ruchardt, C.; Lagerwall, D. R.; Paquette, L. A.; Wahl, F.; Prinzbach, H. *J. Am. Chem. Soc.* **1995**, *117*, 8885.

(49) (a) Engler, E. M.; Andose, J. D.; Schleyer, P. v. R. *J. Am. Chem. Soc.* **1973**, *95*, 8005. (b) Allinger, N. L. *J. Am. Chem.* Soc. **1977**, *99*, 8127. (c) Clark. T.: Knox, T. M.; McKervev, M. A.: Mackle, H.; Rooney, J. J. *J. Am. Chem. Soc.* **1979**, *101*, 2404−2410. (d) Allinger, N. L.; Geise, H. J.; Pyckhout, W.; Paquette, L. A.; Gallucci, J. C. *J. Am. Chem. Soc.* **1989**, *111*, 1106.

(50) (a) Schulman, J. M.; Disch, R. L. *J. Am. Chem. Soc.* **1978**, *100*, 5677. (b) Dixon, D. A.; Deerfield, D.; Graham, G. D. *Chem. Phys. Lett.* **1981**, *78*, 161. (c) Schulman, J. M.; Disch, R. L. *J. Am. Chem. Soc.* **1984**, *106*, 1202. (d) Disch, R. L.; Schulman, J. M.; Sabio, M. L. *J. Am. Chem. Soc.* **1985**, *107*, 1904. (e) Scamehorn, C. A.; Hermiller, S. M.; Pitzer, R. M. *J. Chem. Phys.* **1986**, *84*, 833. (f) Disch, R. L.; Schulman, J. M. *J. Phys. Chem.* **1996**, *100*, 3504.

(51) Ermer, O. *Angew. Chem., Int. Ed.* **1977**, *16*, 411.

(52) Hudson, B. S.; Braden, D. A.; Parker, S. F.; Prinzbach, H. *Angew. Chem., Int. Ed.* **2000**, *39*, 514.

(53) Schulman, J. M.; Venanzi, T.; Disch, R. L. *J. Am. Chem. Soc.* **1975**, *97*, 7, 5335.

(54) (a) McMahon, B. J.; Hagen, S.; Mack, J.; Blank, J.; Wegner, H.; de Meijere, A. *Science*, **2002**, *295*, 1500. (b) Boorum, M. M.; Vasil'ev, Y. V.; Drewello, T.; Scott, L. T. *Science* **2001**, *294*, 828.

(55) (a) Hrovat, D. A.; Borden, W. T. *J. Am. Chem. Soc.* **1988**, *110*, 4710. (b) Borden, W. T. *Chem. Rev.* **1989**, *89*, 1097.

(56) Woodward, R. B.; Hoffmann, R. *The Conservation of Orbital Symmetry*; Academic Press: New York, 1970.

(57) Campbell, E. E. B.; Tellgmann, R.; Wahl, F.; Prinzbach, H. *Int. J. Mass Spectrom. Ion Processes* **1994**, *136*, 209.

(58) Weber, K.; Fritz, H.; Prinzbach, H. *Tetrahedron Lett.* **1992**, *33*, 619.

(59) (a) Prakash, G. K. S.; Krishnamurthy, V. V.; Herges, R.; Bau, R.; Yuan, H.; Olah, G. A.; Fessner, W.-D.; Prinzbach, H. *J. Am.*

Chem. Soc. **1988**, *110*, 7764. (b) Herges, R.; Schleyer, P. v. R.; Schindler, M.; Fessner, W.-D. *J. Am. Chem. Soc.* **1991**, *113*, 3649.
(60) For recent reviews on homoconjugation, see (a) Williams, R. V. *Chem. Rev.* **2001**, *101*, 1185. (b) Williams, R. V. *Eur. J. Org. Chem.* **2001**, 227.
(61) (a) Weber, K.; Prinzbach, H.; Schmidlin, R.; Gerson, F.; Gescheidt, G. *Angew. Chem., Int. Ed. Engl.* **1993**, *32*, 875. (b) Martin, H.-D.; Mayer, B.; Weber, K.; Prinzbach, H. *Liebigs Ann.* **1995**, 2019. (c) Weber, K.; Lutz, G.; Knothe, L.; Mortensen, J.; Heinze, J.; Prinzbach, H. *J. Chem. Soc., Perkin Trans. 2* **1995**, 1991.
(62) (a) McEwen, A. B.; Schleyer, P. v. R., *J. Org. Chem.* **1986**, *51*, 4357. (b) Fokin, A. A.; Jiao, H.; Schleyer, P. v. R. *J. Am. Chem. Soc.* **1998**, *120*, 9364−9365.
(63) (a) Chandrasekhar, J.; Jemmis, E. D.; Schleyer, P. v. R. *Tetrahedron Lett.* **1979**, 3730. (b) Schleyer, P. v. R.; Jiao, H.; Glukhovtsev, M. N.; Chandrasekhar, J.; Kraka, E. *J. Am. Chem. Soc.* **1994**, *116*, 10129.
(64) Guo, B. C.; Kerns, K. P.; Castleman, A. W., Jr. *Science* **1992**, *255*, 1411.
(65) (a) Guo, B. C.; Wei, S.; Purnell, J.; Buzza, S. A.; Castleman, A. W., Jr. *Science* **1992**, *256*, 515. (b) Wei, S.; Guo, B. C.; Deng, H. T.; Kerns, K.; Purnell, J.; Buzza, S. A.; Castleman, A. W., Jr. *J. Am. Chem. Soc.* **1994**, *116*, 4475. (c) Pilgrim, J. S.; Duncan, M. A. *J. Am. Chem. Soc.* **1993**, *115*, 6958. (d) Cartier, S. F.; May, B. D.; Castleman, A. W., Jr. *J. Chem. Phys.* **1994**, *100*, 5384. (e) Cartier, S. F.; May, B. D.; Castleman, A. W., Jr. *J. Am. Chem. Soc.* **1994**, *116*, 5295. (f) Deng, H. T.; Guo, B. C.; Kerns, K. P.; Castleman, A. W., Jr. *Int. J. Mass Spectrom. Ion Processes* **1994**, *138*, 275.
(66) For recent reviews on metallocarbohedrene, see (a) Rohmer, M. M.; Benard, M.; Poblet, J. M. *Chem. Rev.* **2000**, *100*, 495. (b) Leskiw, B. D.; Castleman, A. W. *C. R. Physique* **2002**, *3*, 251.
(67) (a) Dance, I. G. *J. Chem. Soc., Chem. Commun.* **1992**, 1779. (b) Lin, Z.; Hall, M. B. *J. Am. Chem. Soc.* **1993**, *115*, 11165. (c) Hay, P. J. *J. Phys. Chem.* **1993**, *97*, 3081−3083. (d) Dance, I. G. *J. Am. Chem. Soc.* **1996**, *118*, 6309.
(68) Sakurai, H.; Castleman, A. W., Jr. *J. Phys. Chem. A* **1998**, *102*, 10486.
(69) Gueorguiev, G. K.; Pacheco, J. M. *Phys. Rev. Lett.* **2002**, *88*, 115504.
(70) Alder, R. W.; Harvey, J. N.; Schleyer, P. v. R.; Moran, D. *Org. Lett.*, **2001**, *3*, 3233.
(71) Borden, W. T. *Synlett* **1996**, 711.
(72) Evangelisti, S. *Int. J. Quantum Chem.* **1997**, *65*, 83.
(73) Bode, B. M.; Gordon, M. S. *J. Chem. Phys.* **1999**, *111*, 8778.
(74) Pattanayak, J.; Kar, T.; Scheiner, S. *J. Phys. Chem. A* **2004**, *108*, 7681.
(75) (a) Disch, R. L.; Schulman, J. M. *J. Am. Chem. Soc.* **1981**, *103*, 3297. (b) Minkin, V. I.; Minayev, R. M.; Zhdanov. *Nonclassical Structures of Organic Compounds*; MIR: Moscow, 1987; p 238.
(76) For early examples of endohedral fullerenes, see (a) Diederich, F.; Rubin, Y. *Angew. Chem., Int. Ed.* **1992**, *31*, 1101. (b) Chai, Y.; Guo, T.; Jin, C.; Haufler, R. E.; Chibante, L. P. F.; Fure, J.; Wang, L.; Alford, J. M.; Smalley, R. E. *J. Phys. Chem.* **1991**, *95*, 7564.
(77) Jiménez-Vázquez, H. A.; Tamariz, J.; Cross, R. J. *J. Phys. Chem. A* **2001**, *105*, 1315.
(78) (a) Moran, D.; Stahl, F.; Jemmis, E. D.; Schaefer, H. F., III.; Schleyer, P. v. R. *J. Phys. Chem. A* **2002**, *106*, 5144. (b) Chen, Z. F.; Jiao, H. J.; Moran, D.; Hirsch, A.; Thiel, W.; Schleyer, P.v. R. *J. Phys. Chem. A* **2003**, *107*, 2075.
(79) Park, S.; Srivastava, D.; Cho, K. *J. Nanosci. Nanotech.* **2001**, *1*, 1.
(80) (a) Harneit, W.; Waiblinger, M.; Meyer, C.; Lips, K.; Weidinger, A. *Proc. Electrochem. Soc.* **2001**, *11*, 358. (b) Meyer, C.; Harneit, W.; Waiblinger, M.; Lips, K.; Weidinger, A. *AIP Conference Proceedings* **2001**, *591*, 101. (c) Harneit, W.; Waiblinger, M.; Lips, K.; Makarov, S.; Weidinger, A. *AIP Conf. Proc.* **2000**, *544*, 207. (d) Harneit, W. *Phys. Rev. A* **2002**, *65*, 032322.
(81) Cross, R. J.; Saunders: M.; Prinzbach, H. *Org. Lett.* **1999**, *1*, 1479.
(82) (a) Saunders: M.; Jiménez-Vázquez, H. A.; Cross, R. J.; Poreda, R. J. *Science* **1993**, *259*, 1428. (b) Saunders: M.; Cross, R. J.; Jiménez-Vázquez, H. A.; Shimshi, R.; Khong, A. *Science* **1996**, *271*, 1693.
(83) (a) Feyereisen, M.; Gutowski, M.; Simons, J.; Almlöf, *J. Chem. Phys.* **1992**, *96*, 2926. (b) Guo, T.; Scuseria, G. E.; Smalley, R. E. *J. Chem. Phys.* **1993**, *99*, 352. (c) Huang, C. H.; Li, J. Q. *Acta Phys. Sin.* **1993**, *48*, 633. (d) Martin, J. M. L. *Chem. Phys. Lett.* **1996**, *255*, 1. (e) Portmann, S.; Galbraith, J. M.; Schaefer, H. F.; Scuseria, G. E.; Luthi, H. P. *Chem. Phys. Lett.* **1999**, *301*, 98. (f) Klimko, G. T. Mestechkin, M. M.; Whyman, G. E.; Khmelevsky, S. *J. Mol. Struct.* **1999**, *481*, 329. (g) Mishra, K.; Lin, Y. T.; Lee, S. L. *Int. J. Quantum Chem.* **2001**, *84*, 642. (h) Liu, H.; Weng, H. M.; Dong, J. M. *J. Mol. Struct. THEOCHEM* **2004**, *671*, 93. (i) Tuan, D. F.-T.; Pitzer, R. M. *J. Phys. Chem.* **1996**, *100*, 627.
(84) Kent, P. R. C.; Towler, M. D.; Needs, R. J.; Rajagopal, G. *Phys. Rev. R.* **2000**, *62*, 15394.
(85) (a) Pederson, M. R.; Laouini, N. *Phys. Rev. B* **1993**, *48*, 2733. (b) Jackson, K.; Kaxiras, E.; Pederson, M. R. *Phys. Rev. B* **1993**, *48*, 17556. (c) Makurin, Y. N.; Sofronov, A. A.; Gusev, A. I.; Ivanovsky, A. L. *Chem. Phys.* **2001**, *270*, 293. (d) Ionov, S. P.; Kuznetsov, N. T.; Sevast'yanov, V. G. *Russ. J. Coord. Chem.* **2003**, *29*, 766. (e) Dunlap, B. I.; Häberlen, O. D.; Rösch, N. *J. Phys. Chem.* **1992**, *96*, 9095. (f) Häberlen, O. D.; Rösch, N.; Dunlap, B. I. *Chem. Phys. Lett.* **1992**, *200*, 418.
(86) (a) Lu, L. H.; Sun, K. C.; Chen, C. *Int. J. Quantum Chem.* **1998**, *67*, 187. (b) Makurin, Y. N.; Sofronov, A. A.; Ivanovskii, A. L. *Russ. J. Coord. Chem.* **2000**, *26*, 464. Lu, L. H.; Sun, K. C.; Chen, C. *Russ. J. Coord. Chem.* **1998**, *68*, 273.
(87) For investigations on C_{28} solids, see (a) Bylander, D. M.; Kleinman, L. *Phys. Rev. B* **1993**, *47*, 10967. (b) Kaxiras, E.; Zeger, L. M.; Antonelli, A.; Juan, Y. M. *Phys. Rev. B* **1994**, *49*, 8446. (c) Zeger, L. M.; Juan, Y. M.; Kaxiras, E.; Antonelli, A. *Phys. Rev. B* **1995**, *52*, 2125. (d) Canning, A.; Galli, G.; Kim, J. *Phys. Rev. Lett.* **1997**, *78*, 4442. (e) Kim, J.; Galli, G.; Wilkins, J. W.; Canning, A. *J. Chem. Phys.* **1998**, *108*, 2631. (f) Breda, N.; Broglis, R. A.; Colo, G.; Onida, G.; Provasi, D.; Vigezzi, E. *Phys. Rev. B* **2000**, *62*, 130. (g) Enyashin, A. N.; Ivanovskaya, V. V.; Makurin, Yu. N.; Ivanovskii. A. L. *Phys. Solid State* **2004**, *46*, 1569. (h) Romero, N. A.; Kim, J.; Martin, R. M. *Phys. Rev. B* **2004**, *70*, R140504.
(88) Maruyama, S.; Kohno, M.; Inoue, S. In *Fullerenes 2000 Volume 10: Chemistry and Physics of Fullerenes and Carbon Nanomaterials*, Proceedings of the Electrochemical Society, Toronto, Canada, Spring 2000; Kamat, P. V.; Guldi, D. M.; Kadish, K. M., Eds.; Electrochemical Society: Pennington, NJ; p 309.
(89) Ge, M. F.; Feng, J. K.; Cui, M.; Wang, S. F.; Tian, W. Q. *Acta Chim. Sin.* **1999**, *57*, 645.
(90) Sofronov, A. A.; Makurin, Y. N.; Ivanovskii, A. L. *Russ. J. Coord. Chem.* **2000**, *26*, 406.
(91) Rohlfing, E. A.; Cox, D. M.; Kaldor, A. *J. Chem. Phys.* **1984**, *81*, 3322.
(92) For examples, see (a) Kroto, H. W. *Science*, **1988**, *242*, 1139. (b) O'Brien, S. C.; Heath, J. R.; Curl, R. F.; Smalley, R. E. *J. Chem. Phys.* **1988**, *88*, 220. (c) Yang, Y. A.; Xia, P.; Junkin, A. L.; Blomfield, L. A. *Phys. Rev. Lett.* **1991**, *66*, 1205. (d) Kietzmann, H.; Rochow, R.; Gantefor, G.; Eberhardt, W.; Vietze, K.; Seifert, G.; Fowler, P. W. *Phys. Rev. Lett.* **1998**, *81*, 5378. (e) Curl, R. F. *Rev. Mod. Phys.* **1997**, *69*, 691.
(93) Krätschmer, W.; Lamb, L. D.; Fostiropoulos, K.; Huffman, D. R. *Nature* **1990**, *347*, 354.
(94) (a) Fowler, P. W.; Heine, T.; Rogers, K. M.; Sandall, J. P. B.; Seifert, G.; Zerbetto, F. *Chem. Phys. Lett.* **1999**, *300*, 369. (b) Fowler, P. W.; Mitchell, D.; Zerbetto, F. *J. Am. Chem. Soc.* **1999**, *121*, 1, 3218.
(95) Collins, P. G.; Grossman, J. C.; Côte, M.; Ishigami, M.; Piskoti, C.; Louie, S. G.; Cohen, M. L.; Zettl, A. *Phys. Rev. Lett.* **1999**, *82*, 165.
(96) Goel, A.; Howard, J. B.; Vander Sande, J. B. *Carbon* **2004**, *42*, 1907.
(97) (a) Slanina, Z.; Zhao. X.; Osawa, E. *Chem. Phys. Lett.* **1998**, *290*, 311. (b) Grossman, J. C.; Cote, M.; Louie, S. G.; Cohen, M. L. *Chem. Phys. Lett.* **1998**, *284*, 344. (c) Cote, M.; Grossman, J. C.; Cohen, M. L.; Louie, S. G. *Phys. Rev. Lett.* **1998**, *81*, 697. (d) Halac, E.; Burgos, Bonadeo, H. *Chem. Phys. Lett.* **1999**, *299*, 64. (e) Jagadeesh, M. N.; Chandrasekhar, J. *Chem. Phys. Lett.* **1999**, *305*, 298. (f) Yuan, L. F.; Yang, J. L.; Deng, K.; Zhu, Q. S. *J. Phys. Chem. A* **2000**, *104*, 6666. (g) Li, J. Q.; Huang, X.; Wu, L. M.; Zhang, Y. F.; Wu, K. C. *Acta Chim. Sin.* **2000**, *58*, 319. (h) Slanina, Z.; Ulike, F.; Zhao. X.; Osawa, E. *J. Chem. Phys.* **2000**, *113*, 4933. (i) Chen, Z. F.; Jiao, H. J.; Hirsch, A.; Thiel, W. *Chem. Phys. Lett.* **2000**, *329*, 47. (j) Yu, X. Q.; Wu, C. J.; Wang, C. L.; Su, Z. B. *Int. J. Mod. Phys. B* **1999**, *13*, 1513. (k) Jishi, R. A.; Dresselhaus, M. S. *Chem. Phys. Lett.* **1999**, *302*, 533. (l) Ke, X. Z.; Zhu, Z. Y.; Wang, F.; Zhang, F. S.; Wang, Z. X. *Phys. Lett. A* **1999**, *255*, 294. (m) Ito, A.; Monobe, T.; Yoshii, T.; Tanaka, K. *Chem. Phys. Lett.* **2000**, *328*, 32. (n) Ito, A.; Monobe, T.; Yoshii, T.; Tanaka, K. *Chem. Phys. Lett.* **2000**, *330*, 281. (o) Slanina, Z.; Ulike, F.; Zhao. X.; Ueno, H.; Osawa, E. *Fullerene Sci. Technol.* **2000**, *8*, 433. (p) Slanina, Z.; Zhao. X.; Osawa, E. *Mol. Mater.* **2000**, *13*, 13. (q) Gueorguiev, G. K.; Pacheco, J. M. *J. Chem. Phys.* **2001**, *114*, 6068. (r) Takahashi, H.; Tsukada, M. *J. Phys. Soc. Jpn.* **2001**, *70*, 2788. (s) Beu, T. A.; Onoe, J.; Takeuchi, K. *Eur. Phys. J. D* **2001**, *17*, 205. (t) Gong, Z. J.; Xu, W. G.; Li, Q. S. *Chem. J. Chin. Univ.-Chin.* **2001**, *22*, 998. (u) Varganov, S. A.; Avramov, P. V.; Ovchinnikov, S. G.; Gordon, M. S. *Chem. Phys. Lett.* **2002**, *362*, 380. (v) Li, X. D.; Cheng, W. D.; Wu, D. S.; Lan, Y. Z.; Zhang, H.; Gong, Y. J.; Li, F. F.; Shen, J. *J. Chem. Phys.* **2004**, *121*, 5885.
(98) Ito, A.; Monobe, T.; Yoshii, T.; Tanaka, K. *Chem. Phys. Lett.* **1999**, *315*, 348.
(99) Stone, A. J.; Wales, D. J. *Chem. Phys. Lett.* **1986**, *128*, 501.
(100) Jin, Y.; Hao, C. *J. Phys. Chem. A* **2005**, *109*, 2875.
(101) (a) Lin, M. H.; Chiu, Y. N.; Xiao, J. M. *J. Mol. Struct.- TheoChem* **1999**, *489*, 109. (b) Yang, Z. Y.; Wang, G. C.; Shang, Z. F.; Pan, Y. M.; Wu, B. X.; Zhao, X. Z. *Chem. J. Chin. Univ.-Chin.* **2001**,

22, 1539. (c) Grossman, J. C.; Colvin, M. E.; Tran, N. L.; Louie, S. G.; Cohen, M. L. *Chem. Phys. Lett.* **2002**, *356*, 247. (d) Corminboeuf, C.; Fowler, P. W.; Heine, T. *Chem. Phys. Lett.* **2002**, *361*, 405.
(102) Yang, Z. Y.; Wang, G. C.; Shang, Z. F.; Cai, Z. S.; Pan, Y. M.; Zhao, X. Z. *J. Mol. Struct. THEOCHEM* **2001**, *549*, 243.
(103) (a) Xu, X. F.; Shang, Z. F.; Wang, G. C.; Cai, Z. S.; Pan, Y. M.; Zhao, X. Z. *J. Mol. Struct. THEOCHEM* **2002**, *589*, 265. (b) Yang, Z. Y.; Li, R. F.; Yang, X.; Wang, G. C.; Shang, Z. F.; Pan, Y. M.; Wu, B. X.; Zhao, X. Z. *Chem. J. Chin. Univ.-Chin.* **2002**, *23*, 1926.
(104) Xu, X. F.; Yang, Z. Y.; Wang, G. C.; Shang, Z. F.; Wu, B. X.; Pan, Y. M.; Zhao, X. Z. *Chem. J. Chin. Univ.-Chin.* **2003**, *24*, 682.
(105) Slanina, Z.; Chow, T. J. *J. Nanosci. Nanotech.* **2003**, *3*, 303.
(106) (a) Ding, C. G.; Yang, J. L.; Cui, X. Y.; Wang, K. L. *Eur. Phys. J. D* **2000**, *11*, 123. (b) Ding, C. G.; Yang, J. L.; Han, R. S.; Wang, K. L. *J. Chem. Phys.* **2001**, *114*, 9375.
(107) Porezag, D.; Jungnickel, G.; Frauenheim, T.; Seifert, G.; Ayuela, A.; Pederson, M. R. *Appl. Phys. A* **1997**, *64*, 321.
(108) Chen, Y., M.; Li, Y. X.; Huang, Y. H.; Liu, R. Z. *Acta Chim. Sin.* **2000**, *58*, 1511.
(109) Chen, Y., M.; Huang, Y. H.; Liu, R. Z. *Acta Chim. Sin.* **2004**, *62*, 53.
(110) Heine, T.; Fowler, P. W.; Seifert, G. *Solid State Commun.* **1999**, *111*, 19.
(111) (a) Huang, Y. H.; Chen, Y. M.; Liu, R. Z. *J. Phys. Chem. Solids* **2000**, *61*, 1475. (b) Chen, Y. M.; Huang, Y. H.; Liu, R. Z. *Acta Phys.-Chim. Sin.* **2001**, *17*, 196. (c) Huang, Y. H.; Du, S. X.; Chen, Y. M.; Li, Y. X.; Liu, R. Z. *J. Phys.: Condens. Matter* **2002**, *14*, 6777. (d) Du, S. X.; Huang, Y. H.; Liu, R. Z. *Chem. Phys. Lett.* **2003**, *380*, 372.
(112) (a) Gal'pern, E. G.; Stankevich, I. V.; Chernozatonski, L. A.; Chistiakov, A. L. *J. Mol. Graph. Model.* **2001**, *19*, 189. (b) Du, S. X.; Huang, Y. H.; Li, Y. X.; Liu, R. Z. *J. Phys. Chem. B* **2002**, *106*, 4098. (c) Zhang, M. X.; Li, J. Q.; Zhang, Y. F. *Chin. J. Struct. Chem.* **2002**, *21*, 451. (d) Gal'pern, E. G.; Sabirov, A. R.; Stankevich, I. V.; Chernozatonski, L. A.; Chistiakov, A. L. *Fullerene Nanotubes Carbon Nanostruct.* **2004**, *12*, 455.
(113) (a) Grossman, J. C.; Louie, S. G.; Cohen, M. L. *Phys. Rev. B.* **1999**, *60*, R6941. (b) Gal'pern, E. G.; Sabirov, A. R.; Stankevich, I. V.; Chernozatonski, L. A.; Chistiakov, A. L. *JETP Lett.* **2001**, *73*, 491. (c) Rosato, V.; Celino, M.; Benedek, G.; Gaito, S. *Phys. Rev. B* **1999**, *60*, 16928. (d) Burgos, E.; Halac, E.; Bonadeo, H. *Chem. Phys. Lett.* **2000**, *320*, 14. (e) Menon, M.; Richter, E. *Phys. Rev. B* **1999**, *60*, 13322. (f) Menon, M.; Richter, E.; Chernozatonskii, L. *Phys. Rev. B* **2000**, *62*, 15420.
(114) (a) Bakowies, D.; Thiel, W. *J. Am. Chem. Soc.* **1991**, *113*, 3704. (b) Xu, W. G.; Wang, Y.; Li, Q. S. *J. Mol. Struct. THEOCHEM* **2000**, *531*, 119.
(115) Zhechkov, L.; Heine, T.; Seifert, G. *J. Phys. Chem. A* **2004**, *108*, 11733.
(116) Diaz-Tendero, S.; Alcami, M.; Martin, F. *Chem. Phys. Lett.* **2005**, *407*, 153.
(117) (a) Zhao, X. *J. Phys. Chem. B.* **2005**, *109*, 5267. (b) Slanina, Z.; Adamowicz, L.; Bakowies, D.; Thiel. W. *Thermochim. Acta* **1992**, *202*, 249.
(118) Xu, X. F.; Xing, Y. M.; Liang, Y. X.; Shang, Z. F.; Wang, G. C.; Cai, Z. S.; Pan, Y. M.; Zhao, X. Z. *Phys. Chem. Chem. Phys.* **2002**, *4*, 5572.
(119) Wang, X.-B.; Ding, C.-F.; Wang, L.-S. *J. Chem. Phys.* **1999**, *110*, 8217.
(120) Gao, F.; Xie, S. Y.; Huang, R. B.; Zheng, L. S. *Chem. Commun.* **2003**, 2676.
(121) Xie, R. H.; Bryant, G. W.; Cheung, C. F.; Smith, V. H., Jr.; Zhao, J. J. *J. Chem. Phys.* **2004**, *121*, 2849.
(122) Guldi, D. *Chem. Commun.* **2000**, 321.
(123) Yang, Y.; Wang, F. H.; Zhou, Y. S.; Yuan, L. F.; Yang, *J. Phys. Rev. A* **2005**, *71*, 013202.
(124) Xie, S. Y.; Huang, R. B.; Deng, S. L.; Yu, L. J.; Zheng, L. S. *J. Phys. Chem. B* **2001**, *105*, 1734.
(125) Xu, X.; Xing, Y.; Yang, X.; Wang, G.; Cai, Z.; Shang, Z.; Pan, Y.; Zhao, X. *Int. J. Quantum Chem.* **2005**, *101*, 160.
(126) (a) Kimura, T.; Sugai, T.; Shinohara, H. *Int. J. Mass. Spectrom.* **1999**, *188*, 225. (b) Maruyama, S.; Yamaguchi, Y.; Kohno, M. Yoshida, T. *Fuller. Sci. Technol.* **1999**, *7*, 621. (c) Heath, J.; O'Brien, S. C.; Zhang, Q.; Liu, Y.; Curl, R. F.; Kroto, H. W.; Tittel, F. K.; Smalley, R. E. *J. Am. Chem. Soc.* **1985**, *107*, 7779.
(127) Breslavskaya, N. N.; Levin, A. A.; Buchachenko, A. L. *Russ. Chem. Bull.* **2004**, *53*, 18.
(128) Xu, X. F.; Xing, Y. M.; Shang, Z. F.; Wang, G. C.; Cai, Z. S.; Pan, Y. M.; Zhao, X. Z. *Chem. Phys.* **2003**, *287*, 317.
(129) Xu, X.; Shang, Z.; Wang, G.; Li, R.; Cai, Z.; Zhao, X. *J. Phys. Chem. A.* **2005**, *109*, 3754.
(130) (a) Jensen, F. Toftlund, H. *Chem. Phys. Lett.* **1993**, *201*, 89. (b) Raghavachari, K.; Zhang, B.; Pople, J. A.; Johnson, B. G.; Gill, P. M. W. *Chem. Phys. Lett.* **1994**, *220*, 385. (c) Martin, J. M. L.; El-Yazai, J. Francois, J. P. *Chem. Phys. Lett.* **1996**, *255*, 7. (d) Balevicius, L. M.; Stumbrys, E.; Tamulis, A. *Fullerene Sci. Technol.* **1997**, *5*, 85.
(131) Jensen, F.; Koch, H. *J. Chem. Phys.* **1998**, *108*, 3213.
(132) Fowler, P. W.; Heine, T.; Troisi, A. *Chem. Phys. Lett.* **1999**, *312*, 77.
(133) Strout, D. L. *J. Phys. Chem. A* **2000**, *104*, 3324.
(134) (a) Pokropivny, V. V.; Pokropivny, A. V.; Skorokhod, V. V.; Kurdyumov, A. V. *Dopov. Nats. Akad. Nauk Ukr.* **1999**, *4*, 112. (b) Pokropivny, V. V.; Pokropivny, A. V. *Phys. Solid State* **2004**, *46*, 392. (c) Pokropivny, V. V.; Skorokhod, V. V.; Oleinik, G. S.; Kurdyumov, A. V.; Bartnitskaya, T. S.; Pokropivny, A. V.; Sisonyuk, A. G.; Sheichenko, D. M. *J. Solid State Chem.* **2000**, *154*, 214.
(135) For examples of cubic graphite, see (a) Aust, R. B.; Drickamer, H. C. Science **1963**, *140*, 817. (b) Bundy, F. P.; Kasper, J. S. *J. Chem. Phys.* **1967**, *46*, 3437. (c) Slodkevich, V. V. *Dokl. Akad. Nauk SSSR* **1980**, *253*, 697.
(136) (a) Lin, M. H.; Chiu, Y. N.; Lai, S. T.; Xiao, J. M.; Fu, M. Z. *Fullerene Sci. Technol.* **1997**, *5*, 111. (b) Zhao, X.; Slanina, Z.; Ozawa, M.; Osawa, E.; Deota, P.; Tanabe, K. *Fullerene Sci. Technol.* 2000, 8, 595. (c) Sun, Q.; Wang, Q.; Yu, J. Z.; Ohno, G.; Kawazoe, Y. *J. Phys.-Condens. Matter* **2001**, *13*, 1931.
(137) Bühl, M. *Chem. Eur. J.* **1998**, *4*, 734.
(138) (a) Kroto, H. W.; Walton, D. R. M. *Chem. Phys. Lett.* **1993**, *214*, 353. (b) Lin, M. H.; Chiu, Y. N.; Xiao, J. M. *J. Mol. Struct. THEOCHEM* **1999**, *489*, 109.
(139) Liu, G. X.; Zhang, H. X.; Sun, C. C.; Tang, A. Q. *Chem. J. Chin. Univ.-Chin.* **2003**, *24*, 105.
(140) (a) Xiao, J. M.; Lin, M. H.; Chiu, Y. N.; Fu, M. Z.; Lai, S. T.; Li, N. N. *J. Mol. Struct. THEOCHEM* **1998**, *428*, 149. (b) Salcedo, R.; Sansores, L. F. *J. Mol. Struct. THEOCHEM* **1998**, *422*, 245.
(141) Cui, M.; Zhang, H. X.; Ge, M. F.; Feng, J. K.; Tian, W. Q.; Sun, C. C. *Chem. Phys. Lett.* **1999**, *309*, 344.
(142) Lu, L. H.; Chen, C.; Sun, K. C. *Int. J. Quantum Chem.* **1998**, *68*, 273.
(143) (a) Clemmer, D. E.; Hunter, J. M.; Shelimov, K. B.; Jarrold, M. F. *Nature* **1994**, *372*, 248. (b) Shelimov, K. B.; Clemmer, D. E.; Jarrold, M. F. *J. Phys. Chem.* **1994**, *98*, 12819. (c) Clemmer, D. E.; Jarrold, M. F. *J. Am. Chem. Soc.* **1995**, *117*, 8841. (d) Shelimov, K. B.; Clemmer, D. E.; Jarrold, M. F. *J. Phys. Chem.* **1995**, *99*, 11376. (e) Shelimov, K. B.; Clemmer, D. E.; Jarrold, M. F. *J. Chem. Soc., Dalton Trans.* **1996**, 567.
(144) Fan, M. F.; Lin, Z. Y.; Yang, S. H. *J. Mol. Struct. THEOCHEM* **1995**, *337*, 231.
(145) (a) Zhang, B. L.; Wang, C. Z.; Ho, K. M.; Xu, C. H.; Chan, C. T. *J. Chem. Phys.* **1992**, *97*, 5007. (b) Zhang, B. L.; Xu, C. H.; Wang, C. Z.; Chan, C. T.; Ho, K. M. *Phys. Rev. B.* **1992**, *46*, 7333. (c) Lin, M. H.; Chen, M. D.; Zhang, Q. E.; Chiu, Y. N.; Lai, S. T. *Electron. J. Theor. Chem.* **1997**, *2*, 109. (d) White, C. T.; Lyons, M.; Brenner, D. W.; Mintmire, J. W.; Robertson, D. H.; Mowrey, R. C.; Dunlap, B. I. *Mater. Res. Soc. Symp. Proc.* **1994**, *349*, 331. (e) Sun, G.; Nicklaus, M. C.; Xie, R. H. *J. Phys. Chem. A.* **2005**, *109*, 4617.
(146) (a) Chen, Z.; Thiel, W. *Chem. Phys. Lett.* **2003**, *367*, 15. (b) Chen, Z. F. et al., unpublished results.
(147) (a) Balasubramanian, K. J. *Chem. Inf. Comput. Sci.* **1994**, *34*, 421. (b) Hobday, S.; Smith, R. *J. Chem. Soc., Faraday Trans.* **1997**, *93*, 3919. (c) Slanina, Z.; Lee, S. L. *Fullerene Sci. Technol.* **1995**, *3*, 151. (d) Wu, H. S.; Xu, X. H.; Jiao, H. J. *J. Phys. Chem. A* **2004**, *108*, 3813.
(148) (a) Gao, Y. D.; Herndon, W. C. *J. Am. Chem. Soc.* **1993**, *115*, 8459. (b) Dunlap, B. I.; Taylor, R. *J. Phys. Chem.* **1994**, *98*, 11018.
(149) (a) Hu, Y. H.; Ruckenstein, E. *J. Chem. Phys.* **2003**, *119*, 10073. (b) Lee, S. U.; Han, Y.-K. *J. Chem. Phys.* **2004**, *121*, 3941.
(150) (a) Díaz-Tendero, S.; Alcami, M.; Martín, F. *J. Chem. Phys.* **2003**, *119*, 5545. (b) Díaz-Tendero, S.; Martín, F.; Alcami, M. *ChemPhysChem* **2005**, 6, 92.
(151) Ren, X. Y.; Liu, Z. Y. *J. Chem. Phys.* **2005**, *122*, 34306.
(152) (a) Böttcher, A.; Weis, P.; Bihlmeier, A.; Kappes, M. M. *Phys. Chem. Phys. Chem.* **2004**, *6*, 5213. (b) Böttcher, A.; Weis, P.; Jester, S. S.; Löffler, D.; Bihlmeier, A.; Klopper, W.; Kappes, M. M. *Phys. Chem. Chem. Phys.* **2005**, *7*, 2816.
(153) For a recent review on exohedral metallofullerenes, see (a) Balch, A. L.; Olmstead, M. M. *Chem. Rev.* **1998**, *98*, 2123.
(154) For recent reviews on endohedral metallofullerenes, see (a) Shinohara, H. *Rep. Prog. Phys.* **2000**, *63*, 843. (b) Alasak, T.; Nagase, S., Eds.; *Endofullerenes: A New Family of Carbon Clusters*; Kluwer Academic: Dordrecht, Netherlands, 2001.
(155) (a) Branz, W.; Billas, I. M. L.; Malinowski, N.; Tast, F.; Heinebrodt, M.; Martin, T. P. *J. Chem. Phys.* **1998**, *109*, 3425. (b) Billas, I. M. L.; Branz, W.; Malinowski, N.; Tast, F.; Heinebrodt, M.; Martin, T. P. Massobrio, C.; Boero, M. Parrinello, M. *Nanostruct. Mater.* **1999**, *12*, 1071. (c) Poblet, J. M.; Minkler, K.; Cancilla, M.; Hayashi, A.; Lebrilla, C. B.; Balch, A. L. *Chem. Commun.* **1999**, 493. (d) Hayashi, A.; Xie, Y. M.; Poblet, J. M.; Campanera, J. M.; Lebrilla, C. B.; Balch, A. L. *J. Phys. Chem. A* **2004**, *108*, 2192. (e) Kong, Q.; Shen, Y.; Zhao, L.; Zhuang, J.; Qian, S.; Li, Y.; Lin, Y.; Cai, R. *J. Chem. Phys.* **2002**, *116*, 128.

(156) Ding, C. G.; Yang, J. L.; Cui, X. Y.; Chan, C. T. *J. Chem. Phys.* **1999**, *111*, 8481.
(157) Ding, C. G.; Yang, J. L.; Han, R. S.; Wang, K. L. *Phys. Rev. A* **2001**, *64*, 43201.
(158) Wallace, P. R. *Phys. Rev.* **1947**, *71*, 622.
(159) (a) Dresselhaus, M. S.; Dresselhaus, G.; Saito, R. *Phys. Rev. B* **1992**, *45*, 6234. (b) Saito, R.; Fujita, M.; Dresselhaus, G.; Dresselhaus, M. S. *Phys. Rev. B* **1992**, *46*, 1804. (c) Saito, R.; Fujita, M.; Dresselhaus, G.; Dresselhaus, M. S. *Appl. Phys. Lett.* **1992**, *60*, 2204. (d) Hamada, N.; Sawada, S.; Oshiyama, A. *Phys. Rev. Lett.* **1992**, *68*, 1597.
(160) (a) Mintmire, J. W.; Dunlap, B. J.; White, C. T. *Phys. Rev. Lett.* **1992**, *68*, 631. (b) Robertson, D. H.; Brenner, D. W.; Mintmire, J. W. *Phys. Rev. B* **1992**, *45*, 12592. (c) White, C. T.; Robertson, D. H.; Mintmire, J. W. *Phys. Rev. B* **1993**, *47*, 5485. (d) Mintmire, J. W.; Robertson, D. H.; White, C. T. *J. Phys. Chem. Solids* **1993**, *54*, 1835.
(161) (a) Odom, T. W.; Huang, J. L.; Kim, P.; Lieber, C. M. *Nature* **1998**, *391*, 62. (b) Wildöer, J. W. G.; Venema, L. C.; Rinzler, A. G.; Smalley, R. E.; Dekker: C. *Nature* **1998**, *391*, 59. (c) Odom, T. W.; Huang, J. L.; Kim, P.; Lieber, C. M. *J. Phys. Chem. B* **2000**, *104*, 2794.
(162) For example: (a) Cabria, I.; Mintmire, J. W.; White, C. T. *Phys. Rev. B* **2003**, *67*, 121406. (b) Liu, H. J., Chan, C. T. *Phys. Rev. B* **2002**, *66*, 115416.
(163) (a) Blase, X. B.; Benedict, X.; Shirley, E. L.; Louie, S. G. *Phys. Rev. Lett.* **1994**, *72*, 1878. (b) Kane, C. L.; Mele, E. J. *Phys. Rev. Lett.***1997**, *78*, 1932. (c) Zólyomi, V.; Kürti, J. *Phys. Rev. B.* **2004**, *70*, 85403. (d) Gülseren, O.; Yildirim, T.; Ciraci, S. *Phys. Rev. B.* **2002**, *65*, 153405.
(164) (a) Ouyang, M.; Huang, J. L.; Cheung, C. L.; Lieber, C. M. *Science* **2001**, *292*, 702. (b) Ouyang, M.; Huang, J. L.; Lieber, C. M. *Annu. Rev. Phys. Chem.* **2002**, *53*, 201. (c) Kleiner, A.; Eggert, S. *Phys. Rev. B* **2001**, *63*, 73408. (d) Kleiner, A.; Eggert, S. *Phys. Rev. B.* **2001**, *64*, 113402.
(165) (a) Delaney, P.; Choi, H. J.; Ihm, J.; Louie, S. G.; Cohen, M. L. *Nature* **1998**, *391*, 466. (b) Delaney, P.; Choi, H. J.; Ihm, J.; Louie, S. G.; Cohen, M. L. *Phys. Rev. B* **1999**, *60*, 7899. (c) Maarouf, A. A.; Kane, C. L.; Mele, E. J. *Phys. Rev. B* **2000**, *61*, 11156. (d) Kwon, Y. K.; Saito, S.; Tomanek, D. *Phys. Rev. B* **1998**, *58*, 13314.
(166) (a) Fagan, S. B.; da Silva, L. B.; Mota, R. *Nano Lett.* **2003**, *3*, 289. (b) Maiti, A.; Svizhenko, A.; Anantram, M. P. *Phys. Rev. Lett.* **2002**, *88*, 126805. (c) Gülseren, O.; Yildirim, T.; Ciraci, S.; Kiliç, Ç. *Phys. Rev. B* **2002**, *65*, 155410. (d) Gülseren, O.; Yildirim, T.; Ciraci, S. *Phys. Rev. Lett.* **2001**, *87*, 116802. (e) Rochefort, A.; Avouris, Ph.; Lesane, F.; Salahub, D. R. *Phys. Rev. B* **1999**, *60*, 13824.
(167) Ormsby, J. L.; King, B. T. *J. Org. Chem.* **2004**, *69*, 4287.
(168) (a) Clar, E. *Polycyclic Hydrocarbons*; Academic Press: New York, 1964. (b) Clar, E. *The Aromatic Sextet*; Wiley: London, 1972.
(169) For a recent review on the Clar VB model, see Randic, M. *Chem. Rev.* **2003**, *103*, 3449.
(170) Moran, D.; Stahl, F.; Bettinger, H. F.; Schaefer, H. F.; Schleyer, P. v. R. *J. Am. Chem. Soc.* **2003**, *125*, 6746.
(171) (a) Fowler, P. W.; Fujita, M.; Yoshida, M. *J. Chem. Soc., Faraday Trans.* **1996**, *92*, 3673. (b) Fowler, P. W.; Rogers, K. M. *J. Chem. Soc., Faraday Trans.* **1998**, *94*, 2509.
(172) Matsuo, Y.; Tahara, K.; Nakamura, E. *Org. Lett.* **2003**, *5*, 3181.
(173) Bettinger, H. F. *Org. Lett.* **2004**, *6*, 731.
(174) (a) Aihara, J.; Yamabe, T.; Hosoya, H. *Synth. Met.* **1994**, *64*, 309. (b) Aihara, J. *J. Phys. Chem.* **1994**, *98*, 9773.
(175) Aihara, J. *J. Phys. Chem. A* **1999**, *103*, 7487.
(176) Joselevich, E. *ChemPhysChem* **2004**, *5*, 619.
(177) (a) Strano, M. S.; Dyke, C. A.; Ursey, M. L.; Barone, P. W.; Allen, M. J.; Shan, H.; Kittrell, C.; Hauge, R. H.; Tour, J. M.; Smalley, R. E. *Science* **2003**, *301*, 1519. (b) Banerjee, S.; Wong, S. S. *J. Am. Chem. Soc.* **2004**, *126*, 2073.
(178) Chen, Z.; Thiel, W.; Hirsch, A. *ChemPhysChem* **2003**, *4*, 93.
(179) (a) Mauser, H.; Hirsch, A.; Hommes, N. J. R. v. E.; Clark, T. *J. Mol. Model.* **1997**, *3*, 415. (b) Mauser, H.; Hommes, N. J. R. v. E.; Clark, T.; Hirsch, A.; Pietzak, B.; Weidinger, A.; Dunsch, L. *Angew. Chem.* **1997**, *109*, 2859; *Angew. Chem., Int. Ed. Engl.* **1997**, *36*, 2835.
(180) Lu, X.; Tian, F.; Xu, X.; Wang, N.; Zhang, Q. *J. Am. Chem. Soc.* **2003**, *125*, 10459.
(181) Park, H.; Zhao, J. J.; Lu, J. P. *Nanotechnology* **2005**, *16*, 635.
(182) Zheng, G.; Wang, Z.; Irle, S. Morokuma, K., manuscript submitted.
(183) (a) Khabashesku, V. N.; Billups, W. E.; Margrave, J. L. *Acc. Chem. Res.* **2002**, *35*, 1087 and references therein. (b) Mickelson, E. T.; Huffmann, C. B.; Rinzler, A. G.; Smalley, R. E.; Hauge, R. H.; Margrave, J. L. *Chem. Phys. Lett.* **1998**, *296*, 188. (c) Bettinger, H. F. *ChemPhysChem* **2003**, *4*, 1283.
(184) (a) Hafner, J. H.; Bronikowski, M. J.; Azamian, B. R.; Nikolaev, P.; Rinzler, A. G.; Colbert, D. T.; Smith, K. A.; Smalley, R. E. *Chem. Phys. Lett.* **1998**, *296*, 195. (b) Nikolaev, P.; Bronikowski, M. J.; Bradley, R. K.; Rohmund, F.; Colbert, D. T.; Smith, K. A.; Smalley, R. E. *Chem. Phys. Lett.* **1998**, *313*, 91. (c) Bronikowski, M. J.; Willis, P. A.; Colbert, D. T.; Smith, K. A.; Smalley, R. E. *J. Vac. Sci. Technol. A* **2001**, *19*, 1800. (d) Zhou, W.; Ooi, Y. H.; Russo, R.; Papanek, P.; Luzzi, D. E.; Fischer, J. E.; Bronikowski, M. J.; Willis, P. A.; Smalley, R. E. *Chem. Phys. Lett.* **2001**, *350*, 6.
(185) (a) Thess, A.; Lee, R.; Nikolaev, P.; Dai, H.; Petit, P.; Robert, J.; Xu, C.; Lee, Y. H.; Kim, S. G.; Rinzler, A. G.; Colbert, D. T.; Scusseria, G. E.; Tomanek, D.; Fischer, J. E.; Smalley, R. E. *Science* **1996**, *273*, 483. (b) Rinzler, A. G.; Liu, J.; Dai, H.; Nikolaev, P.; Huffman, C. B.; Rodriguez-Macias, F. J.; Boul, P. J.; Liu, A. H.; Heymann, D.; Colbert, D. T.; Lee, R. S.; Fischer, J. E.; Rao, A. M.; Eklund, P. C.; Smalley, R. E. *Appl. Phys. A* **1998**, *67*, 29.
(186) (a) Hirsh, A. *Angew. Chem., Int. Ed.* **2002**, *41*, 1853. (b) Sun, Y.-P.; Fu, K.; Lin, Y.; Huang, W. *Acc. Chem. Res.* **2002**, *35*, 1096.
(187) (a) Dyke, C. A.; Jour, J. M. *J. Phys. Chem. A* **2004**, *108*, 11151−11159. (b) Bahr, J. L.; Tour, J. M. *J. Mater. Chem.* **2002**, *12*, 1952. (c) Banerjee, S.; Hemraj-Benny, T.; Wong, S. S. *Adv. Mater.* **2005**, *17*, 17. (d) Hirsch, A.; Vostrowsky, O. *Top. Curr. Chem.* **2005**, *245*, 193.
(188) Holzinger, M.; Vostrovsky, O.; Hirsch, A.; Hennrich, F.; Kappes, M.; Weiss, R.; Jellen, F. *Angew. Chem., Int. Ed.* **2001**, *40*, 4002.
(189) (a) Ying, Y.; Saini, R. K.; Liang, F.; Sadana, A. K.; Billups, W. E.; *Org. Lett.* **2003**, *5*, 1471. (b) Peng, H.; Alemany, L. B.; Margrave, J. L.; Khabashesku, V. N. *J. Am. Chem. Soc.* **2003**, *125*, 15174.
(190) (a) Chen, Y.; Haddon, R. C.; Fang, S.; Rao, A. M.; Lee, W. H.; Dickey, E. C.; Grulke, E. A.; Pendergrass, J. C.; Chavan, A.; Haley, B. E.; Smalley, R. E. *J. Mater. Res.* **1998**, *13*, 2423. (b) Chen, J.; Hamon, M. A.; Hu, H.; Chen, Y.; Rao, A. M.; Eklund, P. C.; Haddon, R. C. *Science* **1998**, *282*, 95. (c) Kamaras, K.; Itkis, M. E.; Hu, H.; Zhao, B.; Haddon, R. C. *Science* **2003**, *301*, 1501. (d) Hu, H.; Zhao, B.; Hamon, M. A.; Kamaras, K.; Itkis, M. E.; Haddon, R. C. *J. Am. Chem. Soc.* **2003**, *125*, 14893. (e) Coleman, K. S.; Bailey, S. R.; Fogden, S.; Green, M. L. H. *J. Am. Chem. Soc.* **2003**, *125*, 8722. (f) Holzinger, M.; Abraham, J.; Whelan, P.; Graupner, R.; Ley, L.; Hennrich, F.; Kappes, M.; Hirsch. A. *J. Am. Chem. Soc.* **2003**, *125*, 8566. (g) Worsley, K. A.; Moonoosawmy, K. R.; Kruse, P. *Nano Lett.* **2004**, *4*, 1541.
(191) Pekker, S.; Salvelat, J.-P.; Jakab, E.; Bonard, J.-M.; Forro, L. *J. Phys. Chem. B* **2001**, *105*, 7938.
(192) (a) Bahr, J. L.; Yang, J.; Kosynkin, D. V.; Bronikowski, M. J.; Smalley, R. E.; Tour, J. M. *J. Am. Chem. Soc.* **2001**, *123*, 6536. (b) Bahr, J. L.; Tour, J. M. *Chem. Mater.* **2001**, *13*, 3823. (c) Dyke, C. A.; Tour, J. M. *J. Am. Chem. Soc.* **2003**, *125*, 1156−1157. (d) Dyke, C. A.; Tour, J. M. *Nano Lett.* **2003**, *3*, 1215. (e) Dyke, C. A.; Stewart, M. P.; Maya, F.; Tour, J. M. *Synlett* **2004**, 155−160. (f) Hudson, J. L.; Casavant, M. J.; Tour, J. M. *J. Am. Chem. Soc.* **2004**, *126*, 11158. (g) Dyke, C. A.; Tour, J. M. *Chem. Eur. J.* **2004**, *10*, 813.
(193) (a) Georgakilas, D.; Kordatos, K.; Prato, M.; Guldi, D. M.; Holzinger, M.; Hirsch, A. *J. Am. Chem. Soc.* **2002**, *124*, 760. (b) Georgakilas, V.; Voulgaris, D.; Vazquez, E.; Prato, M.; Guldi, D. M.; Kukovecz, A.; Kuzmany, H. *J. Am. Chem. Soc.* **2002**, *124*, 14318. (c) Pantarotto, D.; Partidos, C. D.; Graff, R.; Hoebeke, J.; Briand, J.-P.; Prato, M.; Bianco, A. *J. Am. Chem. Soc.* **2003**, *125*, 6160. (d) Georgakilas, V.; Tagmatarchis, N.; Pantarotto, D.; Bianco, A.; Briand, J.-P.; Prato, M. *Chem. Commun.* **2002**, 3050. (e) Guldi, D. M.; Marcaccio, M.; Paolucci, D.; Paolucci, F.; Tagmatarchis, N.; Tasis, D.; Vázquez, E.; Prato, M. *Angew. Chem., Int. Ed.* **2003**, *42*, 4206. (f) Callegari, A.; Marcaccio, M.; Paolucci, D.; Paolucci, F.; Tagmatarchis, N.; Tasis, D.; Vázquez, E.; Prato, M. *Chem. Commun.* **2003**, 2576. (g) Alvaro, M.; Atienzar, P.; de la Cruz, P.; Delgado, J. L.; Garcia, H.; Langa, F. *J. Phys. Chem. B* **2004**, *108*, 12691.
(194) For recent minireviews, see (a) Tasis, D.; Tagmatarchis, N.; Georgakilas, V.; Prato, M. *Chem. Eur. J.* **2003**, *9*, 4001. (b) Tagmatarchis, N.; Prato, M. *J. Mater. Chem.* **2004**, *14*, 437. (c) Bianco, A.; Kostarelos, K.; Partidos, C. D.; Prato, M. *Chem. Commun.* **2005**, 571.
(195) (a) Banerjee, S.; Wong, S. S. *J. Phys. Chem. B.* **2002**, *106*, 12144. (b) Banerjee, S.; Wong, S. S. *Nano Lett.* **2004**, *4*, 1445. (c) Banerjee, S.; Wong, S. S. *Chem. Commun.* **2004**, 772. (d) Banerjee, S.; Hemraj-Benny, T.; Balasubramanian, M.; Fischer, D. A.; Misewich, J. A.; Wong, S. S. *ChemPhysChem* **2004**, *5*, 1416.
(196) Sun, Y.; Wilson, S. R.; Schuster, D. I. *J. Am. Chem. Soc.* **2001**, *123*, 5348. Sidewall amination of pristine CNTs was proposed to account for the high solubility of CNTs in aniline, but no direct evidence of sidewall amination was provided therein.
(197) Cui, J. B.; Burghard, M.; Kern, K. *Nano Lett.* **2003**, *3*, 613.
(198) Delgado, J. L.; de la Cruz, P.; Langa, F.; Urbina, A.; Casado, J.; Navarrete, J. T. L. *Chem. Commun.* **2004**, 1734.
(199) (a) Lu, X.; Zhang, L.; Xu, X.; Wang, N.; Zhang, Q. *J. Phys. Chem. B* **2002**, *106*, 2136. (b) Kar, T.; Akdim, B.; Duan, X. F.; Pachter, R. *Chem. Phys. Lett.* **2004**, *392*, 176. (c) Yim, W. L.; Liu, Z. F. *Chem. Phys. Lett.* **2004**, *398*, 297. (d) Lu, X.; Chen, Z.; Schleyer, P. v. R. *J. Am. Chem. Soc.* **2005**, *127*, 20.
(200) Lu, X.; Tian, F.; Wang, N.; Zhang, Q. *Org. Lett.* **2002**, *4*, 4313.

(201) Lu, X.; Tian, F.; Feng, Y.; Xu, X.; Wang, N.; Zhang, Q. *Nano Lett*. **2002**, *2*, 1325.
(202) Long, L. S.; Lu, X.; Zhang, Q. *J. Org. Chem*. **2003**, *68*, 4495.
(203) (a) Lu, X.; Tian, F.; Zhang, Q. *J. Phys. Chem. B* **2003**, *107*, 8388. (b) Chen, Z.; Nagase, S.; Hirsch, A.; Haddon, R. C.; Thiel, W.; Schleyer, P. v. R. *Angew. Chem., Int. Ed*. **2004**, *43*, 1552. (c) Chu, Y.-Y.; Su, M. D. *Chem. Phys. Lett*. **2004**, *394*, 231. (d) Zhao. J.; Chen, Z.; Zhou, Z.; Park, H.; Schleyer, P. v. R.; Lu, J. *ChemPhysChem* **2005**, *6*, 598.
(204) Lu, X.; Yuan, Q.; Zhang, Q. *Org. Lett*. **2003**, 5, 3527.
(205) (a) Tada, K.; Furuya, S.; Watanabe, K. *Phys. Rev. B* **2001**, *63*, 5404. (b) Gulseren, O.; Yildirim, T.; Ciraci, S. *Phys. Rev. Lett*. **2001**, *87*, 6802.
(206) (a) Kelly, K. F.; Chiang, I. W.; Mickelson, E. T.; Hauge, R. H.; Margrave, J. L.; Wang, X.; Scuseria, G. E.; Radloff, C.; Smalley, R. E. *Chem. Phys. Lett*. **1999**, *313*, 445. (b) Kudin, K. N.; Bettinger, H. F.; Scuseria, G. E. *Phys. Rev. B* **2001**, *63*, 45413. (c) Bettinger, H. F.; Kudin, K. N.; Scuseria, G. E. *J. Am. Chem. Soc*. **2001**, *123*, 12849. (d) Bauschlicher, C. W., Jr. *Chem. Phys. Lett*. **2000**, *322*, 237. (e) Hayashi, T.; Terrones, M.; Scheu, C.; Kim, Y. A.; Rühle, M.; Nakajima, T.; Endo, M. *Nano Lett*. **2002**, *2*, 491.
(207) For the ONIOM approach, see (a) Dapprich, S.; Komáromi, I.; Byun, K. S.; Morokuma, K.; Frisch, M. J. *J. Mol. Struct. THEOCHEM* **1999**, *461/462*, 1. (b) Maseras, F.; Morokuma, K. *J. Comput. Chem*. **1995**, *16*, 1170. (c) Svensson, M.; Humbel, S.; Froese, R. D. J.; Matsubara, T.; Sieber, S.; Morokuma, K. *J. Phys. Chem*. **1996**, *100*, 19357.
(208) Mickelson, E. T.; Chiang, I. W.; Zimmerman, J. L.; Boul, P. J.; Lozano, J.; Liu, J.; Smalley, R. E.; Hauge, R. H.; Margrave, J. L. *J. Phys. Chem. B*. **1999**, *103*, 4318.
(209) Saini, R. K.; Chiang, I. W.; Peng, H.; Smalley, R. E.; Billups, W. E.; Hauge, R. H.; Margrave, J. L. *J. Am. Chem. Soc*. **2003**, *125*, 3617.
(210) Boul, P. J.; Liu, J.; Mickelson, E. T.; Huffman, C. B.; Ericson, L. M.; Chiang, I. W.; Smith, K. A.; Colbert, D. T.; Hauge, R. H.; Margrave, J. L.; Smalley, R. E. *Chem. Phys. Lett*. **1999**, *310*, 367.
(211) Stevens, J. L.; Huang, A. Y.; Peng, H. Q.; Chiang, I. W.; Khabashesku, V. N.; Margrave, J. L. *Nano Lett*. **2003**, *3*, 331.
(212) (a) *1,3-Dipolar Cycloaddition Chemistry*; Padwa, A., Ed.; John Wiley & Sons: New York, 1984; Vol. 1. (b) Huisgen, R. *Angew. Chem., Int. Ed. Engl*. **1963**, *2*, 562.
(213) (a) Woodward, R. B.; Hoffmann, R. *Angew. Chem., Int. Ed. Engl*. **1969**, *8*, 781. (b) Woodward, R. B.; Hoffmann, R. *Angew. Chem., Int. Ed. Engl*. **1969**, *8*, 817. (c) Fukui, K. In *Molecular Orbitals in Chemistry, Physics and Biology*; Lowdin, P. O.; Pullman, B. Eds.; Academic Press: New York, 1964.
(214) Diederich, F.; Thilgen, C. *Science* **1996**, *271*, 317.
(215) (a) Shaik, S.; Schlegel, H. B.; Wolfe, S. In *Theoretical Aspects of Physical Organic Chemistry*; John Wiley & Sons Inc.: New York, 1992. (b) Pross, A. In *Theoretical and Physical Principles of Organic Reactivity*; John Wiley & Sons Inc.: New York, 1995.
(216) For examples of 1,3-DC on fullerenes, see Prato, M.; Maggini, M. *Acc. Chem. Res*. **1998**, *31*, 519.
(217) Heymann, D.; Bachilo, S. M.; Bruce Weisman, R.; Cataldo, F.; Fokkens, R. F.; Nibbering, N. M. M.; Vis, R. D.; Felipe Chibante, L. P. *J. Am. Chem. Soc*. **2000**, *122*, 11473.
(218) (a) Criegee, R. *Angew. Chem., Int. Ed. Engl*. **1975**, *14*, 745. (b) Atkinson, R.; Carter, W. P. L. *Chem. Rev*. **1984**, *84*, 437. (c) Anglada, J. M.; Crehuet, R.; Bofill, J. M. *Chem. Eur. J*. **1999**, *5*, 1809.
(219) Banerjee, S.; Kahn, M. G. C.; Wong, S. S. *Chem. Eur. J*. **2003**, *9*, 1898.
(220) (a) Rinzler, A. G.; Liu, J.; Dai, H.; Nikolaev, P.; Huffman, C. B.; Rodriguez-Macias, F. J.; Boul, P. J.; Lu, A. H.; Heymann, D.; Colbert, D.; T.; Lee, R. S.; Fischer, J. E.; Rao, A. M.; Eklund, P. C.; Smalley, R. E. *Appl. Phys. A*: *Mater. Sci. Process*. **1998**, *67*, 29. (b) Ichida, M.; Mizuno, S.; Tani, Y.; Saito, Y.; Nakamura, A. *J. Phys. Soc. Jpn*. **1999**, *68*, 3131.
(221) Goodman, M.; Felix, A.; Moroder, L.; Toniolo, C. *Methods of Organic Chemistry* (*Houben-Weyl*); Thieme: Stuttgart, Germany, 2002; Vol. E22a.
(222) Nielsen, O.; Buchardt, O. *Synthesis* **1991**, 819.
(223) (a) Daniel, M.-C.; Ruiz, J.; Astruc, D. *J. Am. Chem. Soc*. **2003**, *125*, 1150. (b) Daniel, M.-C.; Ruiz, J.; Nlate, S.; Blais, J.-C.; Astruc, D. *J. Am. Chem. Soc*. **2003**, *125*, 2617.
(224) Lu, X.; Xu, X.; Wang, N.; Zhang, Q. *J. Org. Chem*. **2002**, *67*, 515.
(225) (a) Wassermann, A. *Diels–Alder Reactions*: *Organic Background and Physico-Chemical Aspect*; Elsevier: New York, 1965. (b) Carruthers, W. *Cycloaddition Chemistry in Organic Synthesis*; Pergamon Press: New York, 1990.
(226) Houk, K. N.; Gonzalez, J.; Li, Y. *Acc. Chem. Res*. **1995**, *28*, 81.
(227) (a) Klundt, I. *Chem. Rev*. **1970**, *70*, 471. (b) Manoharan, M.; Venuvanalingam, P. *J. Phys. Org. Chem*. **1998**, *11*, 133. (c) Manoharan, M.; De Proft, F.; Goerlings, P. *J. Chem. Soc. Perk. Trans. 2* **2000**, 1767. (d) Manoharan, M.; De Proft, F.; Geerlings, P. *J. Org. Chem*. **2000**, *65*, 7971.
(228) (a) Liu, S.; Lu, Y.; Kappas, M. M.; Ibers, J. A. *Science* **1991**, *254*, 410. (b) David, W. I. F.; Ibberson, R. M.; Matthewmann, J. C.; Prassides, K.; Dennis, T. J. S.; Hare, J. P.; Kroto, H. W.; Taylor, R.; Walton, D. R. M. *Nature* **1991**, *353*, 147.
(229) For a recent review, see Kolb, H. C.; VanNieuwenhze, M. S.; Sharpless, K. B. *Chem. Rev*. **1994**, *94*, 2483.
(230) (a) Pidun, U.; Boehme, C.; Frenking, G. *Angew. Chem., Int. Ed. Engl*. **1996**, *35*, 2817. (b) Dapprich, S.; Ujaque, G.; Maseras, F.; Lledos, A.; Musaev, D. G.; Morokuma, K. *J. Am. Chem. Soc*. **1996**, *118*, 11660. (d) Torrent, M.; Den, L.; Duran, M.; Sola, M.; Ziegler, T. *Organometallics* **1997**, *16*, 13.
(231) Hawkins, J. M.; Meyer, A.; Lewis, T. A.; Loren, S.; Hollander, F. J. *Science* **1991**, *252*, 312.
(232) (a) Wallis, J. M.; Kochi, J. K. *J. Am. Chem. Soc*. **1988**, *110*, 8207. (b) Motherwell, W. B.; Williams, A. S. *Angew. Chem*. **1995**, *107*, 2207.
(233) Preliminary QM/MM calculations predicted an activation energy of only 4.6 kcal/mol for the thermal decomposition of the osmyl ester **26** on the sidewall of a (5, 5) SWCNT.
(234) Maiti, A.; Andzelm, J.; Tanpipat, N.; von Allmen, P. *Phys. Rev. Lett*. **2001**, *87*, 155502.
(235) Hou, S.; Shen, Z.; Zhao, X.; Xue, Z. *Chem. Phys. Lett*. **2003**, *373*, 308.
(236) Masnovi, J. M.; Seddon, E. A.; Kochi, J. K. *Can. J. Chem*. **1984**, *62*, 2252.
(237) Strano, M. S. *J. Am. Chem. Soc*. **2003**, *125*, 16148.
(238) Lee, W. H.; Kim, S. J.; Lee, W. J.; Lee, J. G.; Haddon, R. C.; Reucroft, P. J. *Appl. Surf. Sci*. **2001**, *181*, 121.
(239) For examples of Bingel reactions on fullerenes, see (a) Fujiwara, K.; Komatsu, K.; Wang, G.-W.; Tanaka, T.; Hirata, K.; Yamamoto, K.; Saunders: M. *J. Am. Chem. Soc*. **2001**, *123*, 10715. (b) Qian, W.; Rubin, Y. *Angew. Chem., Int. Ed*. **1999**, *38*, 2356. (c) Camps, X.; Hirsch, A. *J. Chem. Soc., Perkin Trans. 1* **1997**, 1595.
(240) Jiao, H.; Hommes, N. J. R. v. E.; Schleyer, P. v. R. *Org. Lett*. **2002**, *4*, 2393.
(241) Lu, J.; Nagase, S.; Zhang, X.; Maeda, Y.; Wakahara, T.; Nakahodo, T.; Tsuchiya, T.; Akasaka, T.; Yu, D.; Gao, Z.; Han, R.; Ye, H. *J. Mol. Struct. THEOCHEM*, **2005**, *725*, 255.
(242) (a) Gasper, P. P.; Holten, D.; Konieczny, S. *Acc. Chem. Res*. **1987**, *20*, 329. (b) Akasaka, T.; Ando, W.; Kobayashi, K.; Nagase, S. *J. Am. Chem. Soc*. **1993**, *115*, 1605.
(243) For experimental studies on the O_2/SWCNTs systems, see: (a) Collins, P. G.; Bradley, K.; Ishigami, M.; Zettl, A. *Science* **2000**, *287*, 1801. (b) Bradley, K.; Jhi, S.-H.; Collins, P. G.; Hone, J.; Cohen, M. L.; Louie, S. G.; Zettl, A. *Phys. Rev. Lett*. **2000**, *85*, 4361. (c) Tang, X.-P.; Kleinhammes, A.; Shimoda, H.; Fleming, L.; Bennoune, K. Y.; Sinha, S.; Bower, C.; Zhou, O.; Wu, Y. *Science* **2000**, *288*, 492. (d) Chen, R. J.; Franklin, N. R.; Kong, J.; Cao, J.; Tombler, T. W.; Zhang, Y.; Dai, H. *Appl. Phys. Lett*. **2001**, *79*, 2258. (e) Ulbricht, H.; Moos, G.; Hertel, T. *Phys. Rev. B* **2002**, *66*, 075404. (f) Ulbricht, H.; Moos, G.; Hertel, T. *Surf. Sci*. **2003**, *532*, 852−856. (g) Goldoni, A.; Larciprete, R.; Petaccia, L.; Lizzit, S. *J. Am. Chem. Soc*. **2003**, *125*, 11329. (h) Heinze, S.; Tersoff, J.; Martel, R.; Derycke, V.; Appenzeller, J.; Avouris, Ph. *Phys. Rev. Lett*. **2002**, *89*, 106801. (i) Derycke, V.; Martel, R.; Appenzeller, J.; Avouris, Ph. *Appl. Phys. Lett*. **2002**, *80*, 2773. (j) Savage, T.; Bhattacharya, S.; Sadanadan, B.; Gaillard, J.; Tritt, T. M.; Sun, Y. P.; Wu, Y.; Nayak, S.; Car, R.; Marzari, N.; Ajayan, P. M.; Rao, A. M. *J. Phys.*: *Condens. Matter* **2003**, *15*, 5915. (k) Dukovic, G.; White, B. E.; Zhou, Z.; Wang, F.; Jockusch, S.; Steigerwald, M. L.; Heinz, T. F.; Friesner, R. A.; Turro, N. J.; Brus, L. E. *J. Am. Chem. Soc*. **2004**, *126*, 15269.
(244) For theoretical studies on the O_2/SWCNTs system, see (a) Jhi, S.-H.; Louie, S. G.; Cohen, M. L. *Phys. Rev. Lett*. **2000**, *85*, 1710. (b) Peng, S.; Cho, K. *Nanotechnology* **2000**, *11*, 57. (c) Zhao, J.; Buldum, A.; Han, J.; Lu, J. P. *Nanotechnology* **2002**, *13*, 195. (d) Sorescu, D. C.; Jordan, K. D.; Avouris, Ph. *J. Phys. Chem. B* **2001**, *105*, 11227. (e) Mann, D. J.; Hase, W. L. *Phys. Chem. Chem. Phys*. **2001**, *3*, 4376. (f) Ricca, A.; Bauschlicher, C. W., Jr.; Maiti, A. *Phys. Rev. B* **2003**, *68*, 035433. (g) Froudakis, G. E.; Schnell, M.; Muhlhauser, M.; Peyerimhoff, S. D.; Andriotis, A. N.; Menon, M.; Sheetz, R. M. *Phys. Rev. B* **2003**, *68*, 115435. (h) Dag, S.; Gulseren, O.; Ciraci, S. *Chem. Phys. Lett*. **2003**, *380*, 1. (i) Dag, S.; Gulseren, O.; Yildirim, T.; Ciraci, S. *Phys. Rev. B* **2003**, *67*, 165424. (j) Grujicic, M.; Cao, C.; Singh, R. *Appl. Surf. Sci*. **2003**, *211*, 166; Grujicic, M.; Cao, G.; Rao, A. M.; Tritt, T. M.; Nayak, S. *Appl. Surf. Sci*. **2003**, *214*, 289. (k) Chan, S. P.; Chen, G.; Gong, X. G.; Liu, Z. F. *Phys. Rev. Lett*. **2003**, *90*, 086403. (l) Zhang, Y.; Liu, Z. F. *J. Phys. Chem. B* **2004**, *108*, 11435.
(245) Ajayan, P. M.; Ebbesen, T. W.; Ichihashi, T.; Iijima, S.; Tanigaki, K.; Hiura, H. *Nature* **1993**, *362*, 522.
(246) (a) Dillon, A. C.; Jones, K. M.; Bekkedahl, T. A.; Kiang, C. H.; Bethune, D. S.; Heben, M. J. *Nature* **1997**, *386*, 377. (b) Heben, M. J.; Dillon, A. C. *Science* **1999**, *287*: 593. (c) Liu, C.; Fan, Y. Y.; Liu, M.; Cong, H. T.; Cheng, H. M., Dresselhaus, M. S. *Science* **1999**, *286*, 1127. (d) Chen, P.; Wu, X.; Lin, J.; Tan, K. L. *Science* **1999**, *285*, 91. (e) Yang, R. T. *Carbon* **2000**, *38*, 623. (f) Ding, R. G.; Lu, G. Q.; Yan, Z. F. *J. Nanosci. Nanotechnol*. **2001**, *1*, 7.

(247) (a) Froudakis, G. E. *Nano Lett*. **2001**, *1*, 179−182. (b) Froudakis, G. E. *Nano Lett*. **2001**, *1*, 531. (c) Froudakis, G. E. *J. Phys.*: *Condens. Matter*, **2002**, *14*, 453.
(248) Khare, B. N., Meyyappan, M., Cassell, A. M. *Nano Lett*. **2002**, *2*, 73.
(249) Haufler, R. E.; Conceicao, J.; Chibante, L. P. F.; Chai, Y.; Byrne, N. E.; Flanagan, S.; Haley, M. M.; O'Brien, S. C.; Pan, C.; Xiao, Z.; Ciufolini, W. E.; Hauge, R. N.; Margrave, J. L.; Wilson, L. J.; Curl, R. F.; Smally, R. E. *J. Phys. Chem*. **1990**, *94*, 8634.
(250) (a) Bergbreiter, D. E.; Killough, J. M. *J. Chem. Soc. Chem. Commun*. **1976**, 913. (b) Bergbreiter, D. E.; Killough, J. M. *J. Am. Chem. Soc*. **1978**, *100*, 2126.
(251) Obushak, M. D.; Lyakhovych, M. B.; Ganushchak, M. I. *Tetrahedron Lett*. **1998**, *39*, 9567.
(252) Gadallah, F. F.; Elofson, R. M. *J. Org. Chem*. **1969**, *34*, 3335.
(253) (a) Delamar, M.; Hitmi, R.; Pinson, J.; Savéant, J. M. *J. Am. Chem. Soc*. **1992**, *114*, 5883. (b) Delamar, M.; Désarmot, G.; Fagebaume, O.; Hitmi, R.; Pinson, J.; Savéant, J.-M. *Carbon* **1997**, *35*, 801. (c) Allongue, P.; Delamar, M.; Desbat, B.; Fagebaume, O.; Hitmi, R.; Pinson, J.; Savéant, J.-M. *J. Am Chem. Soc*. **1997**, *119*, 201. (d) Saby, C.; Ortiz, B.; Champagne, G. Y.; Bélanger, D. *Langmuir* **1997**, *13*, 6805. (e) Ortiz, B.; Saby, C.; Champagne, G. Y.; Bélanger, D. *J. Electroanal. Chem*. **1998**, *455*, 75.
(254) (a) Hashimoto, A.; Suenaga, K.; Gloter, A.; Urita, K.; Iijima, S. *Nature* **2004**, *430*, 870. (b) Watts, P. C. P.; Hsu, W.-K.; Kroto, H. W.; Walton, D. R. M. *Nano Lett*. **2003**, *3*, 549. (c) Charlier, J.-C. *Acc. Chem. Res*. **2002**, *35*, 1063. (d) Ouyang, M.; Huang, J. L.; Cheung, C. L.; Lieber, C. M. *Science* **2001**, *291*, 97−100. (e) Louie, S. G. *Top. Appl. Phys*. **2001**, *80*, 113. (f) Orlikowski, D.; Nardelli, M. B.; Bernholc, J.; Roland, C. *Phys. Rev. Lett*. **1999**, *83*, 4132. (g) Ebbesen, T. W.; Takada, T. *Carbon* **1995**, *33*, 973. (h) Charlier, J. C. Ebbesen, T. W.; Lambin, Ph. *Phys. Rev. B*. **1996**, *53*, 11108. (i) Crespi, V. H.; Cohen, M. L. *Phys. Rev. Lett*. **1997**, *79*, 2093. (j) Chico, L.; Sancho, M. P. L.; Muñoz, M. C. *Phys. Rev. Lett*. **1998**, *98*, 1278. (k) Kim, H.; Lee, J.; Kahng, S. J.; Son, Y. W.; Lee, S. B.; Lee, C. K.; Ihm, J.; Kuk, Y. *Phys. Rev. Lett*. **2003**, *90*, 216107.
(255) (a) Bom, D.; Andrews, R.; Jacques, D.; Anthony, J.; Chen, B.; Meier, M. S.; Selegue, J. P. *Nano Lett*. **2002**, *2*, 615. (b) Chakrapani, N.; Zhang, Y. M.; Nayak, S. K.; Moore, J. A.; Carroll, D. L.; Choi, Y. Y.; Ajayan, P. M. *J. Phys. Chem. B* **2003**, *107*, 9308. (c) Lu, A. J.; Pan, B. C. *Phys. Rev. Lett*. **2004**, *92*, 105504.
(256) (a) Li, X.; Niu, J.; Zhang, J.; Li, H.; Liu, Z. *J. Phys. Chem. B* **2003**, *107*, 2453. (b) Fan, Y.; Burghard, M.; Kern, K. *Adv. Mater*. **2002**, *14*, 130. (c) Liu, J.; Rinzler, A. G.; Dai, H.; Hafner, J. H.; Bradley, R. K.; Boul, P. J.; Lu, A.; Iverson, T.; Shelimov, K.; Huffman, C. B.; Rodriguez-Macias, F.; Shon, Y.-S.; Lee, T. R.; Colbert, D. T.; Smalley, R. E. *Science* **1998**, *280*, 1253.
(257) For recent reviews, see (a) Xie, R. H.; Zhao, J.; Rao, Q. In *Encyclopedia of Nanoscience and Nanotechnology;* Nalwa, H. S, Eds.; Stevenson Ranch, Calif.: American Scientific Publishers, 2004; Vol. 2, p 505. (b) Zhao, J.; Xie, R. H. *J. Nanosci., Nanotech*. **2003**, *3*, 459. For some experiments on the synthesis of B- or/and N-doped CNTs and $B_xC_yN_z$ nanotubes, see (c) Han, W.; Cumings, J.; Huang, X.; Bradley, K.; Zettl, A. *Chem. Phys. Lett*. **2001**, *346*, 368. (d) Weng-Sieh, Z.; Cherry, K.; Chopra, N. G.; Blase, X.; Miyamoto, Y.; Rubio, A.; Cohen, M. L.; Louie, S. G.; Zettl, A.; Gronsky, R. *Phys. Rev. B* **1995**, *51*, 11229. (e) Czerw, R.; Terrones, M.; Charlier, J.-C.; Blase, X.; Foley, B.; Kamalakaran, R.; Grobert, N.; Terrones, H.; Tekleab, D.; Ajayan, P. M.; Blau, W.; Ruehle, M.; Carroll, D. L. *Nano Lett*. **2001**, *1*, 457.
(258) (a) Peng, S.; Cho, K. *Nano Lett*. **2003**, *3*, 513. (b) Nevidomskyy, A. H.; Csányi, G.; Payne, M. C. *Phys. Rev. Lett*. **2003**, *91*, 105502.
(259) (a) Zhou, Z.; Gao, X. P.; Yan, J.; Song, D. Y.; Morinaga, M. *J. Phys. Chem. B* **2004**, *109*, 9023. (b) Zhou, Z.; Gao, X. P.; Yan, J.; Song, D. Y.; Morinaga, M. *Carbon* **2004**, *42*, 2677.
(260) Zhou, Z.; Zhao, J.; Gao, X.; Chen, Z.; Yan, J.; Schleyer, P. v. R.; Morinaga, M. *Chem. Mater*. **2005**, *17*, 992.
(261) Miyamoto, Y.; Rubio, A.; Berber, S.; Yoon, M.; Tomänek, *Phys. Rev. B*. **2004**, *69*, 121413.
(262) (a) Bettinger, H. F. *J. Phys. Chem. B* **2005**, *109*, 6922. (b) Picozzi, S.; Santucci, S.; Lozzi, L.; Valentini, L.; Delley, B. *J. Chem. Phys*. **2004**, *120*, 7147.
(263) See recent reviews (a) Monthioux, M. *Carbon* **2002**, *40*, 1809. (b) Iijima, S. Carbon, *Physica B* **2002**, *323*, 1. (c) Vostrowsky, O.; Hirsch, A. *Angew. Chem., Int. Ed*. **2004**, *43*, 2326.
(264) Smith, B. W.; Monthioux, M.; Luzzi, D. E. *Chem. Phys. Lett*. **1999**, *315*, 31.
(265) Smith, B. W.; Monthioux, M.; Luzzi, D. E. *Nature* **1998**, *296*, 323.
(266) (a) Hirahara, K.; Suenaga, K.; Bandow, S.; Kato, H.; Okazaki, T.; Shinohara, H.; Iijima, S. *Phys. Rev. Lett*. **2000**, *85*, 5384. (b) Luzzi, D. E.; Smith, B. W. *Carbon* **2000**, *38*, 1751. (c) Smith, B. W.; Luzzi, D. E.; *Chem. Phys. Lett*. **2000**, *321*, 169.
(267) (a) Hirahara, K. Bandow, S.; Suenaga, K.; Kato, H.; Okazaki, T.; Shinohara, H.; Iijima, S. *Phys. Rev. B* **2001**, *64*, 115420. (b) Kataura, H.; Maniwa, Y.; Abe, M.; Fujiwara, A.; Kodama, T.; Kikuchi, K.; Imahori, H.; Misaki, Y.; Suzuki, S.; Achiba, Y. *Appl. Phys. A* **2002**, *74*, 349.
(268) (a) Suenaga, K.; Tence, M.; Mory, C.; Colliex, C.; Kato, H.; Okazaki, T.; Shinohara, H.; Hirahara, K.; Bandow, S.; Iijima, S. *Science* **2000**, *290*, 2280. (b) Shimada, T.; Okazaki, T.; Taniguchi, R.; Sugai, T.; Shinohara, H.; Suenaga, K.; Ohno, Y.; Mizuno, S.; Kishimoto, S.; Mizutani, T. *Appl. Phys. Lett*. **2002**, *81*, 4067.
(269) Chiu, P. W.; Gu, G.; Kim, G. T.; Philipp, G.; Roth, S.; Yang, S. F.; Yang, S. *Appl. Phys. Lett*. **2001**, *79*, 3845.
(270) Suenaga, K.; Okazaki, T.; Wang, C. R.; Bandow, S.; Shinohara, H.; Iijima, S. *Phys. Rev. Lett*. **2003**, *90*, 055506.
(271) Khlobystov, A. N.; Porfyrakis, K.; Kanai, M.; Britz, D. A.; Ardavan, A.; Shinohara, H.; Dennis, T. J. S.; Briggs, G. A. D. *Angew. Chem., Int. Ed*. **2004**, *43*, 1386.
(272) Smith, B. W.; Luzzi, D. E.; Achiba, Y. *Chem. Phys. Lett*. **2000**, *331*, 137.
(273) Suenaga, K.; Taniguchi, R.; Shimada, T.; Okazaki, T.; Shinohara, H.; Iijima, S. *Nano Lett*. **2003**, *3*, 1395.
(274) Britz, D. A.; Khlobystov, A. N.; Wang, J.; O'Neil, A. S.; Poliakoff, M.; Ardavan, A.; Briggs, G. A. D. *Chem. Commun*. **2004**, 176.
(275) Britz, D. A.; Khlobystov, A. N.; Porfyrakis, K.; Ardavan, A.; Briggs, G. D. *Chem. Commun*. **2005**, 37.
(276) Berber, S.; Kwon, Y. K.; Tomanek, D. *Phys. Rev. Lett*. **2002**, *88*, 185502.
(277) Hornbaker, D. J.; Kahng, S.-J.; Misra, S.; Smith, B. W.; Johnson, A. T.; Mele, E. J.; Luzzi, D. E.; Yazdani, A. *Science* **2002**, *295*, 828.
(278) (a) Okada, S.; Saito, S.; Oshiyama, A. *Phys. Rev. Lett*. **2001**, *86*, 3835. (b) Otani, M.; Okada, S.; Oshiyama, A. *Phys. Rev. B*. **2003**, *68*, 125424. (c) Melle-Franco, M.; Kuzmany, H.; Zerbetto, F. *J. Phys. Chem. B*. **2003**, *107*, 6986. (d) Rochefort, A. *Phys. Rev. B*. **2003**, *67*, 115401.
(279) Bandow, S.; Takizawa, M.; Hirahara, K.; Yudasaka, M.; Iijima, S. *Chem. Phys. Lett*. **2001**, *337*, 48.
(280) Okada, S.; Otani, M.; Oshiyama, A. *Phys. Rev. B*. **2003**, *67*, 205411.
(281) (a) Liu, Y.; Jones, R. O.; Zhao, X.; Ando, Y. *Phys. Rev. B*. **2003**, *68*, 125413. (b) Lu, J.; Nagase, S.; Zhang, S.; Peng, L. *Phys. Rev. B*. **2003**, *68*, 121402. (c) Zhang, Z. X.; Pan, Z. Y.; Wei, Q.; Li, Z. J.; Zang, L. K.; Wang, Y. X. *Int. J. Mod. Phys. B*. **2003**, *17*, 4667.
(282) Sofronov, A. A.; Ivanosvskaya, V. V.; Makurin, Y. N.; Ivanovskii, A. L. *Chem. Phys. Lett*. **2002**, *351*, 35.
(283) Perdew, J. P.; Burke, K.; Ernzerhof, M. *Phys. Rev. Lett*. **1996**, *77*, 3865.
(284) For example, (a) Nunzi, F.; Mercuri, F.; Sgamellotti, A.; Re, N. *J. Phys. Chem. B*. **2002**, *106*, 10622. (b) Irle, S.; Mews, A.; Morokuma, K. *J. Phys. Chem. A*. **2002**, *106*, 11973.
(285) Irle, S.; Stanley, D. M.; Morokuma, K., manuscript submitted.
(286) Morokuma, K.; Musaev, D. G.; Vreven, T.; Basch, H.; Torrent, M.; Khoroshun, D. V. *IBM J. Res., Dev*. **2001**, *45*, 367.
(287) Troshin, P. A.; Avent, A. G.; Darwish, A. D.; Martsinovich, N.; Abdul-Sada, A.; Street, J. M.; Taylor, R. *Science* **2005**, *309*, 278.
(288) Hata, K.; Futaba, D. N.; Mizuno, K.; Namai, T.; Yumura, M.; Iijima, S. *Science* **2004**, *306*, 1362.
(289) (a) Zheng, M.; Jagota, A.; Strano, M. S.; Santos, A. P.; Barone, P.; Grace Chou, S.; Diner, B. A.; Dresselhaus, M. S.; Mclean, R. S.; Bibiana Onoa, G.; Samsonidze, G. G.; Semke, E. D.; Usrey, M.; Walls, D. J. *Science* **2003**, *302*, 1545. (b) Krupke, R.; Hennrich, F.; von Lohneysen, H.; Kappes, M. *Science* **2003**, *301*, 344. (c) Chattopadhyay, D.; Galeska, L.; Papadimitrakopoulos, F. *J. Am. Chem. Soc*. **2003**, *125*, 3370. (d) Chen, Z.; Du, X.; Du, M.; Rancken, C. D.; Cheng, H.; Rinzler, A. G. *Nano Lett*. **2003**, *3*, 1245. (e) Li, H. P.; Zhou, B.; Lin, Y.; Gu, L.; Wang, W.; Fernando, K. A. S.; Kumar, S.; Allard, L. F.; Sun, Y. *J. Am. Chem. Soc*. **2004**, *126*, 1014. (f) Samsonidze, G. G.; Chou, S. G.; Santos, A. P.; Brar, V. W.; Dresselhaus, G.; Dresselhaus, M. S.; Selbst, A.; Swan, A. K.; Ünlü, M. S.; Goldberg, B. B.; Chattopadhyay, D.; Kim, S. N.; Papadimitrakopoulos, F. *Appl. Phys. Lett*. **2004**, *85*, 1006.
(290) Maeda, Y.; Kimura, S.; Kanda, M.; Hirashima, Y.; Hasegawa, T.; Wakahara, T.; Lian, Y.; Nakahodo, T.; Tsuchiya, T.; Akasaka, T.; Lu, J.; Zhang, X.; Gao, Z.; Yu, Y.; Nagase, S.; Kazaoui, S.; Minami, N.; Shimizu, T.; Tokumoto, H.; Saito, R. *J. Am. Chem. Soc*. **2005**, *127*, 10287.
(291) Seifert, G.; Enyashin, A. N.; Heine, T. *Phys. Rev. B* **2005**, *72*, 012102.
(292) Chattopadhyay, J.; Sadana, A. K.; Liang, F.; Beach, J. M.; Xiao, Y.; Hauge, R. H.; Billups, W. E. *Org. Lett*. **2005**, *7*, 4067.
(293) Liang, F.; Alemany, L. B.; Beach, J. M.; Billups, W. E. *J. Am. Chem. Soc.*, published online September 9, 2005, http://dx.doi.org/10.1021/ja052870s.
(294) Kam, N. W. S.; O'Connell, M.; Wisdom, J. A.; Dai, H. *Proc. Natl. Acad. Sci*. **2005**, *102*, 11600.
(295) Henry, C. *Chem. Eng. News* **2005**, *83*, 16.

CR030093D